SYNTHESIS AND CHARACTERIZATION OF MONODISPERSE SILICA BASED FUNCTIONAL NANOPARTICLES FOR MULTI-PURPOSE APPLICATIONS

A Thesis Submitted to
the Graduate School of Engineering and Science of
İzmir Institute of Technology
in Partial Fulfillment of the Requirements for the Degree of

MASTER OF SCIENCE

in Chemistry

by
Burcu ALTIN

July 2009
İZMİR

ACKNOWLEDGEMENTS

I would like to thank and express my deepest gratitude to Professor Serdar ÖZÇELİK for his supervision, guidance, support, understanding and encouragement during this study. It was an invaluable experience for me to work with him.

I would also like to thank Associate Professor Ali Çağır for giving a chance to work on this project in his laboratory.

Also, I would like to thank Pınar KASAPLAR for her constructive comments on this thesis and for being an exceptional collaborator.

I am very grateful to İlker ERDEM, Berna TOPUZ and A. Emrah ÇETİN for their valuable comments and recommendations.

I am pleased to pay my thanks to Scientific and Technological Research Council of Turkey (TÜBİTAK) for funding the project (108T446) and providing scholarship. Next, I wish to express my appreciation to Murat ÇOKAKLI from Dokuz Eylül University and Specialist Özgür YILMAZER from IYTE for the help of the biological activity tests.

Special thanks to group members of Materials Research Center, Evrim YAKUT, Mine BAHÇECİ, Duygu OĞUZ, and Gökhan ERDOĞAN for their helps in XRD, SEM, TGA and BET analyses.

I would like to thank my labmates for their invaluable help and the kindness in the laboratory. Additionally, I would like to appreciate deeply to my friends, especially Özlem KEPENEKCİ, Sabiha ÖRER, Yasemin KAYA, İpek SAYHAN, Burcu KAYA, Ahmet SIRLAN and Esra YAYICI for their friendships and supports. They have made my school life much more enjoyable than it would have otherwise been.

Finally, I would like to express my endless thanks to my mother, my father and my sisters and also to my nephews Yiğit Emre and Saltuk Alp for their love, endless motivation and continuous support all through my life. I know without their support and understanding I would never have been able to achieve what I have.

ABSTRACT

SYNTHESIS AND CHARACTERIZATION OF MONODISPERSE SILICA BASED FUNCTIONAL NANOPARTICLES FOR MULTI-PURPOSE APPLICATIONS

The Stöber method was performed to tune the size of monodisperse silica nanoparticles in the range of 10 to 500 nm. It was observed that increasing amount of reactants favors the formation of larger particles.

A Stöber method in the presence of L-lysine as a catalyst instead of ammonia was developed to prepare well-ordered, highly monodisperse silica nanoparticles based on the hydrolysis and condensation of TEOS. The effect of medium temperature, amounts of L-lysine, TEOS, octane and dye on the size of particle was investigated. It was found that L-arginine increased the size of particles. The amount of TEOS was determined to be 50.0 mmol to obtain the smallest size of particle. The mole of L-lysine slightly altered the size of particles, however the surface of particles was substantially covered by L-lysine. The presence of octane does not change the size of particles. The amount of dye molecule Rhodamine B isothiocyanate (RBITC) does not alter the size of nanoparticles. We showed that temperature plays important role tuning the particle size from 5.0 nm to 80.0 nm.

MTT assay indicates no cytotoxicity of the silica particles against MCF-7 (human breast cancer cell lines) and PC-3 (human prostate cancer cell lines) cancer cell lines. The particles enter to the cells within 5 minutes with a concentration of 0.1μg/mL.

We propose that these particles can be used in the field of bioimaging and drug delivery.

ÖZET

ÇOK AMAÇLI UYGULAMALAR İÇİN TEK DAĞILIMLI SİLİKA TABANLI İŞLEVSEL NANOPARÇACIKLARIN SENTEZİ VE KARAKTERİZASYONU

Su, amonyak ve etanol içerisinde TEOS'un hidroliz ve yoğuşma reaksiyonlarının gerçekleştiği, Sol-jel yöntemine dayalı olan Stöber metodu kullanılarak tek dağılımlı eş büyüklükte silika nanoparçacıklar sentezlenmiştir. Bu yöntemle farklı mol miktarlarına sahip reaktantların –amonyak, TEOS ve su- silika parçacığın büyüklüğünde ve büyüklük dağılımındaki etkisi araştırılmıştır. Amonyak, TEOS ve su miktarının artması silika parçacıklarının büyümesine neden olduğu belirlenmiştir. Bu yöntemle büyüklüğü 10 nm ile 500 nm arasında silika nanoparçacıklar sentezlenmiştir.

L-lizin kullanılarak tek dağılımlı silika nanoparçacıkların sentezlendiği yeni Stöber yöntemi geliştirilmiştir. Oktan, su ve kataliz olarak L-lizin ortamında TEOS'un hidroliz ve yoğuşma reaksiyonlarının gerçekleştiği sentez sonucunda silika parçacıklar elde edilmiştir. Sıcaklık, L-lizin, TEOS, oktan ve boya miktarının parçacık büyüklüğü üzerindeki etkisi araştırılmıştır. Oda sıcaklığında parçacık büyüklüğü 5.0 nm'ye kadar küçülürken, 100^0C'de 80.0 nm'ye kadar çıkmaktadır. En küçük parçacık büyüklüğüne TEOS miktarı 50.0 mmol olduğunda ulaşılmıştır. L-lizin miktarı arttıkça parçacıkların çok az oranda büyürken, parçacık yüzeyinin daha çok L-lizin ile kaplandığı gözlenmiştir. Boya moleküllerinin silika parçacıkların büyüklüğü üzerinde önemli bir etkisi olmadığı ortaya konmuştur. Oktanın varlığının parçacık büyüklüğüne etkisi ise sınırlıdır.

Silika parçacıkların ne MCF-7 ne de PC-3 hücreleri üzerinde herhangi bir toksik etki uyarmadığı ve hücrelerin çoğalmalarına devam ettiği sonucuna varılmıştır. Konfokal mikroskobu çalışmaları parçacıkların hücre sitoplazmasına geçtiklerini göstermiştir. Parçacıkların hücre içerisine geçmeleri için 5 dakika süre ve 0.1µg/mL konsantrasyonla inkübasyonlarının yeterli olduğu belirlenmiştir.

Sonuç olarak, sentezlenen silika nanoparçacıkları biyogörüntüleme ve ilaç-taşıma uygulamalarında kullanımları beklenmektedir.

TABLE OF CONTENTS

LIST OF FIGURES

LIST OF TABLES

CHAPTER 1

INTRODUCTION

Nanotechnology is a multidisciplinary branch in science that deals with the creation and utilization of materials, devices, and systems through the control of matter on the nanometer scale (10^{-9}m). The term 'nanotechnology' is described in various research areas where the characteristic dimensions are in the nanometer range, typically between 0.1nm and 100nm. The list of typical nanomaterials of different dimensions is shown in Table 1.1. Properties of materials of nanometric dimensions are significantly different from those of atoms as well as those of bulk materials. Appropriate control of the properties of nanometer-scale structures can lead to new science as well as new devices and technologies. Advances in science have made it possible to manipulate atoms and molecules in order to construct materials with nanometer size accuracy.

Table 1.1 Examples of Nanomaterials (Source: Rao 2004).

	Size (approx.)	*Materials*
Nanocrystals and clusters (quantum dots)	diam. 1–10 nm	Metals, semiconductors, magnetic materials
Other nanoparticles	diam. 1–100 nm	Ceramic oxides
Nanowires	diam. 1–100 nm	Metals, semiconductors, oxides, sulfides, nitrides
Nanotubes	diam. 1–100 nm	Carbon, layered metal chalcogenides
Nanoporous solids	pore diam. 0.5–10 nm	Zeolites, phosphates etc.
2-Dimensional arrays (of nano particles)	several nm2–μm2	Metals, semiconductors, magnetic materials
Surfaces and thin films	thickness 1–1000 nm	A variety of materials
3-Dimensional structures (superlattices)	Several nm in the three dimensions	Metals, semiconductors, magnetic materials

Nanotechnology is one of the key technologies of the 21st century. It refers mostly to a field of applied science and technology whose unifying theme is the control of matter on the atomic and molecular scale as shown in Figure 1.1, generally 100

nanometers or smaller, and the fabrication of devices with critical dimensions that lie within this size range.

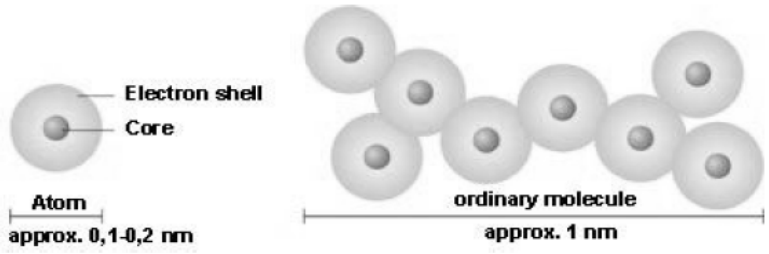

Figure 1.1. Schematic representations for atom and molecule.
(Source: Viswanathan 2008)

Besides areas such as electronics and robotics, nanotechnology makes important developments at the molecular levels, atom by atom, combining biological materials and the rules of physics, chemistry, and genetics to create small synthetic structures. The result of this technology, highly functional nanoscale materials are created.

In the past decades, nanoscience and nanotechnology has been making significant progress, and the effect of nanoscience and nanotechnology on every field has been acknowledged in the world. The study of nanomaterials and nanostructures is one field with the earliest starting that obtained rich achievements in nanoscience and nanotechnology. The synthesis of nanosized particles is one of the fastest expanding research in materials science according to the extensive development of nanotechnology. There is no accepted international definition of a nanoparticle, but one given is a particle having one or more dimensions of the order of 100nm or less. During the past years a rapid development of nano structures, which allow making high-quality products at a very low cost, and also making new nanomaterials the same low cost and at a very rapid speed. Unique changes occur in the electronic structure and chemical properties of solids when their dimensions are reduced to the nanoscale, including development of discrete electronic structure, quantum confinement, structural strain and distortion, and altered surface reactivity. These changes translate into new physical and chemical behavior which is not observed in the ‘bulk’ form of the material (Viswanathan 2008).

The use of nanomaterials offer many advantages in the field of fabrication, such as technologies, energy sources, environments, health and medical treatments, etc. due to their unique size, high surface-to-volume ratio, and other size dependent qualities.

Interest in synthesis techniques for preparation of nanoparticles have increased in the past ten years. Especially, the synthesis of nanoparticles with uniform size, shape and composition exhibit improved properties in many widely used applications. Although many preparation techniques are available for the synthesis of nanoparticles, there are mainly two methods that are being actively studied in many laboratories all over the world from past to present. One is the *Stöber Method*, which includes the Sol-gel processing that consists of hydrolysis and condensation reactions –in general hydrolysis and condensation reactions of tetraethyl orthosilicate in a mixture of alcohol, water and ammonia-. The other is the *Microemulsion Method*, which includes single-phase system consisting of three primary components: water, oil and a surfactant. The resulting particle size and morphology of both techniques strongly depend on the amount of reactants and temperature.

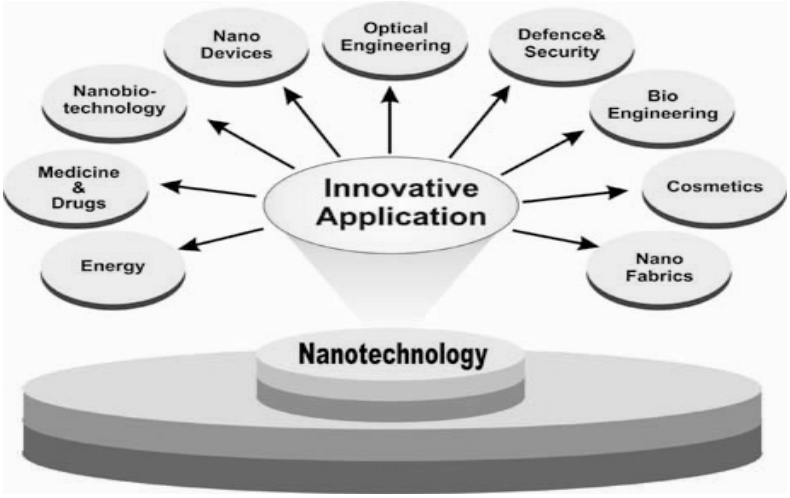

Figure 1.2. An overview of areas of nanotechnology.
(Source: nstc 2009)

The use of silica nanoparticles occupy a major position in scientific research, because of their easy preparation and adequate surface modification, and their wide uses in various industrial applications, not only in the field of physical chemistry dealing with dynamic behavior and stability of particles system but also in industries including pigments, pharmacy, photographic emulsions, ceramics, chromatography, catalysts, electronic and thin film substrates, electronic and thermal insulators, and humidity sensors and chemical mechanical polishing. Silica particles are also used as stabilizers, coatings, glazes and binders. The need for well-defined silica nanoparticles is hence

constantly increasing as high-tech industries (e.g., biotechnology, pharmaceuticals or photonics) provide a tremendous demand for such materials. Figure 1.2) shows the overview of nanotechnology areas that is widely used.

In addition, there is enormous interest in using silica nanoparticles in biomedical applications especially including biolabelling (fluorescent markers in vivo and in vitro), imaging and drug delivery. The sol-gel process, originally developed for glass production, includes extremes of alcohol concentration, temperature and pH, which are detrimental to biomaterial. To avoid the denaturation of proteins the process was modified. The resulting silica gel is chemically inert and biocompatible due to their biocompatible properties. Especially, there has been an exponentially increasing interest and demand for nanoparticles that have 10-100nm size range. The size of the particles is important in this biological usage because most cell uptake occurs in this size range. The importance of nanoparticles for biomedical applications cannot be overestimated. For instance, targeted entry into cells is an increasingly important area of research. Figure 1.3 demonstrates how the nano size is important for biological applications.

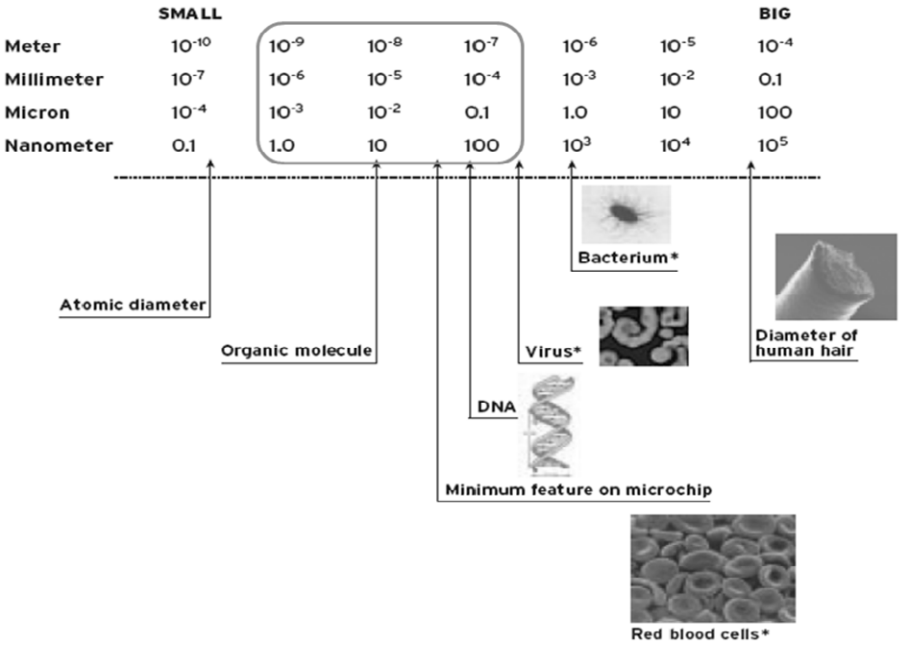

Figure 1.3. Basic illustration of nanostructure size scales.
(Source: Cornell Nanobiotechnology Center 2009)

Furthermore, dye-doped (core-shell) nanoparticles have also widespread interesting application areas of material science because of the ease with which the properties of the core can be changed by building a shell layer on a core. Core-shell

nanoparticles have extensive applications in biology due to their biocompatible properties. The use of nanoparticles with a fluorescent core and a non-fluorescent shell allow monitoring a local structure, such as tracking intracellular structures and also in drug delivery systems (encapsulating the drugs) by confocal microscopy. Also these particles may help in developing some treatment techniques such as delivering or targeting the particles to the cells due to their nanosize and coating materials.

1.1. The Purpose of the Study

The aim of this study is to synthesize silica nanoparticles by controlling their and to modify the surface of these particles for multi-purpose applications, such as bio-imaging and drug delivery. The modification and optimization in preparation methods of silica nanoparticles were investigated. Highly monodisperse silica nanoparticles were prepared by developing methods based on the sol-gel chemistry. Dynamic Light Scattering (DLS) was used to determine the particle size of the resulting silica nanoparticles. Scanning Electron Microscopy (SEM) and Fourier transform infrared spectroscopy (FTIR) were used to investigate the effects of the amounts of reactants and the mole ratio on the catalysis of the hydrolysis and condensation reactions. The effects of parameters like temperature, amount of ammonia and water were also investigated. This research lays in the development of new sol-gel chemistry synthetic approaches for the preparation of advanced silica nanoparticles. The cytotoxic test –MTT Assay- was applied on these synthesized silica nanoparticles to determine whether the particles induce cellular toxicity. Particles being determined as non-toxic, these particles were incubated with MCF-7(breast cancer cell lines) and PC-3(prostate cancer cell line) cells to obtain images to monitor location of silica nanoparticles inside of the cell by using confocal microscopy.

CHAPTER 2

SOL-GEL CHEMISTRY AND PROCESSING

Inorganic polymerization, better known as the ‘sol-gel process’, is a versatile new approach of versatile for preparation of gelation in the sols. In general, this process involves the transition of a system from a liquid *sol*, which is a dispersion of the solid particle in a liquid media that in the size range of 1- 100nm, into a solid "gel" phase that is a state where both liquid and solid are dispersed in each other, which presents a three dimensional network of the dispersed solid particles (solid network) containing liquid components. In case of sol-gel process, an oxide network is obtained via organic polymerization by starting from molecular precursors. These reactions occur in solutions and because of that the term of sol-gel is often used to describe the synthesis of inorganic oxide by wet chemistry methods.

The sol-gel process generally consists of 4 steps (Brinker and Scherer 1990);

1) The desired colloidal particles once dispersed in a liquid to form a sol.
2) The deposition of sol solution produces the coatings on the substrates by spraying, dipping or spinning.
3) The particles in sols are polymerized through the removal of the stabilizing components and produce a gel in a state of a continuous network.
4) The final heat treatments pyrolyze the remaining organic or inorganic components and form an amorphous or crystalline coating.

The main and unique property of the sol-gel process is the ability to all the way from the molecular precursor to the product, allowing a better control of the whole process and synthesis of tailor made materials for various applications in many active areas.

Figure 2.1 shows the schematic representation of sol-gel process of synthesis of nanoparticles. Applying the sol-gel process, it is possible to manufacture nanoparticles in a wide variety of forms such as, ultra-fine or spherical shaped powders, thin film

coatings, ceramic fibers, microporous inorganic membranes, monolithic ceramics and glasses, or extremely porous aerogel materials.

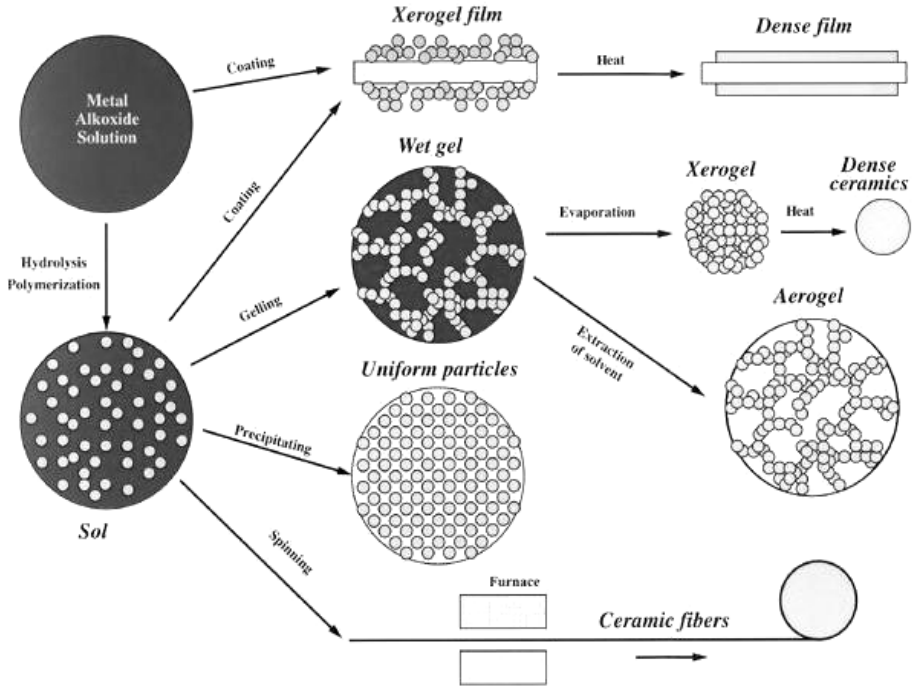

Figure 2.1. Schematic representation of sol-gel process of synthesis of nanomaterials. (Source: chemat 2009)

The sol-gel process appears attractive because it offers many advantages, such as (Brinker and Scherer 1990);

a) Homogeneous multi-component systems can be easily obtained by mixing the molecular precursor solutions,
b) The potential ability in a viscous liquid to minimize the sources of defects introduced in the processing of powders,
c) The ability to visually examine many gel products for defects after drying,
d) Temperatures required for glass and ceramic processing can be significantly reduced by mixing the precursors at the molecular level,
e) The rheological properties of sols or gels allow the formation of fibers, films or composites by such techniques as spinning, dip coating or impregnation.

2.1. Sol-gel Chemistry

In the synthesis of sol-gel, monomer of metal alkoxides can form by hydrolysis and link together in condensation reactions, then one molecule reaches macroscopic dimensions so that it extends throughout solution, the substance is said to be a gel. The starting materials used in the preparation of the sol are usually inorganic metal salts or metal organic compounds such as metal alkoxides. Gelation can occur after a sol is cast into a mold, in which case it is possible to make objects of a desired shape. After the desirably shaped gel has been formed, it must be dried to remove the solvents from the gel structure due to obtaining of amorphous oxide structure from sol-gel processed gel. Flexibility of sol-gel processing enables one to synthesize materials with different chemical composition and geometrical shape. Main possibilities for shaping of metal alkoxides based sol-gel materials are represented in Figure 2.2.

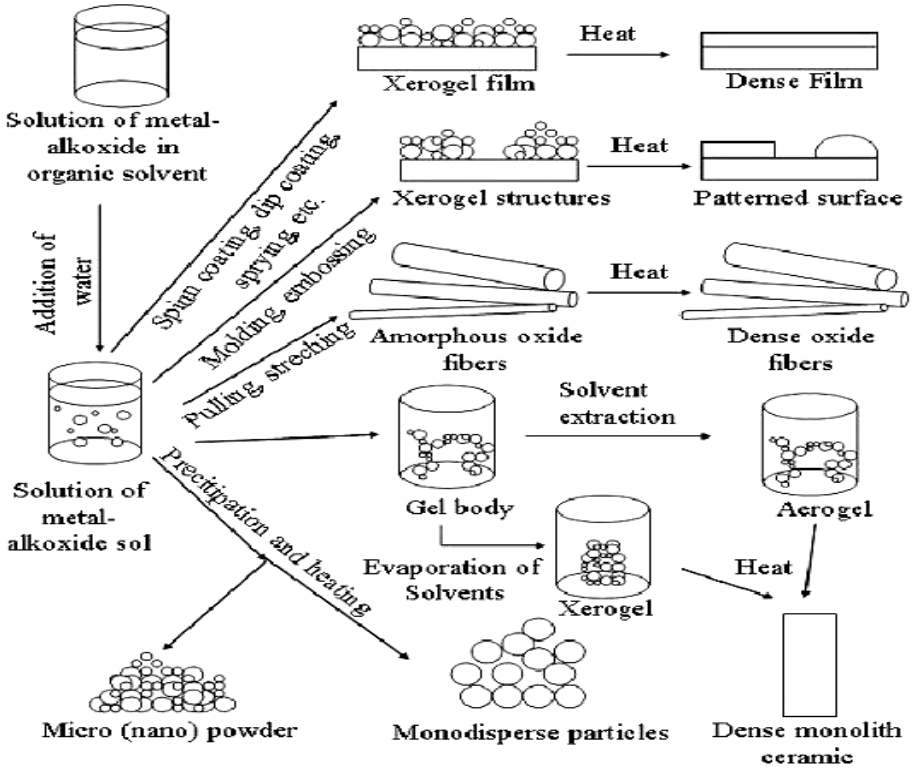

Figure 2.2. Main possibilities for shaping of metal alkoxides based sol-gel materials. (Source: Reedo 1980)

During the drying process, the most evident physical change that occurs when amorphous gel is heated above room temperature (at ambient pressure), is considerable

shrinkage and weight loss. Weight loss is mostly affected by choice of synthesis route or starting compounds. Weight loss and shrinkage are assigned to the number of physical, chemical and structural changes that occur during the heat treatment of resulting material, is known as a xerogel. When solvent removal occurs under hypercritical (supercritical) conditions, the network does not shrink and a highly porous, low-density material known as an aerogel is produced. Heat treatment of a xerogel at elevated temperature produces viscous sintering (shrinkage of the xerogel due to a small amount of viscous flow) and effectively transforms the porous gel into a dense glass.

Many of these nanomaterials are made directly as dry powders or removed the solvents from the gel structure due to obtaining of amorphous oxide structure, and it is a common myth that these powders will stay in the same state when stored as dry forms. In fact, they will rapidly aggregate through a solid bridging mechanism in as little as a few seconds. Whether these aggregates are detrimental will depend entirely on the application of the nanomaterials. If the nanoparticles need to be kept separate, then they must be prepared and stored in a liquid medium designed to facilitate sufficient interparticle repulsion forces to prevent aggregation (wet chemistry). By applying this technique, nanoparticles are already in the form of dispersion, thus high inter-particle forces can be designed in to prevent agglomeration. Hence, the chemical composition and morphology can be closely controlled. This is especially important for research purposes where the quality of the material must be very high to ensure repeatable and meaningful results.

2.2. Sol-gel Processing of Silicates

Silicon is the most abundant metal in the earth's crust and evidence of silicate hydrolysis and condensation to form polysilicate gels and particles are seen in many natural systems. For example, precious opal is composed of amorphous silica particles glued together by a lower density silica gel (Iler 1979). The essential ingredients required to form opals are an abundant supply of readily soluble silica and a source of water. Repeated hydrolysis and condensation steps including the soluble silica lead to aqueous polysilicate species that, under suitable chemical conditions, evolve into spherical particles of essentially anhydrous SiO_2.

The discovery of the exceptional tendency of organosilicon compounds to form siloxane polymers containing organic side groups (silicones) caused an explosion of activity in the late 1930s that established a chemical and physical basis for understanding the process of hydrolysis and condensation. More recently, the rediscovery of monolithic gel formation and the low temperature conversion of gels to glasses without melting have caused renovated interest in the topic of the hydrolysis and condensation of silicates (Battisha 2007).

Today there are wide varieties of materials that can be synthesized and shaped by sol-gel processing. Most of the studies on sol-gel processing and synthesis principles have been done on silica (an oxide of silicon- SiO_2). In particular, recent research efforts were concentrated on sol-gel processes involving the formation of particulate materials or glass-precursor gels from silicon alkoxides such as tetraethyl orthosilicate (TEOS) and tetramethoxysilane (TMOS). Silica sols and gels can be produced very easily both by the colloidal suspension and by the polymeric gel route (de Vos and Verweij 1998)

Reaction kinetic of hydrolysis and condensation is strongly influenced by the electronegativity of metal atom in reactions. It is known that silicon alkoxides are not very reactive with water. Conversely, transition metal alkoxides react vigorously as soon as the alkoxide is brought in contact with water. An approximation of the partial charge distribution in metal alkoxides shows that partial positive charge is much higher for transition metals than that of silicon. This makes clear why transition metal alkoxides are very unstable toward hydrolysis.

2.2.1. Aqueous Silicates

The +4 oxidation state (z=4) is the only important one in the chemistry of silicon in naturally occurring systems, and the coordination number of silicon, N, is most often four. Compared to transition metals, silicon is generally less electropositive, thus coordination expansion does not spontaneously occur with nucleophilic reagents. These factors make the kinetics of hydrolysis and condensation considerably slower than in transition metal systems or Group III systems (Brinker and Scherer 1990).

For expanding the applications of sol–gel method, studies on aqueous precursor solutions are of great importance, because water is inexpensive, nontoxic and less volatile. Especially for applications in an industrial scale, the usual solvents in sol–gel

method, alcohols and the other organic solvents, are very dangerous due to their flammability. Water, a safe and low cost medium, is thus desired.

As silicic acid solutions slowly thicken and finally gel, appearing externally like organic gels, most researches had believed that $Si(OH)_4$ polymerized into siloxane chains that branched and cross-linked like many organic polymers. However, Iler states, "There is no relation or analogy between silicic acid polymerized in an aqueous system and condensation type organic polymer". Instead, silicic acid polymerizes into discrete particles that in turn aggregate into chains and networks as recognized then.

Polymerization process occurs in mainly three steps (Iler 1990);

1. Polymerization of monomer to form particles,
2. Growth of particles,
3. Linking particles into chains, then networks that extend throughout the liquid medium, thickening it to a gel.

Condensation occurs to maximize the number of Si-O-Si bonds and minimize the number of terminal hydroxyl groups through internal condensation. Hence, three dimensional particles are formed. According to Iler, the three dimensional particles serve as nuclei.

Polymerization to form siloxane bonds occurs by either an alcohol-producing or a water-producing condensation reaction. A typical sequence of condensation products is monomer, dimer, linear trimer, cyclic trimer, cyclic tetramer, and higher order rings. The rate of these ring opening polymerizations and monomer addition reactions is dependent upon the environmental pH. Figure 2.3 represents that in basic solution (B) particles grow in size with decreases in number; in acid solution or in the presence of salt (A), particles aggregates into three dimensional networks and forms gel.

pH 7 appears as a boundary because both the silica solubility and dissolution rates are maximized at or above pH 7 and because the silica particles are ionized above pH 7 so that particle growth occurs without aggregation or gelation.

Further growth occurs by addition of lower molecular weight species to more highly condensed species and by aggregation of the condensed species to form chains and networks. In any case, the solubility of silica in this pH range is again low and particle growth stops when the particles reach 2-4 nm in diameter.

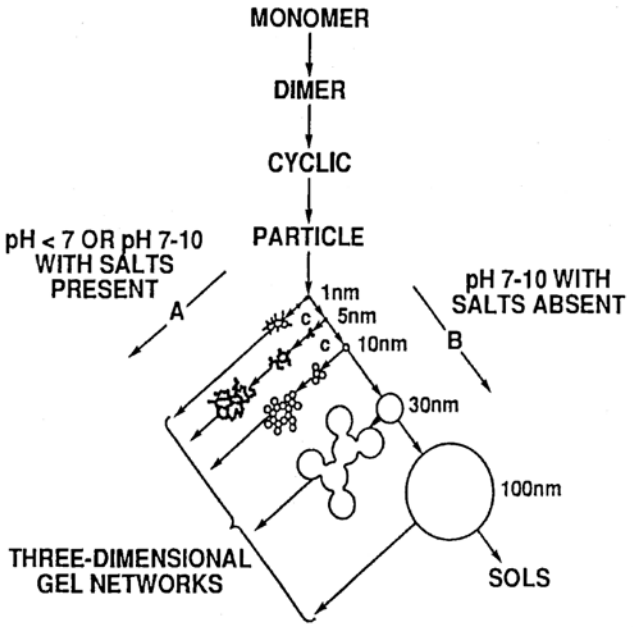

Figure 2.3. Polymerization behavior of aqueous silica.
(Source: Brinker 1990)

Above pH 7, all the condensed species are ionized and therefore, mutually repulsive. Growth occurs primarily through the addition of monomers to the more highly condensed particles rather than by particle aggregation. Particles 1- 2nm in diameter are formed in a few minutes above pH 7. Due to the greater solubility of silica and the greater size dependence of solubility above pH 7, particles grow in size and decrease in number as highly soluble small particles dissolve and reprecipitate on larger, less soluble particles. Growth stops when the difference in solubility between the smallest and largest particles becomes indistinguishable. This process is referred to as Ostwald ripening (ageing) (Brinker and Scherer 1979).

Particle size is therefore, mainly temperature dependent, in that higher temperatures produce a larger particle that can be seen in Figure 2.4 Since growth occurs by the dissolution of smaller particles and deposition of soluble silica on larger particles, the growth rate depends upon the particle size distribution.

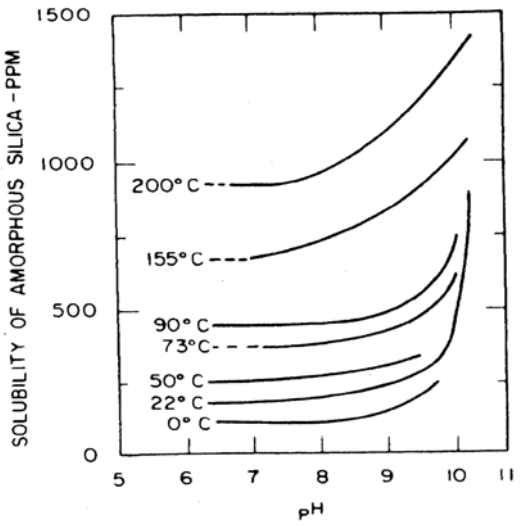

Figure 2.4. Solubility of amorphous silica versus pH at different temperatures.
(Source: Brinker and Scherer 1990)

2.2.2. Hydrolysis and Condensation of Silicon Alkoxides

In the sol-gel process, the use of inorganic or metal organic precursors for preparation of a sol is followed by the formation of a gel. The most commonly used organic precursors are metal alkoxides [M $(OR)_n$], where R is an alkyl group. The preparation of silica is a two step process starting from a suitable metal alkoxide which is the most commonly used organic precursors, mixed with water and a common solvent to form a solution, resulting in an amorphous gel particle. The most frequently used material in this method is silica, being very stable, versatile and inexpensive, which has broad applications in most active areas, due to its easy and adequate surface modifications.

In general, the hydrolysis reaction (Eqn.1), through the addition of water, replaces alkoxide groups (OR) with hydroxyl groups (OH).

$$\equiv Si - OR + H_2O \overset{\text{hydrolysis}}{\rightleftharpoons} \equiv Si - OH + ROH \qquad (2.1)$$

Hydrolysis leads to the formation of silanol groups (Si-OH). These species are only intermediates. Following condensation reactions (Eqns.2- 3) involving the silanol groups (Si-OH) produce siloxane bonds (Si-O-Si) and in most cases the by-products are water or alcohol as shown below for silicate condensation:

Alcohol condensation
- alcoholysis-

$$\equiv Si - OR + HO - Si \rightleftharpoons \equiv Si - O - Si \equiv + ROH \qquad (2.2)$$

Water condensation
- hydrolysis-

$$\equiv Si - OH + HO - Si \equiv \rightleftharpoons \equiv Si - O - Si \equiv + H_2O \qquad (2.3)$$

Subsequent condensation reactions produce siloxane bonds (Si-O-Si) plus the by-products alcohol ROH. This reaction scheme is a simplification of the complex condensation processes. The silica gel formed by this process leads to a rigid, interconnected three-dimensional network which is caused by TEOS (has four ethoxy groups three- and fourfold reaction lead to 3D networks) consisting of submicrometer pores and polymeric chains. The reverse of reaction 2 and 3, siloxane bond alcoholysis and siloxane bond hydrolysis, promote bond breakage and renovation process that permit complete restructuring of the growing polymer. The overall reaction can be dissected into two parts. The first is the initiation step where the primary particles are formed which is followed by the growth of the particles as long as silicic acid is available.

Under most conditions, condensation begins before hydrolysis is complete. Because water and alkoxides are immiscible, a common solvent such as an alcohol is used as a homogenizing agent. With the presence of this homogenizing agent, alcohol, hydrolysis is facilitated due to the miscibility of the alkoxide and water. It is known that alcohol is not simply a solvent. As indicated in the reverse of Eqns.1-2, it can participate in esterification and alcoholysis reactions (Brinker and Scherer 1990).

Although hydrolysis can occur without addition of an external catalyst, it is most rapid and complete when catalysts are employed. The catalyst can either be protons (acid catalysis) or hydroxyl ions (base catalysis) such as mineral acids (HCl) and ammonia which are the most generally used; other known catalysts are acetic acid, KOH, amines, KF, and HF. In addition, the rate and extent of the hydrolysis reaction is most influenced by the strength and concentration of the acid- or base catalyst. Temperature and solvent were of secondary importance. Furthermore, the condensation reactions are also acid and base specific.

It is generally believed that the acid-catalyzed condensation mechanism involves a protonated silanol species. Protonation of the silanol makes the silicon more electrophilic and thus susceptible to nucleophilic attack. The most basic silanol species

are the most likely to be protonated. Therefore, condensation reactions may occur preferentially between neutral species and protonated silanols situated on monomers, end groups of chains, etc.

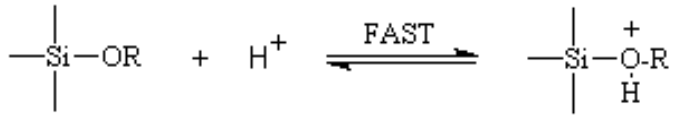

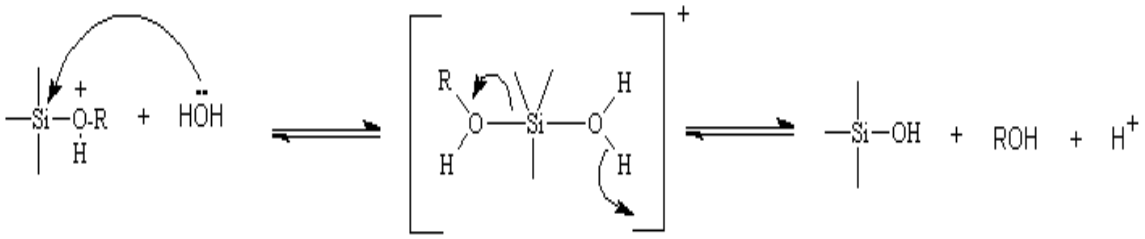

Base-catalyzed hydrolysis of silicon alkoxides proceeds much more slowly than acid-catalyzed hydrolysis at an equivalent catalyst concentration. Basic alkoxide oxygen tend to repel the nucleophile, -OH. However, once an initial hydrolysis has occurred, following reactions proceed stepwise, with each subsequent alkoxide group more easily removed from the monomer then the previous one. Thus, under basic conditions, it is likely that water dissociates to produce hydroxyl anions in a rapid first step.

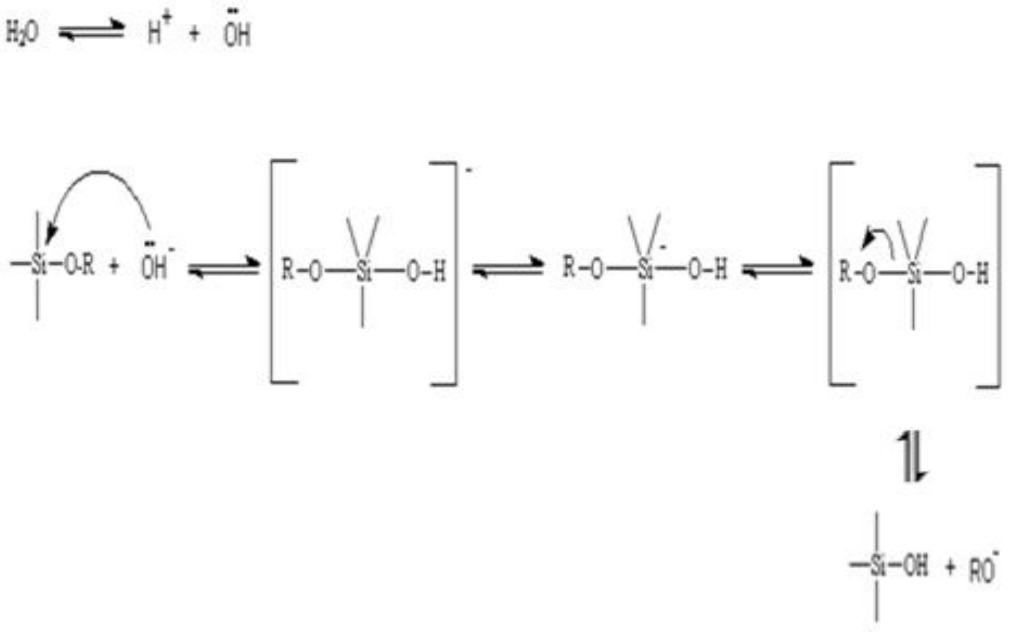

However, it can generally be said that sol-gel derived silicon oxide networks, under acid-catalyzed conditions, yield primarily linear or randomly branched polymers which entangle and form additional branches resulting in gelation. On the other hand, silicon oxide networks derived under base-catalyzed conditions yield more highly branched clusters which do not interpenetrate prior to gelation and thus behave as discrete clusters. In Figure 2.5 shows the summary of acid/base sol-gel conditions.

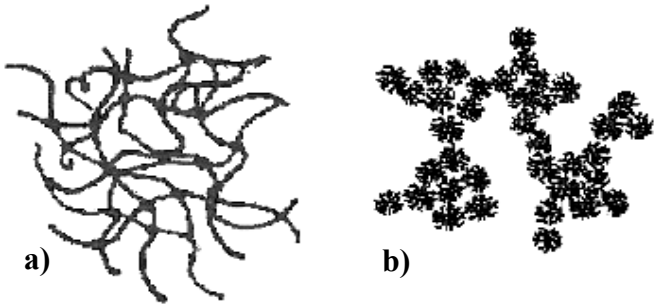

Figure 2.5. Summary of a) Acid and b) Base Sol-gel Conditions.
(Source: Brinker and Scherer 1979)

Nevertheless, the characteristics and properties of a particular sol-gel inorganic network are related to a number of views that affect the rate of hydrolysis and condensation reactions, such as pH, temperature and time of reaction, reagent concentrations (TEOS), catalyst nature and concentration, H_2O/Si molar ratio (R), and drying. Hence, by controlling these factors, it is possible to change the structure and properties of the sol-gel-derived inorganic network over wide ranges.

CHAPTER 3

NANOTOXICOLOGY

Nanotechnology depends in part on exploiting the size-specific properties of nanoscale materials, which in some cases includes an expression of quantum effects that are unique to nanoparticles. Additionally, these size dependent properties also lead to the possibility of size-dependent biological activity. The concept of uniqueness is often used when discussing what makes “nano” different—usually in the context of physical or chemical properties. Recent research has demonstrated that nanoparticles may exhibit unique biological behavior, even when physical and chemical properties remain unchanged from those observed in larger particles. Perhaps the most striking examples are those in which particle size enables nanoscale particles to cross or circumvent barriers that are impenetrable to larger particles. Research showing the potential for nanoparticles to move up the olfactory nerves to the brain in rodents is a prime example of this unanticipated and size-unique behavior. But given that many biological processes occur at the nanoscale, there are numerous additional opportunities for precisely sized nanoparticles to interfere with normal biological functions. Therefore, the studies were started to investigate the effect of particle size in the nanometer range (app. 1–100 nm) on health impact (Figure3.1).

It is well established that nanomaterials display properties and behavior that can be very different compared to the corresponding bulk materials of the same chemical composition. Size, shape, and surface state are properties accounting for most of their differences. The physical and chemical characterization of nanomaterials are important steps in toxicological studies in order to correctly evaluate and assess their potential exposure routes, toxicity, and related risk. Both physical (e.g., particle size and morphology, water solubility) and chemical (e.g., chemical composition and structure, type of coating) properties are important, but other parameters, such as surface/volume ratio, phase transfer, chemical stability, tendency to aggregation, may be important as well. No individual characterization technique can provide sufficient information to completely support the potential risk assessment for a given nanomaterials (Nanotoxicology 2007).

It is certainly necessary to measure or derive not only the nanomaterials characteristics but also to assess and document the nanomaterials involved synthetic methods and its related properties (e.g., dispersion media, dispersion procedure, solution pH, stabilization procedures) in order to understand the associations between nanomaterials features and observed biological responses.

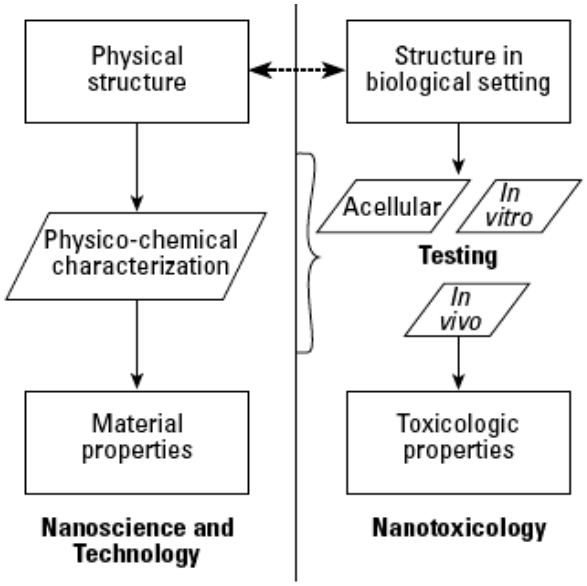

Figure 3.1. The parallel relationship between nanotechnology and nanotoxicology. (Source: ehponline 2009)

The interaction of nanomaterials with biological systems is affected by several factors that should be characterized and determined during in vivo/in vitro experimentation as a preliminary activity included in the adopted experimental protocol. Firstly, size plays a key role in determining the final properties of nanomaterials. The biological activity of nanomaterials is already known to increase as the particle size decreases: nanometer-sized particles are being discovered to be more biologically active (more toxic) than the same material of larger (even in the microrange) size, since they can reach places not accessible to larger particles, as when they are inhaled. Additionally, nanomaterials can exhibit various shape and structures, such as spheres, needles, tubes, rods, platelets, etc. The shape can have two main effects: one, in solution and under aerosol form, is the variation of the hydrodynamic radius between spherical particles and oblong ones (larger for the latter) with the same mass, which triggers a variation in their mobility and diffusion in both gas and liquid phases. The second effect is that the shape influences the deposition and adsorption kinetics in biological media,

since the blocking mechanisms of ion channels in cell walls appear to be dependent on the shape of tested nanomaterials.

The chemical composition, in terms of elemental composition and chemical structure, is an intrinsic property of all materials and it is consequently an important parameter for the comprehension of nanomaterials biological behavior. They can have very different chemical compositions, from completely inorganic, e.g., metals (iron, nickel, zinc, titanium, gold, silver, palladium, iridium, and platinum), and metal oxides (titanium oxide, zinc oxide, silica, iron oxide, etc.), to entirely organic.

Nanomaterials, when dispersed in liquid media, may carry an electric charge on their surface. This charge can depend upon the particle nature and the surrounding medium. Their size and surface charge are major factors affecting the nanomaterials dispersion characteristics. Also, size and charge can influence the adsorption of ions, contaminants, and biomolecules, and the way cells react when exposed to them. Surface charge is also known to influence the biological response to nanomaterials.

Although cells die in many different ways, sometimes they die due to be exposed to toxic effect (Figure 3.2). Therefore, the toxic effects of (nano) materials can be investigated by using some in vitro/in vivo cell tests.

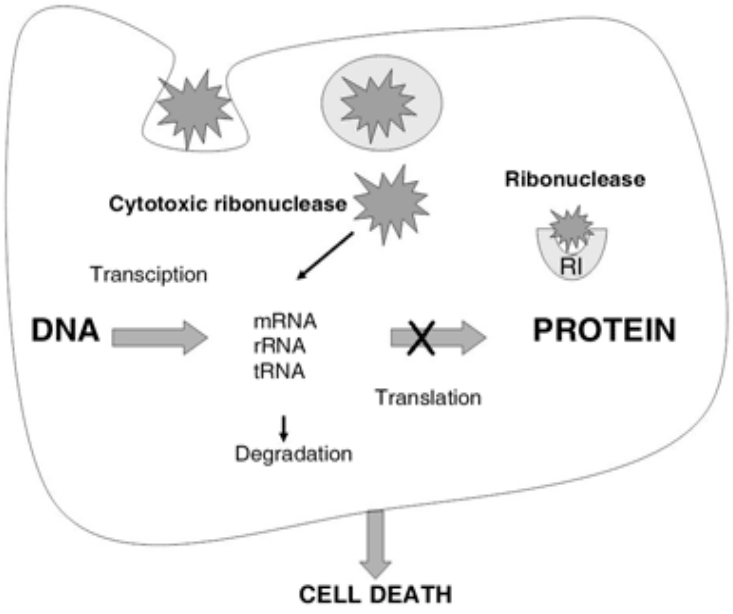

Figure 3.2. Basic scheme of the process of cell death.
(Source: Matsumato 2002)

3.1. Cytotoxicity Assays

In general, toxicity is the degree to which a substance is able to damage an exposed organism and for cells, it is defined as cytotoxicity which is the quality of being toxic to cell. Many cytotoxicity assays are used in biological applications, especially by the pharmaceutical industry-in the field of new drug development- to screen for cytotoxicity in compound libraries. Researchers can either look for cytotoxic compounds, if they are interested in developing a therapeutic that target rapidly dividing cancer cells, for instance; or they can screen hits from initial high-throughput drug screens for unwanted cytotoxic effects before investing in their development as a pharmaceutical.

The predictive value of *in vitro* cytotoxicity tests is based on the idea of 'basal' cytotoxicity – that toxic chemicals affect basic functions of cells which are common to all cells, and that the toxicity can be measured by assessing cellular damage. There are 3 basic parameters upon which these measurements are based. The first assay type is the measurement of cellular metabolic activity. An early indication of cellular damage is a reduction in metabolic activity. Another parameter often tested is the measurement of membrane integrity. When cells are damaged, they become 'leaky' and this forms the basis for the second type of assay. The third type of assay is the direct measure of cell number, since dead cells normally detach from a culture plate, and are washed away in the medium. Cell number can be measured by direct cell counting, or by the measurement of total cell protein or DNA, which are proportional to the number of cells.

There are many techniques that are used to evaluate the cytotoxic effect in cells. Compounds that have cytotoxic effects often compromise cell membrane integrity. Vital dyes, such as trypan blue or propidium iodide are normally excluded from the inside of healthy cells; however, if the cell membrane has been compromised, they freely cross the membrane and stain intracellular components. Alternatively, membrane integrity can be assessed by monitoring the passage of substances that are normally sequestered inside cells to the outside. One commonly used measure molecule is lactate dehydrogenase (LDH). Protease biomarkers have been identified that allow researchers to measure relative numbers of live and dead cells within the same cell population. The live-cell protease is only active in cells that have a healthy cell membrane, and looses

activity once the cell is compromised and the protease is exposed to the external environment. The dead-cell protease cannot cross the cell membrane, and can only be measured in culture media after cells have lost their membrane integrity.

Cytotoxicity can also be monitored using the MTT or MTS assay. This assay measures the reducing potential of the cell using a calorimetric reaction. Viable cells will reduce the MTS reagent to a colored formazan product. A similar redox-based assay has also been developed using the fluorescent dye, resazurin. In addition to using dyes to indicate the redox potential of cells in order to monitor their viability, researchers have developed assays that use ATP content as a marker of viability. Such ATP-based assays include bioluminescent assays in which ATP is the limiting reagent for the luciferase reaction. Cytotoxicity can also be measured by the sulforhodamine B (SRB) assay, WST assay and clonogenic assay. Figure 3.3 represents the principle of measurement assays for cytotoxicity.

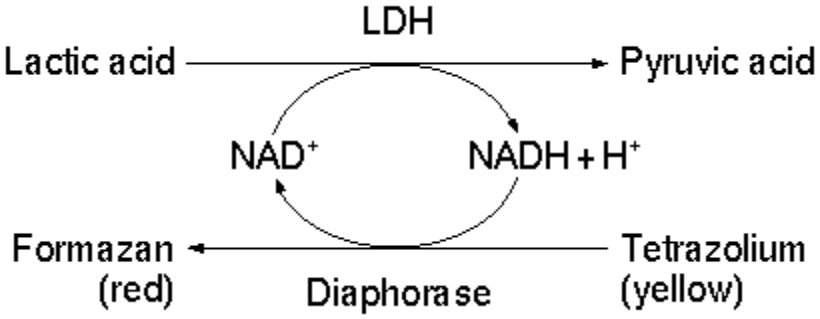

Figure 3.3. Principle of measurement assays for cytotoxicity.
(Source: Papazoglou 2007)

In our study, we deal with the cytotoxic effect of our synthesized nanoparticles on cells that are MCF-7(Human breast cancer cell lines) and PC3 (Human prostate cancer cell lines) cells. MTT assay was applied, to determine the cell viability of these cancer cells.

3.2. Live/ Dead Cell Assay

Cell viability is a determination of living or dead cells, based on a total cell sample. It can be used as a quantitative parameter to assess the cytotoxicity of exogenous substrates or drugs, cytotoxic cellular interactions or as a method to

eliminate dead cells from immunofluorescence analysis since non-viable cells may show different patterns of non-specific antibody binding compared to intact viable, competent cells. Cell viability measurements may be used to evaluate the death or life of cancerous cells and the rejection of implanted organs. There are several methods that can be used to quantitative viability of cells. When samples are applied to cells, they may perform several actions, which allow scientists to examine cells in many different ways. There are numerous tests and methods for measuring cell viability. Testing for cell viability usually involves looking at a sample cell population and staining the cells or applying chemicals to show which are living and which are dead.

3.3. MTT Assay

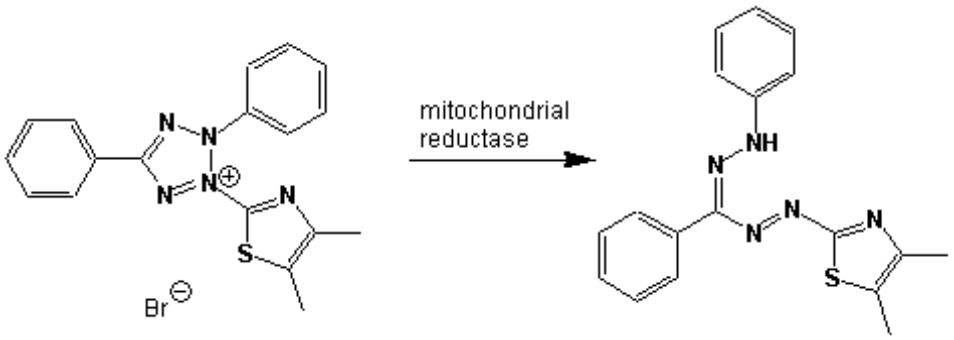

Figure 3.4. Scheme showing the reduction of MTT to formazan.
(Source: Mosmann 1983)

MTT Assay has been widely used as a rapid and sensitive method for measuring the cytotoxicity. This test is a quantitative calorimetric assay - measures changes in color- for measuring the activity of enzymes that reduces yellow water-soluble tetrazolium salt [3-(4,5-Dimethylthiazol-2-yl)-2,5-diphenyltetrazolium bromide, a tetrazole] -MTT- to formazan (Figure 3.4), giving a purple color that is insoluble in aqueous solution. Dimethyl sulfoxide (DMSO) is added to dissolve the insoluble purple formazan product into a colored solution. The absorbance of this colored solution can be quantified by measuring at a certain wavelength (usually between 500 and 600 nm) by a spectrophotometer. The absorption maximum is dependent on the solvent employed.

Changes in metabolic activity can give large changes in MTT result while the number of viable cells is constant. When the amount of purple formazan produced by cells treated with an agent is compared with the amount of formazan produced by

untreated control cells, the effectiveness of the agent in causing death, or changing metabolism of cells, can be deduced through the production of a dose-response curve. Before applying MTT assay, MTT stock solution should be prepared. In briefly, MTT is dissolved in phosphate buffer solution (PBS) to yield 5mg/mL stock solution and then resulting MTT stock solution is filter sterilized and kept no more than 6 weeks at 4ºC.

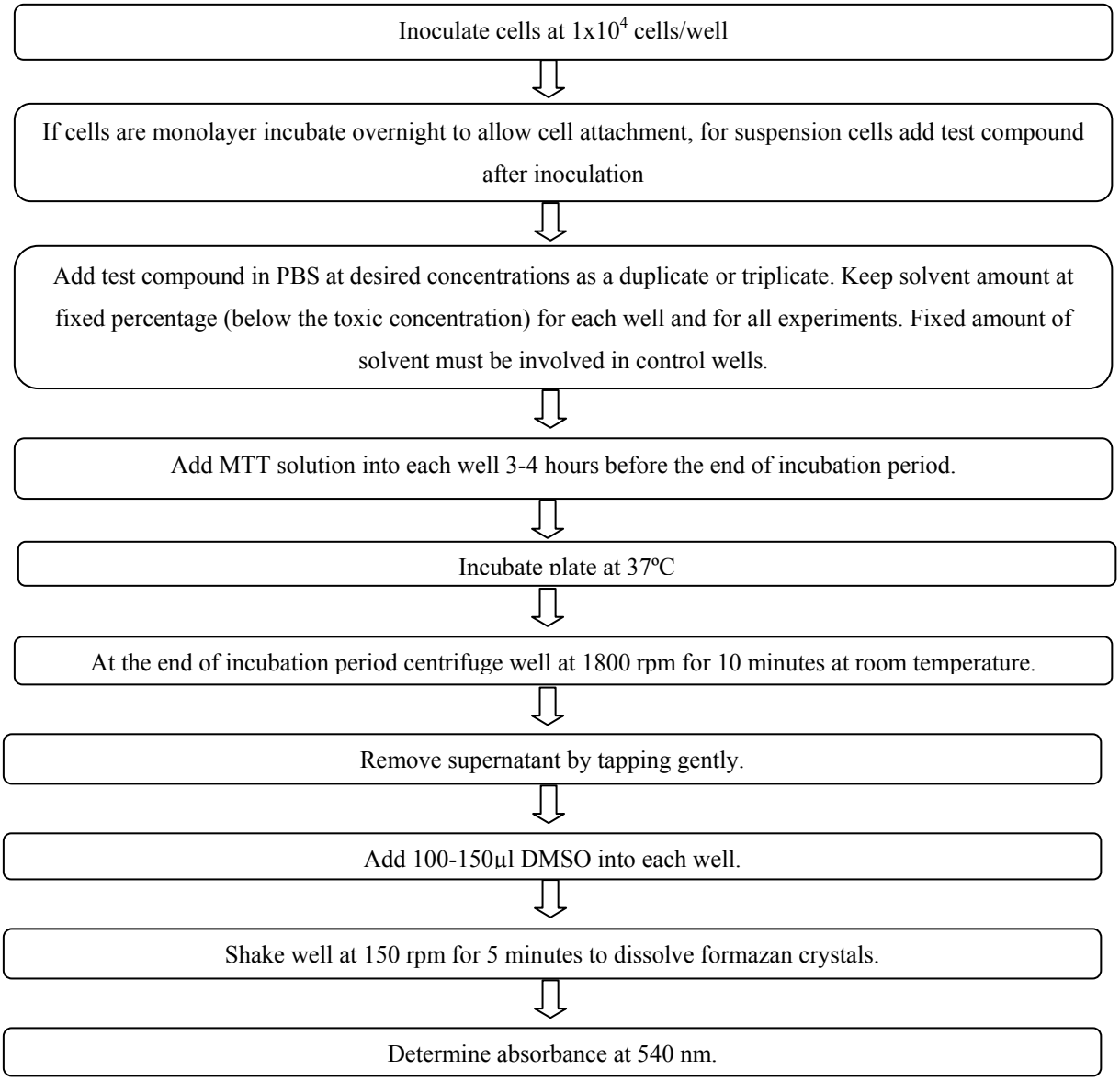

Figure 3.5 Principles of MTT Assay Procedure for cytotoxicity test

By applying these steps that is written above in Figure 3.5, cells treated with our samples and after the incubations, we can measure cell viability of cells and determine whether our samples are toxic or non-toxic according to cell viability.

3.4. Biological Imaging

The nanoparticles internalization (uptake) in cell may be monitored by common cell and molecular biology methods, such as fluorescence microscopy, TEM, SEM, differential interference contrast microscopy, and confocal microscopy. By these microscopy techniques except confocal microscopy, the presence and distribution of individual particles and their aggregates with components at the cellular level can be observed, but it is impossible to ascertain if the aggregation took place before or after particle uptake by the cells. Transmission electron microscopy offers superb resolution; however, it is damaging to living specimens and suffers from fixation and sectioning artifacts. Conventional light microscopy allows examination of living and fixed cells with a variety of imaging modes including fluorescence. However, ultrastructural details cannot be obtained because of the relatively low resolution of the light microscope (0.2 μm).

On the other hand, confocal microscopy offers several advantages over conventional light and electron microscopy which can be applied to a wide range of investigations in the biological and medical sciences for imaging the structural and functional detail of in living and fixed cells and tissues in thin (up to 100 mm) optical sections. First, the confocal microscope optically sections the specimen. This eliminates any physical sectioning artifacts observed with conventional light and electron microscopic techniques. Since optical sectioning is relatively noninvasive, living as well as fixed samples can be observed with greater clarity. Another advantage of confocal microscopy is that optical sections can be taken in different planes, that is, the *xy* plane (perpendicular to the optical axis of the microscope) and the *xz* and *yz* planes (parallel to the optical axis of the microscope).

Although Immunofluorescent labeling is commonly used for biological imaging which involves incubating the sample with a fluorophores-conjugated antibody that is specific to the antigen of interest; in our study, silica nanoparticles-synthesized particles- were used instead of fluorophore-antibody conjugates. By using both living and fixed cells exposed to fluorescent silica particles, it can determine both presence and the sub-cellular localization of fluorescent silica particles and in some cases can also be quantified to yield relative concentrations of sub-cellular biomolecules.

Imaging living tissues with the Confocal Microscopy is substantially more difficult than imaging fixed specimens, and is not always a practical option because the specimen may not tolerate the conditions involved. Some specimens simply will not physically fit on the stage of the microscope, or they cannot be kept alive on the stage during observation. The phenomenon or structures of interest may not be accessible to the objective lens field of view.

The most common protocols for Immunofluorescence labeling are Direct and Indirect. Direct labeling involves incubating the sample with a fluorophores-conjugated antibody that is specific to the antigen of interest. With Indirect labeling, the specimen is incubated first of all with an unconjugated antibody, specific for the antigen under study. Then a second fluorophore-conjugated antibody is introduced that is specific for the first antibody.

Immuno-labeled specimens are examined under a fluorescent microscope, generally confocal microscopy. Confocal microscopy has developed into a universally accessible technique for study of fluorescently labeled cells and tissues. Over the last few decades, this drive has been accelerated by improvements in fluorescent probes, labeling chemistry, optical instrumentation (such as filters and objectives) and detector technology. On the other hand, as with most fluorescence techniques, a significant problem with immunofluorescence is photobleaching. Often to achieve an adequate signal to noise, a high intensity excitation light must be employed, that also causes accelerated photobleaching of fluorophore labels. "Anti-fade" mounting media agents can be used that retard the rate of photo-bleaching, but the most effective ones invariably cause emission intensity to deplete also, and can sometimes result in higher photon background and diffused fluorescence.

In this study, fixed cells exposed to our synthesized dye-doped silica nanoparticles are used to determine the localization of our synthesized nanoparticles and observe whether nanoparticles on cell walls or in cell nucleous by imaging with confocal microscopy. Before the imaging of fixed cells, specimen should be prepared according to immunofluorescence protocol that is outlined below in Figure 3.6.

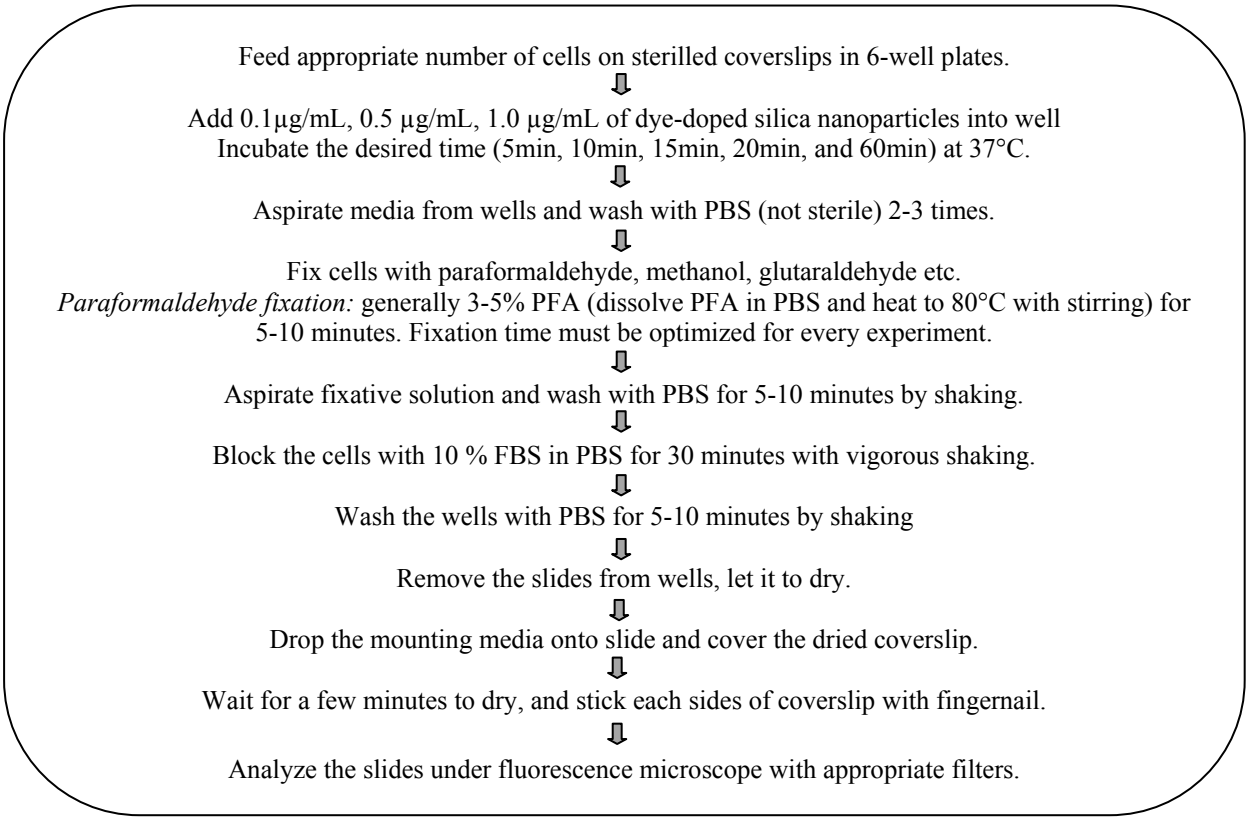

Figure 3.6 Principles of Immunofluorescence protocol

CHAPTER 4

SYNTHESIS AND CHARACTERIZATION METHODS

4.1. Chemicals and Reagents

Tetraethyl Orthosilicate (TEOS 98%, Aldrich), ammonium hydroxide (NH_4OH 28-30%, Aldrich), absolute ethanol (99.9%, Fluka), L-Lysine (98%, Fluka), L-Arginine (98%, Fluka), octane (99%, Fluka), (3-aminopropyl)triethoxysilane (APTES 98%, Aldrich) were used to prepare silica particles. Rhodamine B isothiocyanante (RITC-B, Fluka) was used as a dye. These were used without any further purification.

For MTT Assay, dimethyl sulfoxide (DMSO, 99% Sigma Chemical Co.), tetrazolium (3-(4,5-dimethylthiazol-2-yl)-2,5-diphenyl tetrazolium bromide) (Sigma Chemical Co.) were used.

Ultra pure water (18MΩ) was used throughout the study. Glassware and plasticware were cleaned by soaking them in dilute nitric acid (10%) and rinsed with distilled water prior to use.

4.2. Synthesis of Silica Nanoparticles

4.2.1. Silica Nanoparticles Synthesized by Stöber Method

Silica nanoparticles were prepared by the sol-gel process on the basis of well-known Stöber method (Stöber 1968). The synthesis of these nanoparticles was performed by the hydrolysis and condensation of tetraethyl orthosilicate as a silica source, in a mixture of ethanol and water with ammonia solution as a catalyst to initiate the reaction. The use of ethanol and water were as a solvent.

Briefly, 3.35 mL (0.015 mol) of tetraethyl orthosilicate was mixed with 14.5 mL (0.5 mol) of absolute ethanol. The solution was stirred at room temperature. After 5

minutes, 2.27 mL (0.12 mol) of ammonium hydroxide, 0.5 mL (0.03 mol) of pure water and 14.0 mL of absolute ethanol was added into the solution which yields a total volume of ~35.0 mL. The reaction was allowed to continue for 6 h for completion at room temperature. The resulted solution was directly evaporated at 45^0C. Precursors (ammonia, TEOS and water content) were systematically varied to figure out the change of the size of Silica nanoparticles. The effects of these changing parameters were observed from DLS (Dynamic Light Scattering) technique. The procedure for the preparation of silica nanoparticles was illustrated in Figure 4.1 with the experimental parameters tabulated in Table 4.1.All concentrations were calculated based on the final concentration in the reaction mixture.

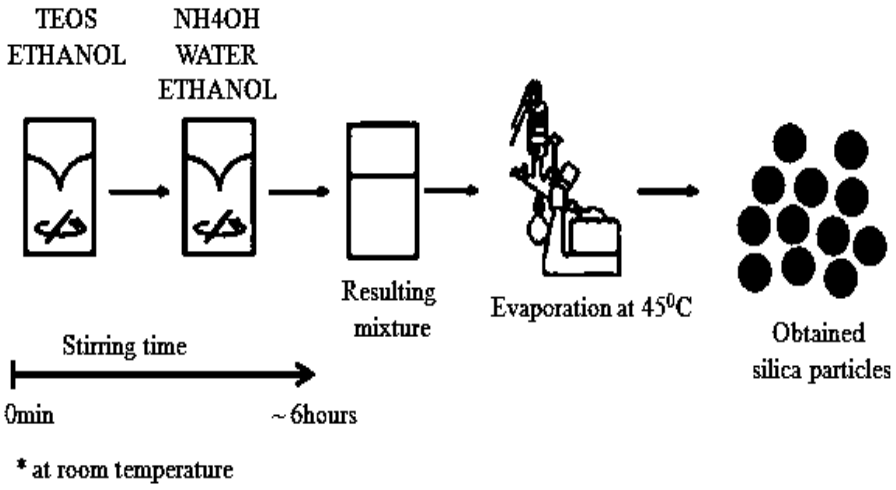

Figure 4.1. A schematic of preparation procedure of the silica nanoparticles

According to appearance of the resulting mixture, we can make a rough estimate whether the particle size is small or large. In this case, the particle size from small to large results that the transparent mixture becomes white turbid suspension. In addition, we can determine the drying step that includes the centrifuge process and evaporation process according to particle size. If the size of the particles is smaller than ~ 20nm, the evaporation process should be applied to get solid powder. However, if the size of the particles is larger than ~ 20nm, both centrifuge and evaporation processes can be applied to obtain solid powder.

Table 4.1. Precursor amounts to prepare silica nanoparticles.

Sample	TEOS	Ethanol	Ammonium Hydroxide	Water
S1	0.015 mol (3.35 mL)	0.5 mol (29 mL)	0.12 mol (2.27 mL)	0.03 mol (0.5 mL)
S2	0.015 mol	0.5 mol	0.06 mol	0.03 mol
S3	0.015 mol	0.5 mol	0.03 mol	0.03 mol
S4	0.015 mol	0.5 mol	0.04 mol	-
S5	0.005 mol	0.05 mol	0.015 mol	-
S6	0.005 mol	0.05 mol	0.03 mol	-
S7	0.005 mol	0.05 mol	0.06 mol	-
S8	0.005 mol	0.05 mol	0.12 mol	-
S9	0.0008 mol	0.24 mol	0.032 mol	-
S10	0.0016 mol	0.24 mol	0.032 mol	-
S11	0.0032 mol	0.24 mol	0.032 mol	-
S12	0.0064 mol	0.24 mol	0.032 mol	-
S13	0.06 mol	3.45 mol	0.95 mol	0.84mol

4.2.2. Synthesis of Silica Nanoparticles Assisted by Amino Acids

The monodisperse uniform-sized silica nanoparticles were prepared following a modified Stöber method, which proceeds with the hydrolysis and condensation of tetraethyl orthosilicate (TEOS) in a mixture of octane and water in the presence of basic amino acid, L-lysine or L-arginine, instead of ammonia -as a catalyst-.

In this study, amino acids were used to synthesize biocompatible particles and with the amino group of the basic amino acids, this well-ordered arrangement of the silica nanoparticles has been synthesized.

In a typical synthesis, 1.0 mmol (0.146 g) of L-lysine was dissolved in the solution containing pure water (139.0 g) and 10.4 mL (7.3 g) of octane with vigorous stirring at 60^0C under N_2 atmosphere. An oil bath was used to control the temperature of the reactions. The solution was stirred overnight at 60^0C under N_2 atmosphere after 11.4 mL of TEOS was added dropwise through a syringe. To obtain silica powder, the resulting mixture was directly evaporated at 70^0C. To determine the effects of amount of L-lysine, amount of TEOS and temperature on particle size, silica nanoparticles were synthesized by changing the amount of TEOS (5.0 mmol-100 mmol), amount of L-lysine (0.1 mmol- 4.0 mmol) and the temperature (20^0C-100^0C).

Figure 4.2 shows the experimental procedure of the silica nanoparticles assisted by L-lysine (L-arginine). Experimental precursor amounts (L-lysine, H_2O, Octane and TEOS) are tabulated in Table 4.2.

Table 4.2. Precursor amounts to prepare silica nanoparticles assisted by amino acids.

Sample	Amino Acids	Water	Octane	TEOS	Temperature (^{0}C)
L1	1 mmol (0.146 g)	7.7 mol (139 g)	64 mmol (10.4 mL)	50 mmol (11.4 mL)	60
A1	1 mmol (0.174 g)	7.7 mol	64 mmol	50 mmol	60
N1	1 mmol (0.075 mL)	7.7 mol	64 mmol	50 mmol	60
L2	0.1 mmol	7.7 mol	64 mmol	50 mmol	60
L3	0.5 mmol	7.7 mol	64 mmol	50 mmol	60
L4	1.0 mmol	7.7 mol	64 mmol	50 mmol	60
L5	2.0 mmol	7.7 mol	64 mmol	50 mmol	60
L6	4.0 mmol	7.7 mol	64 mmol	50 mmol	60
L7	1.0 mmol	7.7 mol	64 mmol	5.0 mmol	60
L8	1.0 mmol	7.7 mol	64 mmol	25 mmol	60
L9	1.0 mmol	7.7 mol	64 mmol	50 mmol	60
L10	1.0 mmol	7.7 mol	64 mmol	75 mmol	60
L11	1.0 mmol	7.7 mol	64 mmol	100 mmol	60
L12	1.0 mmol	7.7 mol	64 mmol	50 mmol	20
L13	1.0 mmol	7.7 mol	64 mmol	50 mmol	30
L14	1.0 mmol	7.7 mol	64 mmol	50 mmol	40
L15	1.0 mmol	7.7 mol	64 mmol	50 mmol	50
L16	1.0 mmol	7.7 mol	64 mmol	50 mmol	60
L17	1.0 mmol	7.7 mol	64 mmol	50 mmol	70
L18	1.0 mmol	7.7 mol	64 mmol	50 mmol	80
L19	1.0 mmol	7.7 mol	64 mmol	50 mmol	90
L20	1.0 mmol	7.7 mol	64 mmol	50 mmol	100

(**L** -- Lysine **A** -- Arginine **N** -- NH_40H)

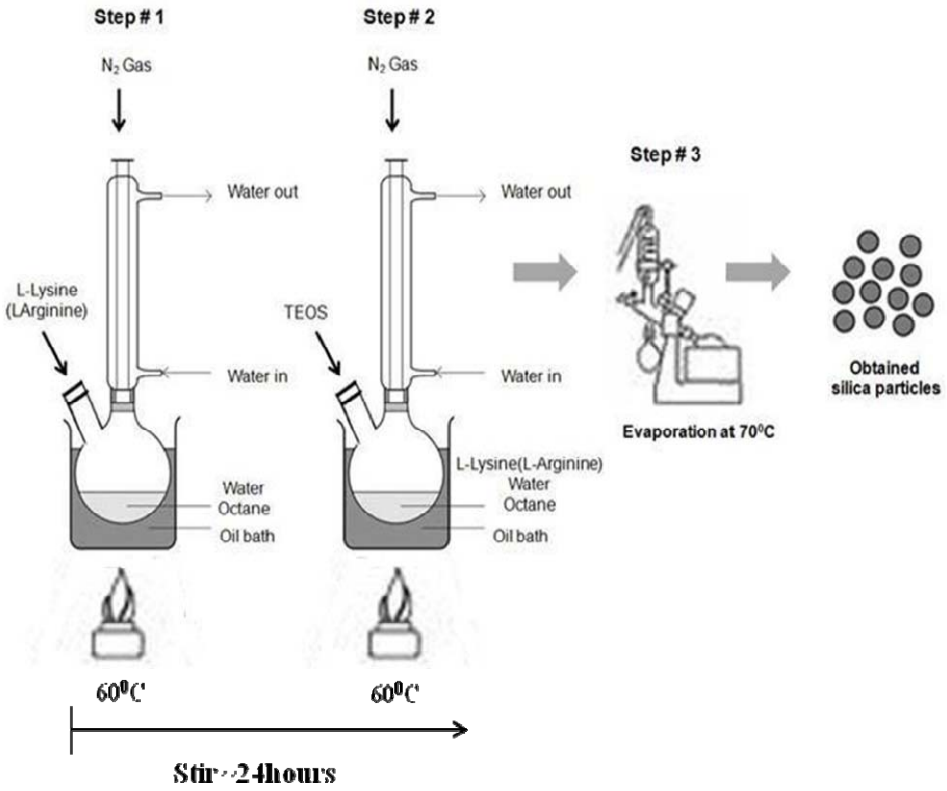

Figure 4.2. A schematic of preparation procedure of silica nanoparticles assisted by amino acids

4.2.3. Dye-doped (RBITC) Silica Particles Assisted by Amino Acids

We have synthesized dye-doped silica nanoparticles for bioimaging applications. By confocal microscopy, the location of the dye-doped silica nanoparticles relative to the cells was verified.

4.2.3.1. Synthesis of RBITC-APTES Conjugate

Rhodamine B isothiocyanate (RBITC) is an amine reactive fluorescent compound that forms a stable fluorescent conjugate (RBITC- APTES) when the amine group of APTES reacts with the thioisocyanate group of RBITC. In the first step, dye was prepared. Briefly, 0.22 mL (220 mg) of APTES was added to 10 mg of RBITC in a 20 mL of absolute ethanol under dry nitrogen atmosphere and stirred for ~24h. The RBITC- APTES conjugate solution is protected from light during reaction and to prevent bleaching of the dye (photobleaching). Figure 4.3 shows the APTES-RBITC conjugate.

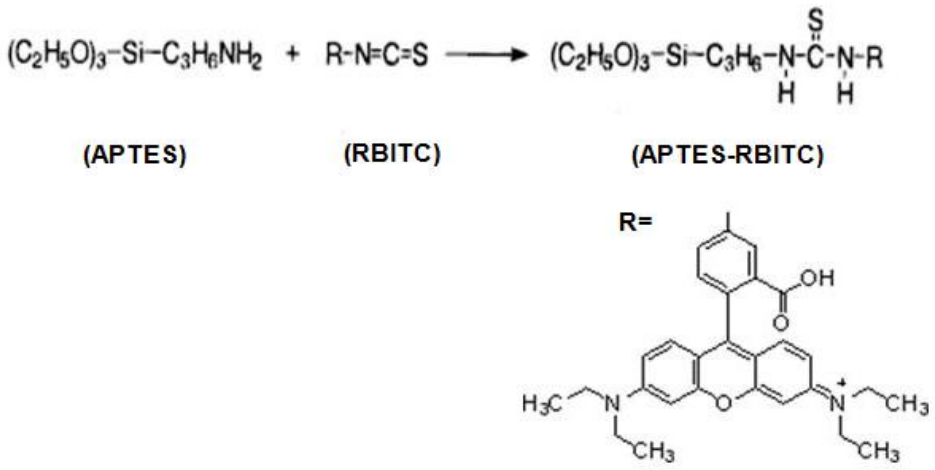

Figure 4.3. Schematic representation of APTES-RBITC conjugation.

4.2.3.2. Synthesis of dye-doped Silica Nanoparticles

In the second step, 1.0 mmol (0.146 g) of L-lysine was dissolved in the solution containing pure water (139.0 g) and 10.4 mL (7.3 g) of with stirring octane under vigorous stirring at 60^0C under N_2 atmosphere. After 5 minutes, 11.4 mL of TEOS was added through the syringe dropwise, followed by 1 mL/ 100 µL of the APTES-RBITC conjugate another 5 minutes later. The solution was stirred vigorously overnight at 60^0C under N_2 atmosphere.

Following the reaction, the samples were centrifuged at 5000 rpm for 60 minutes to collect the silica particles. The synthesized silica nanoparticles were centrifuged from the solution and redispersed in ethanol at least 3 times to remove excess reactants, and then disperse in 20ml of absolute ethanol.

Figure 4.4 shows the experimental steps of dye-doped silica nanoparticles assisted by L-lysine. All experimental amounts for L-lysine, H_2O, Octane, TEOS and Dye are given in Table 4.3.

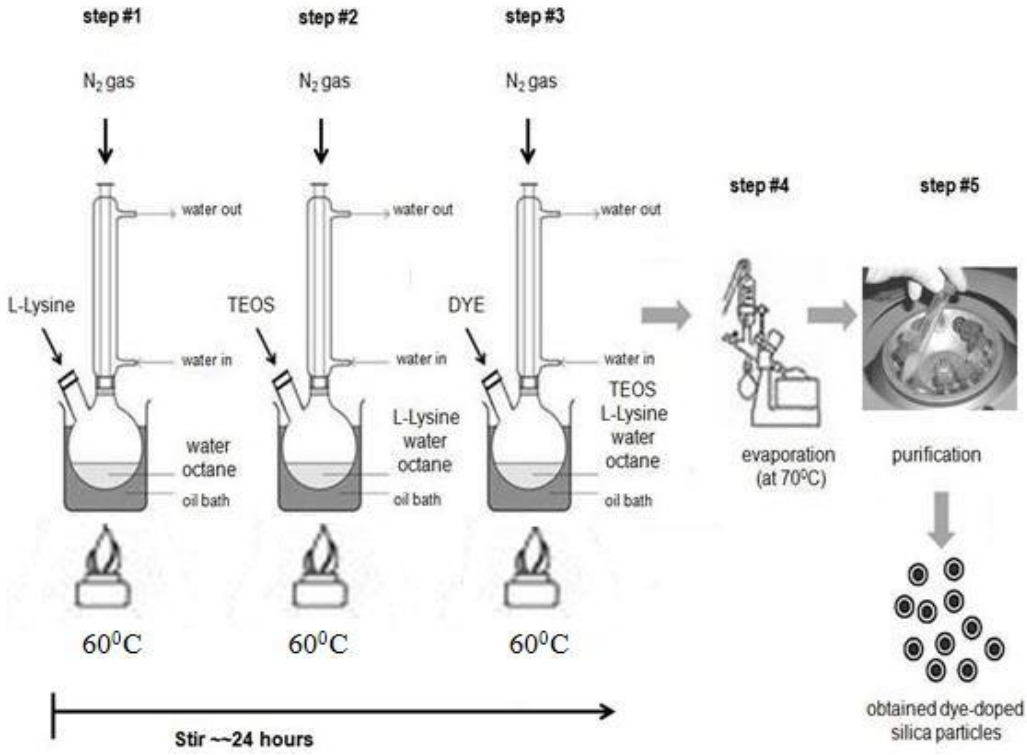

Figure 4.4. A Schematic of preparation procedure of dye-doped silica nanoparticles assisted by L-lysine.

Table 4.3 Precursor amounts to prepare dye-doped silica nanoparticles

Sample	Amount of Dye/ APTES	Amino Acids	Water	Octane	TEOS
L21	1mL	1 mmol (0.146 g)	7.7 mol (139 g)	64 mmol (10.4 mL)	50 mmol (11.4 mL)
L22	100 µL	1.0 mmol	7.7 mol	64 mmol	50 mmol
L23*	12 µL	1.0 mmol	7.7 mol	64 mmol	50 mmol
L24**	0.2 mg	1.0 mmol	7.7 mol	64 mmol	50 mmol

*** L23** was synthesized by addition of APTES (44 µL)
**** L24** was synthesized by addition of RBITC (0.2 mg in 1mL ethanol).

4.3. Biological Evaluations

There are many techniques that are used to evaluate the cytotoxic effect in cells. In this study, MTT assay was applied to investigate the cytotoxic activity of silica particles -synthesized in the presence of ammonia and basic amino acids- on MCF-7(human breast cancer cell lines) and PC-3(human prostate cancer cell lines) cancer cells.

4.3.1. Cell Viability

Human Prostate Cancer (PC-3) cell line was kindly provided by Associate Professor Kemal Sami Korkmaz (Ege University, Engineering Faculty, Department of Bioengineering), human breast cancer (MCF-7) cell line was obtained from Professor Neşe Atabey (Dokuz Eylül University, Medical School, Department of Medical Biotechnology and Genetics). PC3 cells were maintained in Dulbecco's modified Eagle's medium (DMEM) containing 5% fetal bovine serum (FBS), 100µg/mL streptomycin/100IU/mL penicillin. MCF7 cell line was maintained in Roswell Park Memorial Institude-1640 (RPMI-1640) containing 15% FBS (BIO-IND), 100µg/mL streptomycin/100IU/ml penicillin incubated at 37 ºC in the dark with 5% CO_2 humidified incubator. The cells were passaged when they reached 80-85% confluency. Cells used in experiments were maintained from up to 20^{th} passages.

4.3.1.1. MTT Assay for Silica Nanoparticles

To investigate the cytotoxic activity of silica nanoparticles, 95µL of cell suspension was inoculated into 96-well microculture plates at $1x10^4$ cells density per well in culture media containing FBS, penicillin/streptomycin. Compounds were dissolved in dimethyl sulfoxide (DMSO), filter sterilized, diluted at the appropriate concentrations with the culture medium. In all well, 1% DMSO concentration was fixed. Dilutions of compounds were freshly prepared before each experiment. After 24h cultivation for cell attachment, silica nanoparticles were added at final concentration of 5000, 1000, 500, 100, 10, 1 0.1 µg/mL, for triplicate assay. Cells were treated with silica nanoparticles for 24- 48 and 72 hours and cytotoxic effects were determined by

tetrazolium (3-(4,5-dimethylthiazol-2-yl)-2,5-diphenyl tetrazolium bromide) based colorimetric assay. Briefly; 4 hours before the end of incubation period, medium of the cells was removed and wells were washed by pre-warmed phosphate-buffered saline (PBS) to remove any trace of compounds and to prevent colour interferance while optical density determination. MTT stock solution (5mg/ml) was diluted at 1:10 ratio into complete culture media, 100 µL of MTT dilution was added into each well and incubated. After 3.5 hours plates were centrifuged at 1800 rpm for 10 minute at room temperatures to avoid accidental removal of formazan crystals. Crystals were dissolved with 100 µL DMSO. The absorbance was determined at 540nm/570nm. Results were represented as percentage viability and calculated by the following formula:

$$\%viability=[(OD_s-OD_b)/(OD_c-OD_b)x\ 100] \quad (4.1)$$

where OD_b indicates the optical density of blank, OD_s indicates the optical density of sample and OD_c indicates the optical density of control.

4.3.2. Confocal Imaging

Cells exposed to our synthesized dye-doped silica nanoparticles are used to determine the localization nanoparticles and to observe the nanoparticles on cell walls or in sitoplasma by imaging with confocal microscopy. Before the imaging of fixed cells, specimen should be prepared according to immunofluorescence protocol. In briefly, feed appropriate number of cells on sterile coverslips in 6-well plates. Add 0.1µg/mL, 0.5 µg/mL, 1.0 µg/mL of dye-doped silica nanoparticles into well and then incubate 5min, 10min, 15min, 20min, and 60min at 37°C. After the incubation, the media was removed from the wells and wash with PBS 2-3 times. Cells were fixed with paraformaldehyde for 5-10 minutes. Fixative solution was aspirated and washed with PBS for 5-10 minutes by shaking. Then the cells were blocked with 10% FBS in PBS for 30 minutes with vigorous shaking. The wells were washed with PBS for 5-10minutes. Then the slides were removed from wells let it to dry. The mounting media was droped onto slide and covered the dried coverslip with fingernail. We analyzed the slides under confocal microscope. The slides were excited at 488nm and imaged with an emission filter.

CHAPTER 5

PHYSICOCHEMICAL PROPERTIES AND BIOLOGICAL EVALUATION OF SILICA NANOPARTICLES

Morphologies of the synthesized silica nanoparticles were investigated with Phillips XL-30S FEG Scanning Electron Microscopy (SEM) which 5-50keV electron beam scans the specimen surface and Transmission Electron Microscopy (TEM).The average particle size and size distribution based on intensity, volume and number of silica nanoparticles were measured with Zetasizer 3000HS by using Dynamic Light Scattering (DLS) technique. The wavelength of the laser light employed in the instrument was 633nm, which could detect a minimal particle size 2nm. X-Ray Diffraction (XRD) analysis was performed to determine the crystal structure of silica nanoparticles. Diffraction patterns were recorded with Cuκα radiation (λ=0.1541nm) over a 2Θ-range of 1^0- 30^0 for silica particles, 1^0- 2^0 for silica nanoparticles assisted by L-Lysine. Fourier transformed infrared (FTIR) was used with Spectrum 100 FTIR spectrometer (Perkin Elmer, Waltham, MA) to identify the molecular functional groups in particles. Thermal Gravimetric analysis was performed with Perkin Elmer Diamond Thermo Gravimetric Analyzer (TGA) to perform the thermal behavior analysis. The samples were heated at a rate of 10^0C per minute to 1000^0C. A plot of the percent weight loss with increasing temperature was produced as TGA curves. Uv-visible absorption spectra were recorded by using Varian Cary 50 spectrophotometer and Fluorescence spectra were measured with Cary Eclipse Fluorescence Spectrophotometer.

MTT Assay was applied to determine cytotoxicity effects of the synthesized silica particles against MCF-7(human breast cancer cell lines) and PC-3 (human prostate cancer cell lines) cancer cell lines. Confocal Microscopy (Andor Revolution) was used to monitor and determine the locations of the silica nanoparticles exposed to cells.

5.1. Measurement of Particle Size

5.1.1. Silica Nanoparticles Synthesized by Stöber Method

The silica nanoparticles were synthesized by general Stöber method which utilizes two main precursor's amount; TEOS and ammonia, which control the particle size. Amount of water in the reaction medium affects the particle size as well. The results of the average particle size and size distributions based on intensity, volume and number of synthesized silica nanoparticles was measured by DLS technique. Measurements for each sample were repeated three times.

5.1.1.1. Effect of Amount of Ammonia

Firstly, the effect of ammonia on particle size was investigated. Silica particles with different concentrations of ammonia were synthesized by keeping amount of TEOS, ethanol and water unchanged. The particle size of each samples were measured by DLS techniques. According to DLS results, increase in the amount of ammonia favors the formation of larger particles that can be seen in Figures 5.1-5.3. In addition, all the synthesized silica nanoparticles had sharp peaks which indicate of the monodipersity of the particle size distribution. Table 5.1 also summarizes results of silica nanoparticles by varying amount of ammonia.

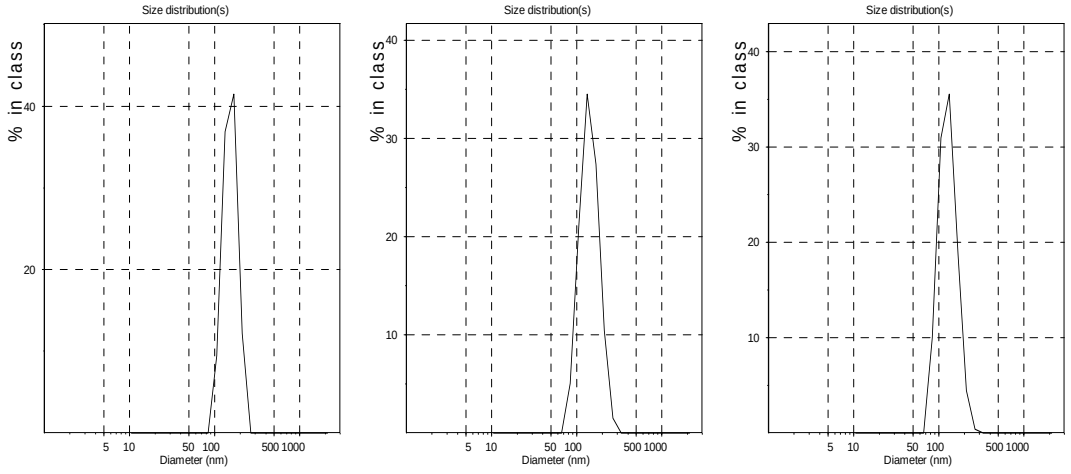

Figure 5.1. Size distributions of **(S1)** based on intensity, volume and number.

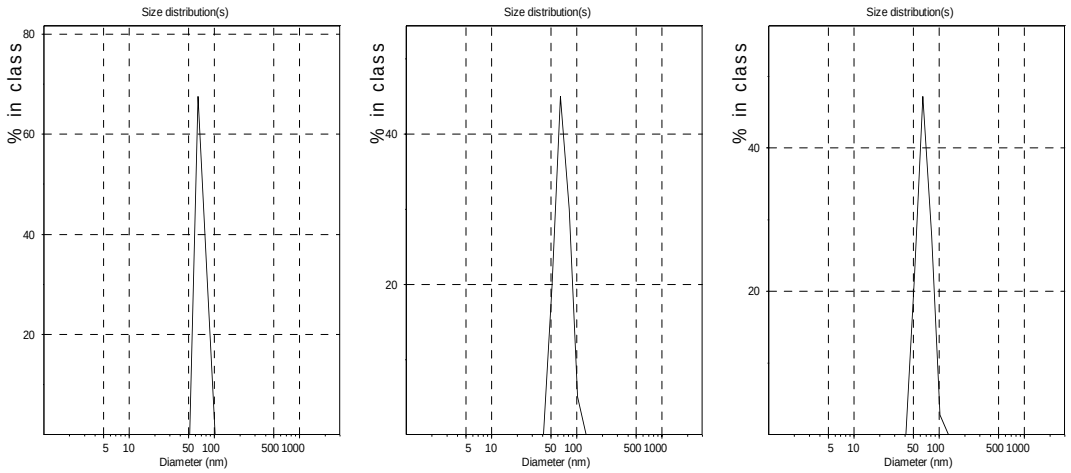

Figure 5.2. Size distributions of **(S2)** based on intensity, volume and number.

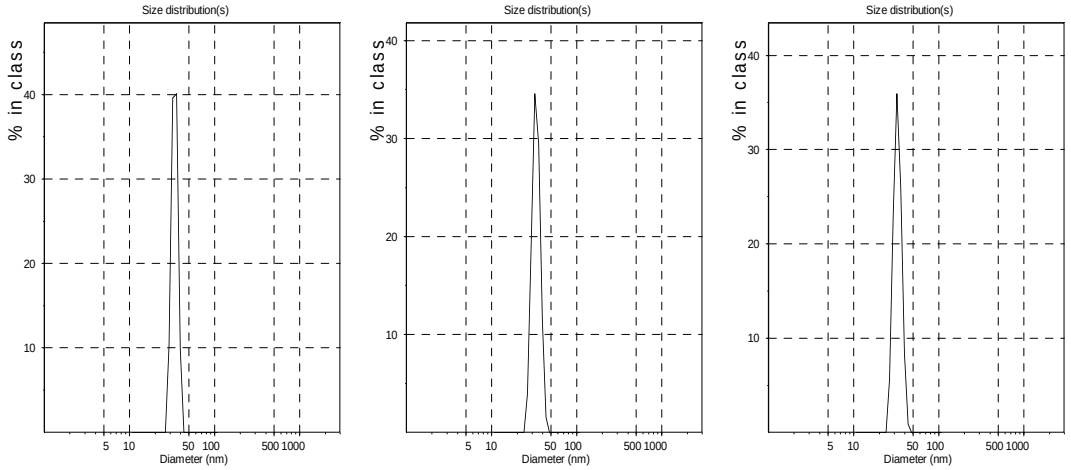

Figure 5.3. Size distributions of **(S3)** based on intensity, volume and number.

Table 5.1 Size Distribution Values of Silica Particles (Effect of Amount of Ammonia).

Sample	Hydrodynamic Diameter (nm)	Intensity Distribution Peak Means (nm)	Volume Distribution Peak Means (nm)	Number Distribution Peak Means (nm)
S1	149	154±40.6	144±46.5	130±39.1
S2	91	70±11.4	69±17.5	67±16.4
S3	34	34±4	33±4.6	33±4.5
S5	15	12±1.4	12±2.4	12±2.4
S6	31	22±2.9	22±3.8	22±3.6
S7	149	105±5.4	105±10.8	105±10.7
S8	169	159±6.4	159±12.1	159±12.9

5.1.1.2. Effect of Amount of TEOS

We have investigated the effect of amount of TEOS on the particle size. Silica nanoparticles with different amount of TEOS were synthesized by keeping amount of ammonia, ethanol and water constant. The size of synthesized silica particles were measured by DLS. As shown in Figures 5.4- 5.7, an increase in the amount of TEOS was resulted in formation of larger particles. According to DLS results, almost all of the synthesized nanoparticles had sharp size distribution peaks; however, polydispersity of the particle size distribution may have resulted in the broadening of peaks due to the impurity of sample container tubes. Hence, these particles are detected during the analysis and resulted large size distribution and broad size distribution peaks.

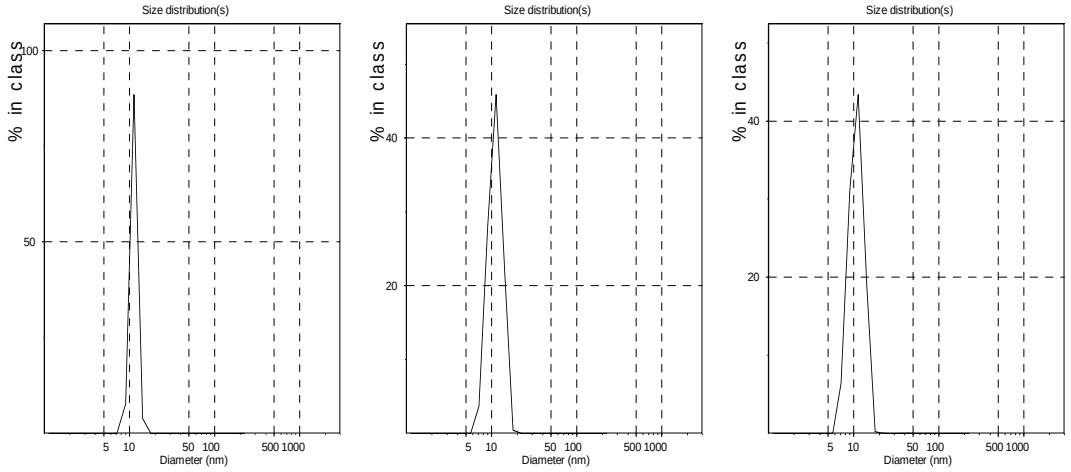

Figure 5.4. Size distributions of **(S9)** based on intensity, volume and number.

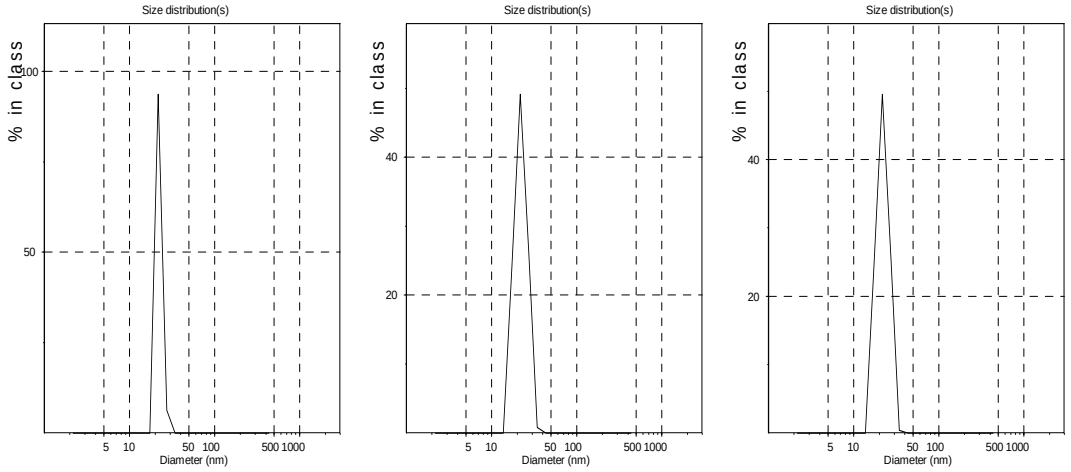

Figure 5.5. Size distributions of **(S10)** based on intensity, volume and number.

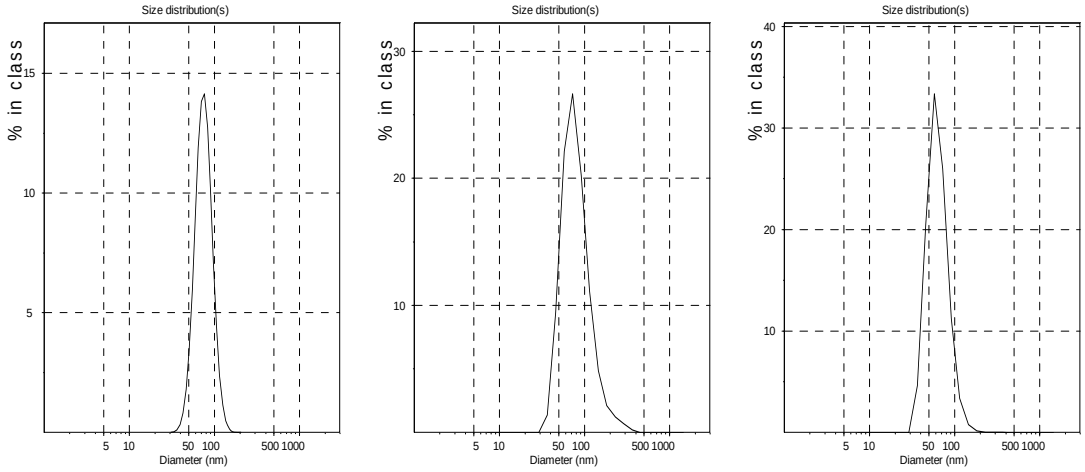

Figure 5.6. Size distributions of (**S11)** based on intensity, volume and number.

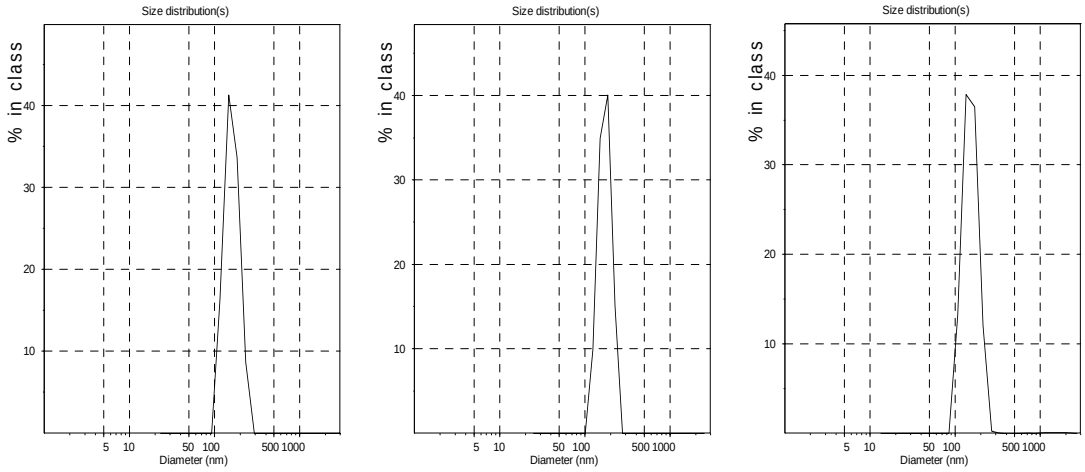

Figure 5.7. Size distributions of (**S12)** based on intensity, volume and number.

The mean particle size distributions of these synthesized silica particles at different amount of TEOS are summarized in Table 5.2.

Table 5.2. Size Distribution Values of Silica Particles (Effect of Amount of TEOS).

Sample	Hydrodynamic Diameter (nm)	Intensity Distribution Peak Means (nm)	Volume Distribution Peak Means (nm)	Number Distribution Peak Means (nm)
S9	15.9	11.2±1.4	11.2±2.8	11±2.8
S10	30.7	22.1±2.7	22.2±5.2	22.1±5.1
S11	92.4	67.3±16.4	84.6±29.9	64.7±20.4
S12	189.6	173.4±41.4	161.7±43.9	132.9±31.8

5.1.1.3. Effect of Amount of Water

The effect of water content on particle size was also investigated. The silica particles were synthesized in the presence of water and in the absence of water. When no water is added to the solution, the amount of water in ammonium hydroxide was calculated and the amount of ammonium hydroxide corresponding to a certain amount of water was added. When we compared the particle size distributions of **S3** (water addition) and **S4** (no water addition), the results of the DLS show that the water content favors the formation of larger particles that can be seen in Figures 5.3 and 5.8. Additionally, **S3** had a sharp peak around 34 nm, 33 nm and 33 nm at intensity, volume and number based distribution, respectively. On the other hand, **S4** had a sharp peak around 27 nm, 28 nm and 27 nm at intensity, volume and number based distribution, respectively. It is observed that the difference of particle size between **S3** and **S4** is about 6nm, which is resulted from water content.

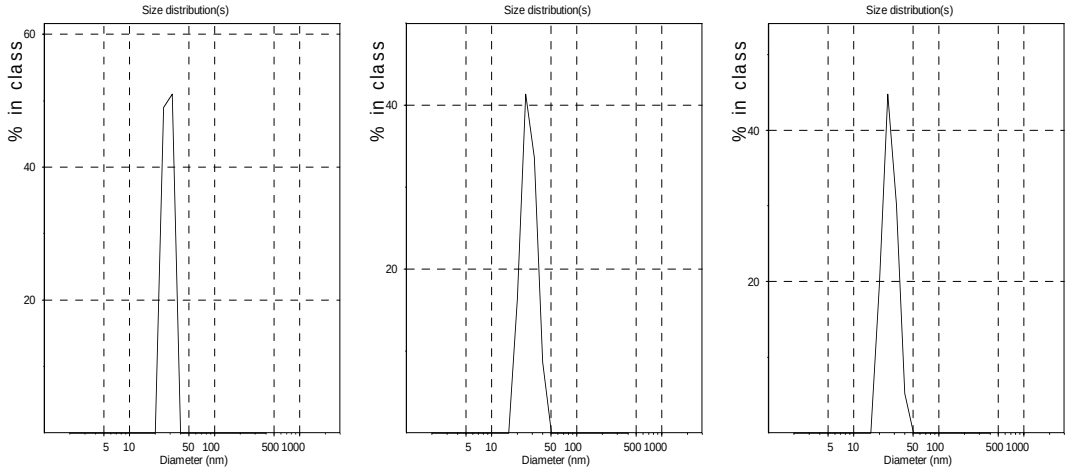

Figure 5.8. Size distributions of **(S4)** based on intensity, volume and number.

5.1.2. Synthesis of Silica Nanoparticles Assisted by Amino Acids

The silica nanoparticles were synthesized by using a modified Stöber method (Yokoi 2006) and the effects of different types of amino acids, temperature, amount of L-Lysine and dye addition on particle size were investigated. The measurement of average particle size and size distributions based on intensity, volume and number of synthesized silica nanoparticles was analyzed by DLS that were repeated three times.

5.1.2.1. Effect of Type of Amino Acids

Firstly, we have investigated the effect of use of L-Lysine (**L1**) and L-Arginine (**A1**) instead of ammonia (**N1**) on the particle size. The particle size of each sample was measured by DLS. According to DLS results that can be shown in Figure 5.9-5.11, the use of L-Lysine was resulted in the formation of smaller particles with size of 9.7±4.1nm, 9.7±5.3 nm and 9.8±5.4 nm based on intensity, volume and number particle size distributions, respectively. However, the use of L-Arginine favors the formation of larger particles with size of 27.8±6.0 nm, 25.2±5.1 nm and 22.8±5.1 nm and use of ammonia results the 41.3±3.8 nm, 41.1±5.1 nm and 40.8±4.9 nm particle size distributions based on intensity, volume and number, respectively.

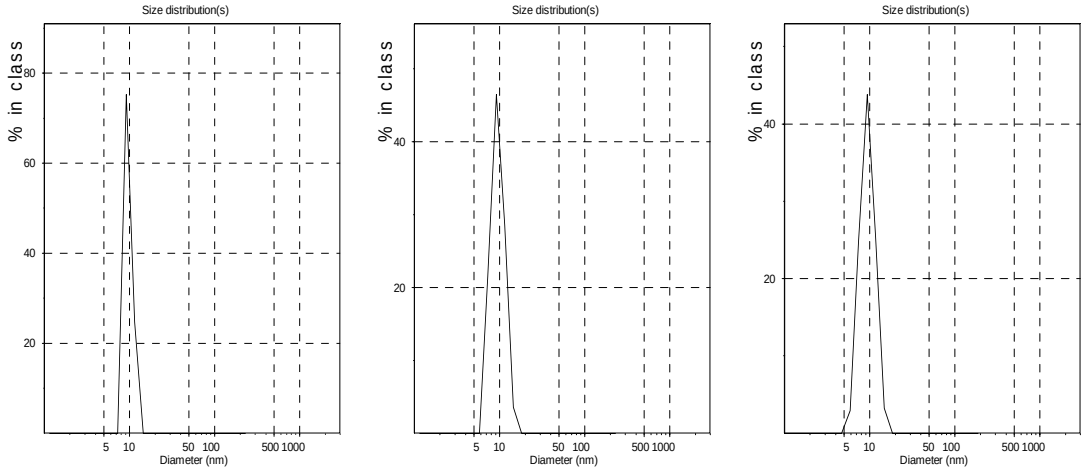

Figure 5.9. Size distributions of (**L1**) based on intensity, volume and number.

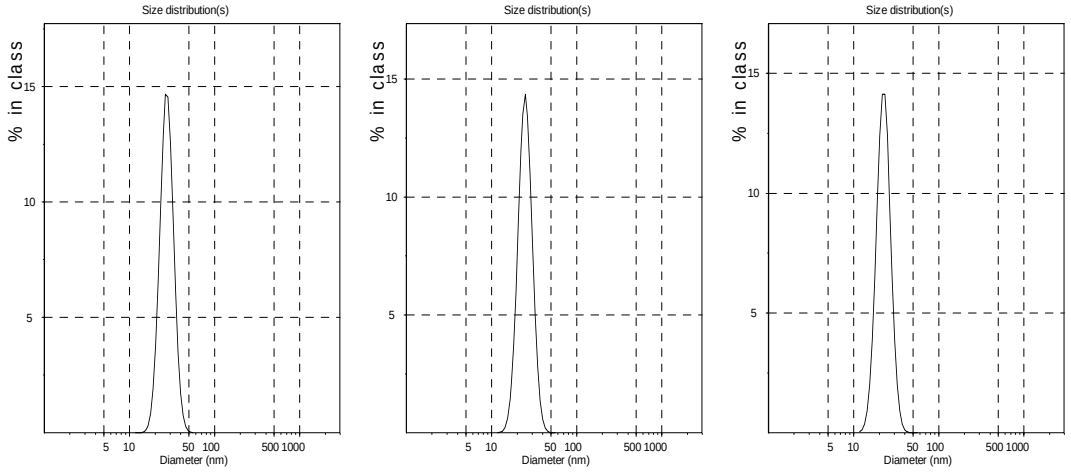

Figure 5.10. Size distributions of (**A1)** based on intensity, volume and number.

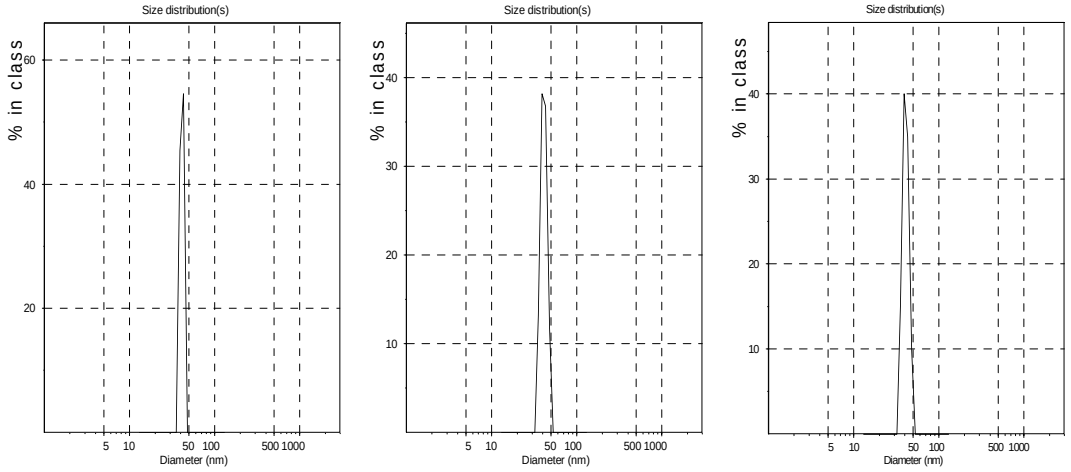

Figure 5.11. Size distributions of Si-np (**N1)** based on intensity, volume and number.

5.1.2.2. Effect of Amount of Lysine

We investigated the effect of amount of L-Lysine on particles size. To optimize the amount of L-Lysine, silica nanoparticles were synthesized in the presence of 0.1 mmol, 0.5 mmol, 1.0mmo, 2.0mmol and 4.0mmol of L-Lysine. The size of synthesized particles was measured by DLS as can be seen in Figure 5.12- 5.16. According to these results, it is observed that the particle size increases with the amount of L-Lysine. All the mean particle size distributions of these synthesized particles are tabulated in Table 5.3. Also, Figure 5.12 represents the size distributions of **L2-L6** against amount of L-Lysine based intensity, volume and number.

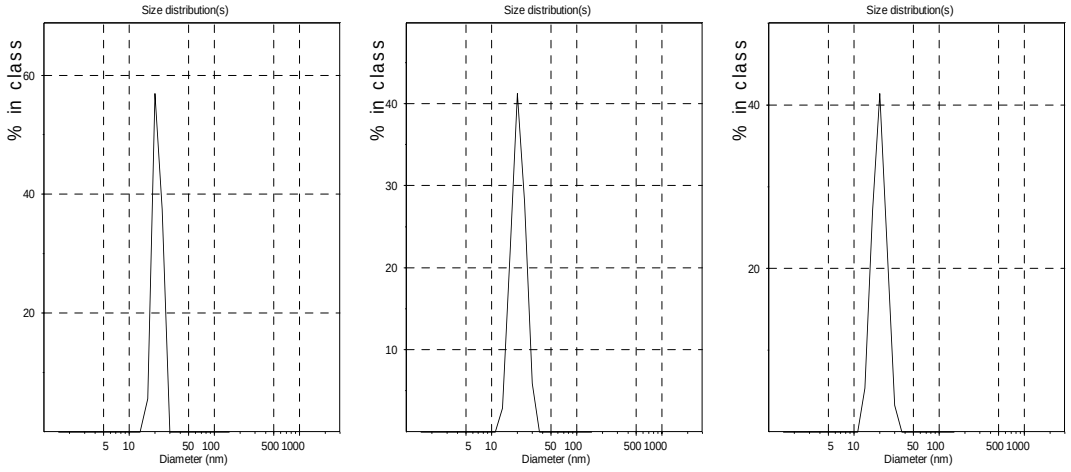

Figure 5.12. Size distributions of (**L2)** based on intensity, volume and number.

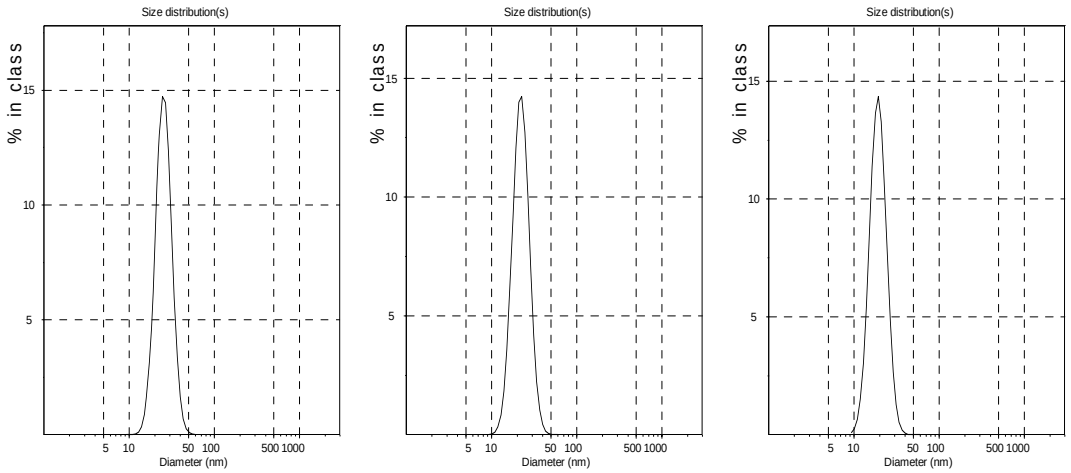

Figure 5.13. Size distributions of (**L3)** based on intensity, volume and number.

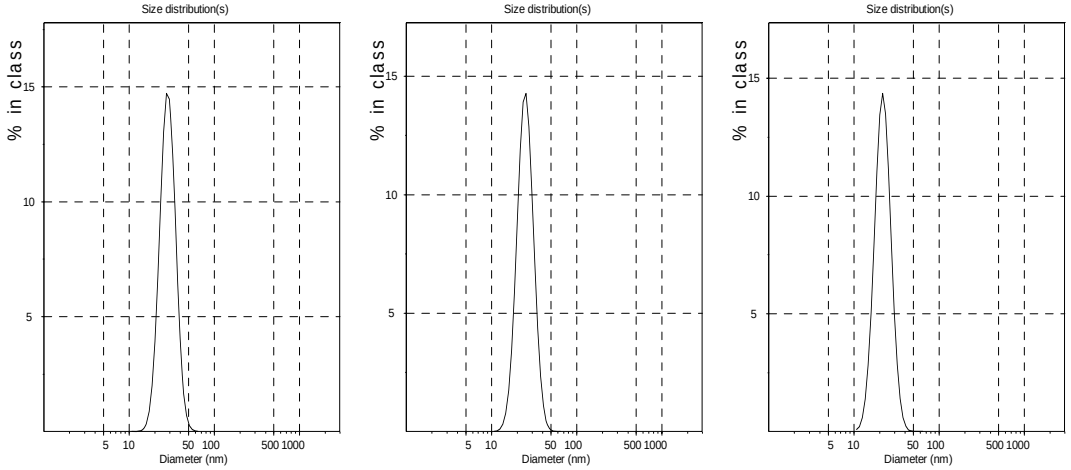

Figure 5.14. Size distributions of (**L4)** based on intensity, volume and number.

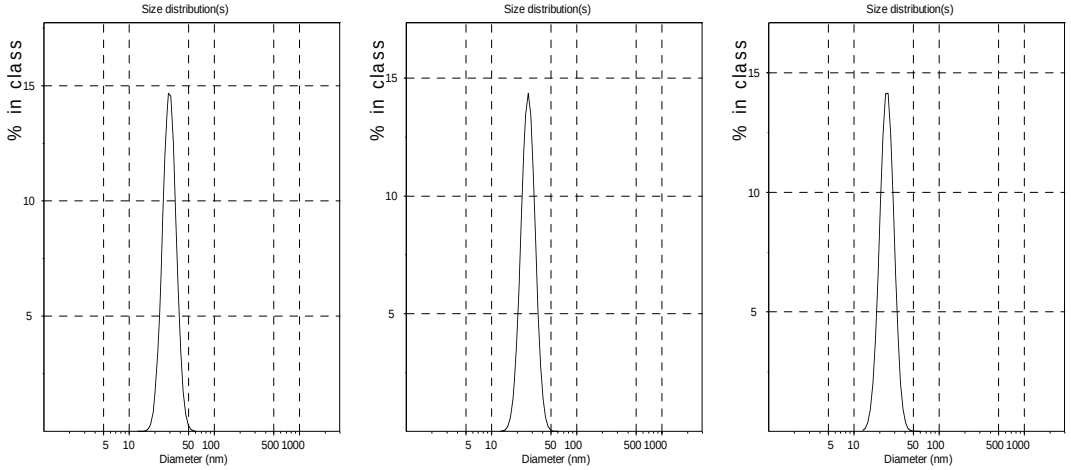

Figure 5.15. Size distributions of (**L5)** based on intensity, volume and number.

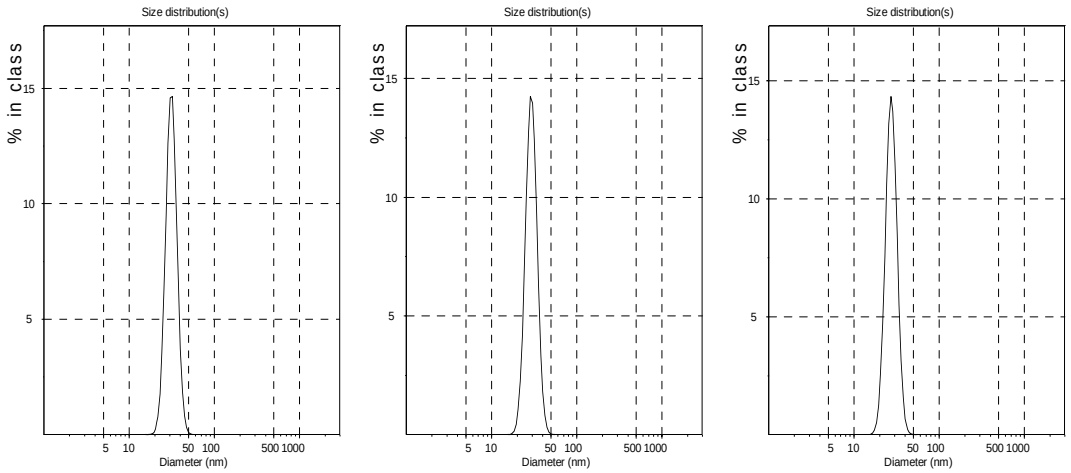

Figure 5.16. Size distributions of (**L6)** based on intensity, volume and number.

Table 5.3. Size Distribution Values of Silica Particles (Effect of Amount of L-lysine).

Sample	Amount of L-Lysine (mmol)	Hydrodynamic Diameter (nm)	Intensity Distribution Peak Means (nm)	Volume Distribution Peak Means (nm)	Number Distribution Peak Means (nm)
L2	0.1	21.0	21.6±3.9	20.9±5.0	20.1±4.8
L3	0.5	25.3	25.9±6.6	22.6±5.9	20.6±5.1
L4	1.0	28.2	28.8±7.1	25.3±6.4	22.2±5.6
L5	2.0	29.6	30.1±6.5	27.3±6.0	24.7±5.5
L6	4.0	31.2	31.5±5.5	29.6±5.2	27.7±5.0

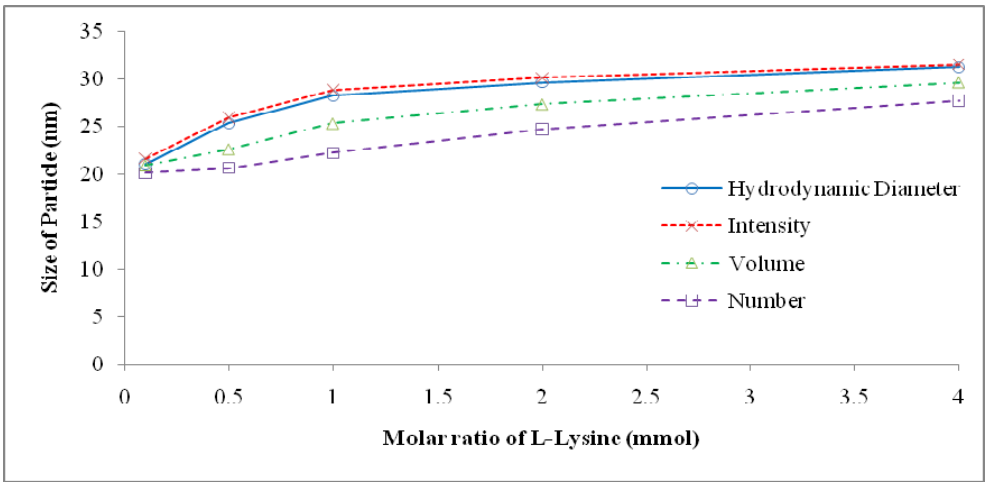

Figure 5.17. Particle size distributions of **L2- L6** against amount of L-Lysine (mmol).

5.1.2.3. Effect of Amount of TEOS

We examined the effect of amount of TEOS on particles size. To optimize the amount of TEOS, silica nanoparticles were synthesized in the presence of 5 mmol, 25 mmol, 50 mmol, 75 mmol and 100 mmol of TEOS. The size of synthesized particles was measured by DLS as can be seen in Figure 5.18- 5.22. According to these results, it is observed that the particle size increases above the 1.0 mmol and decreases below the 1.0 mmol of TEOS. Hence, we decided that 1.0 mmol of TEOS is more suitable amount for our synthesis. All the mean particle size distributions of these synthesized particles are tabulated in Table 5.4.

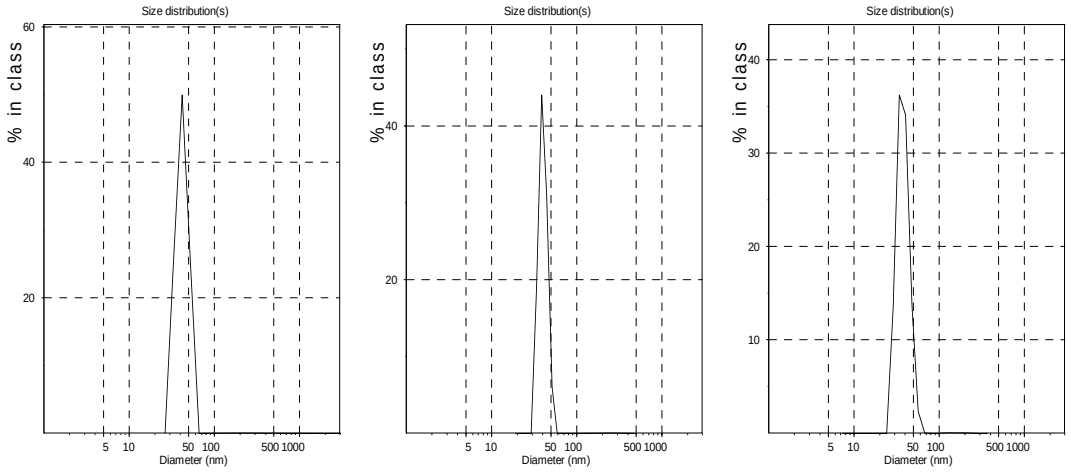

Figure 5.18. Size distributions of (**L7)** based on intensity, volume and number.

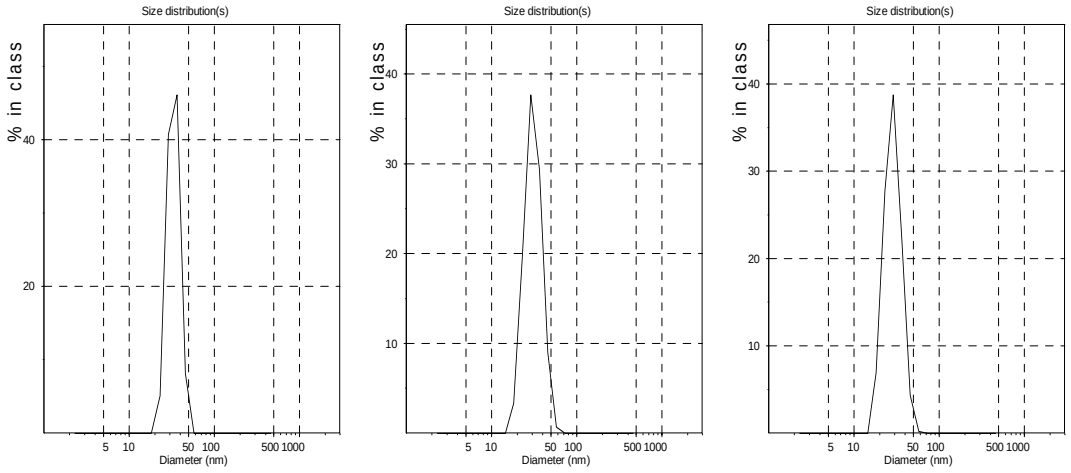

Figure 5.19. Size distributions of (**L8)** based on intensity, volume and number.

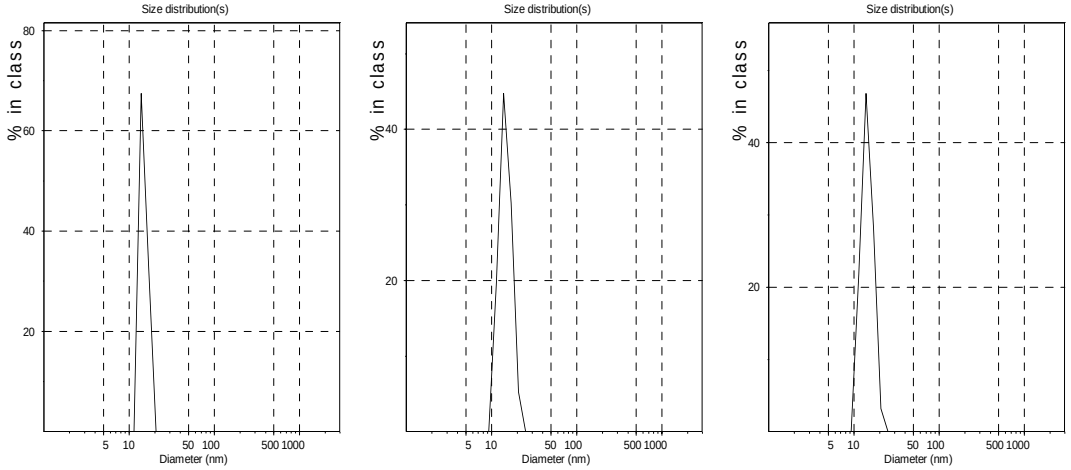

Figure 5.20. Size distributions of (**L9)** based on intensity, volume and number.

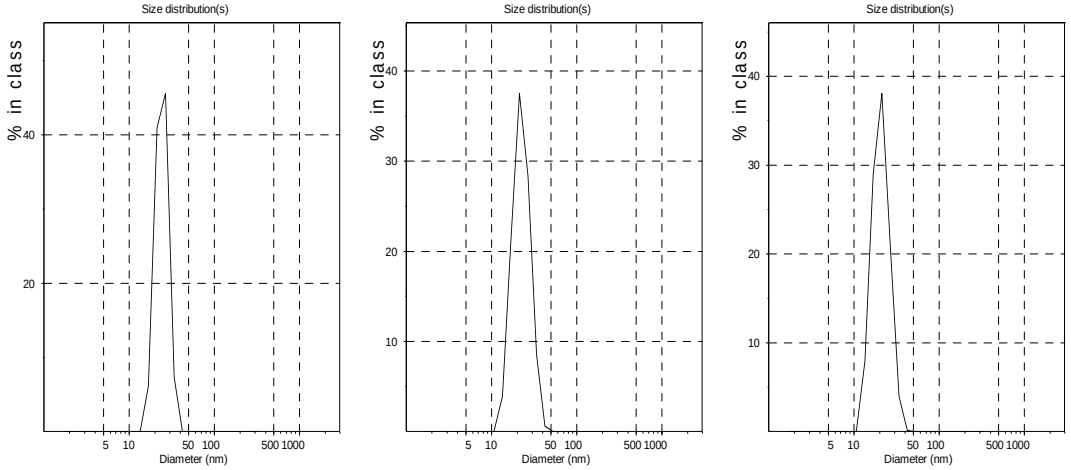

Figure 5.21. Size distributions of (**L10)** based on intensity, volume and number.

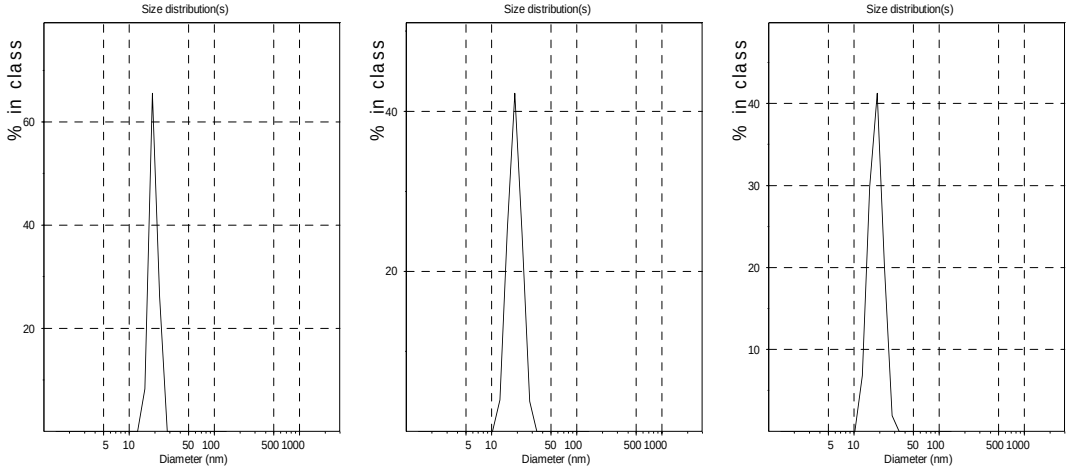

Figure 5.22. Size distributions of (**L11)** based on intensity, volume and number.

Table 5.4. Size Distribution Values of Silica Particles (Effect of Amount of TEOS).

Sample	Amount of TEOS (mmol)	Hydrodynamic Diameter (nm)	Intensity Distribution Peak Means (nm)	Volume Distribution Peak Means (nm)	Number Distribution Peak Means (nm)
L7	5.0	52.2	41.3±8.3	39.7±6.3	38.0±8.2
L8	25	32.5	33.5±8.1	31.3±9.3	29.0±8.4
L9	50	14.5	14.9±2.1	14.6±3.2	14.4±3.0
L10	75	23.8	24.4±6.0	22.8±6.8	21.0±6.1
L11	100	19.6	19.5±2.7	19.0±4.5	18.3±4.3

5.1.2.4. Effect of Temperature

We also examined the effect of temperature on particle size. To optimize the temperature, silica nanoparticles were synthesized at various temperatures in the range of 20 - 100^{0}C. The size of silica particles was measured by DLS. According to DLS results, the particle size increases with increasing temperature. Figures 5.23-26 represent the size distribution of synthesized silica particles that **L12**, **L15, L17** and **L21** at 20^{0}C, 50^{0}C, 70^{0}C and 100^{0}C. The other particle sizes of silica nanoparticles synthesized at different temperatures are tabulated in Table 5.5.

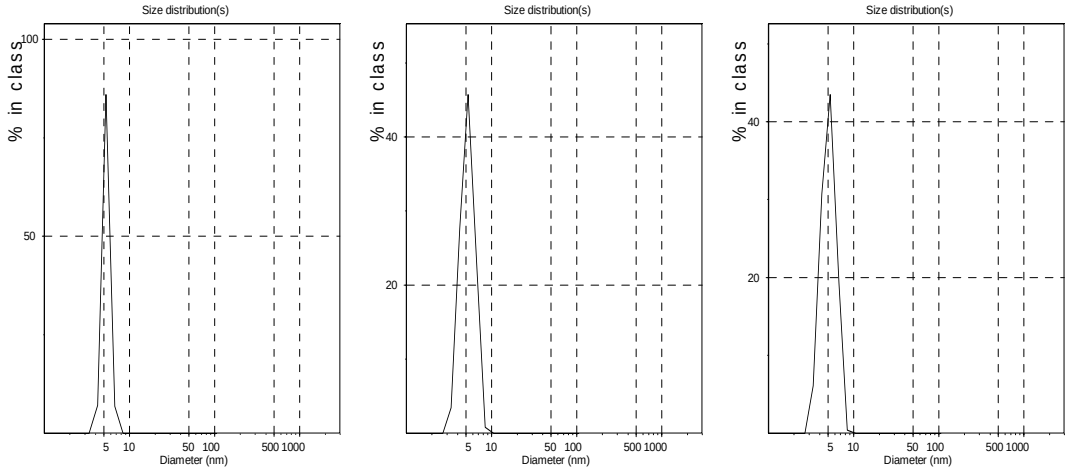

Figure 5.23. Size distributions of (**L12)** at 20^{0}C based on intensity, volume and number.

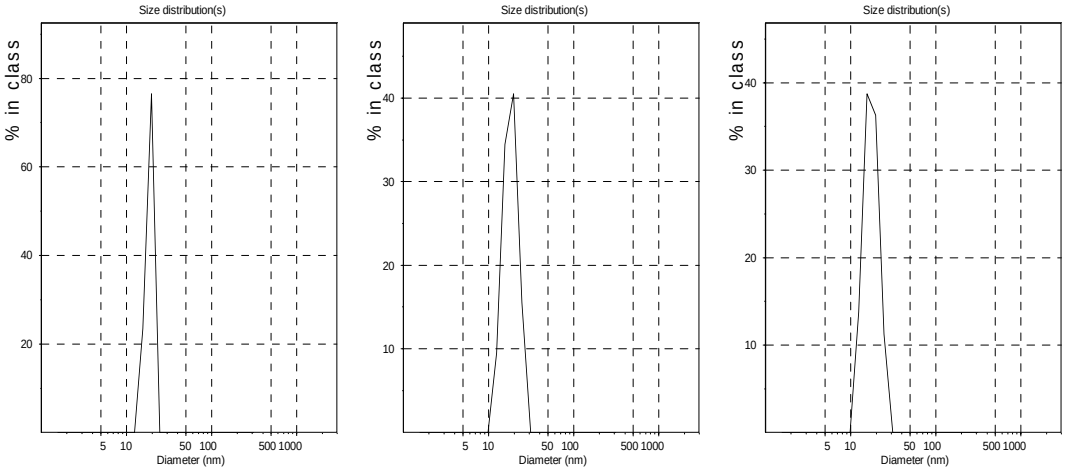

Figure 5.24. Size distributions of (**L15)** at 50^0C based on intensity, volume and number.

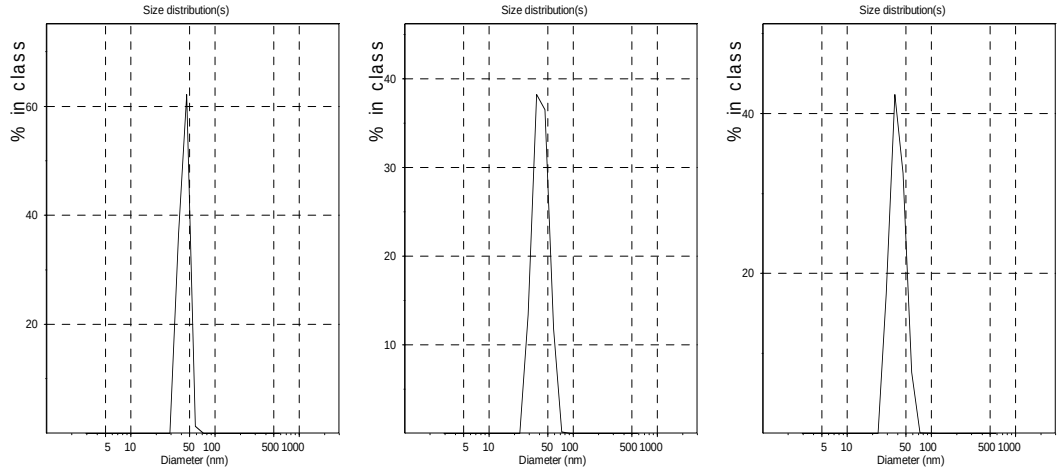

Figure 5.25. Size distributions of (**L17)** at 70^0C based on intensity, volume and number.

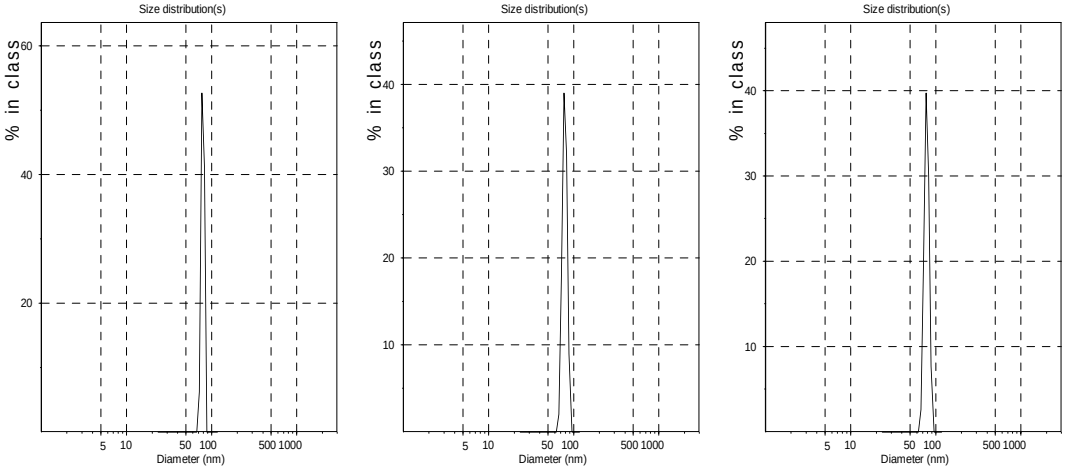

Figure 5.26. Size distributions of (**L20)** at 100^0C based on intensity, volume and number

Table 5.5. Size Distributions of Silica Particles (Effect of Temperature).

Sample	Temperature (^{0}C)	Hydrodynamic Diameter (nm)	Intensity Distribution Peak Means (nm)	Volume Distribution Peak Means (nm)	Number Distribution Peak Means (nm)
L12	20	7.5	5.3± 0.6	5.3±1.3	5.1±1.3
L13	30	10.7	9.6±1.1	9.6±2.2	9.6±2.3
L14	40	15.4	11.2±2.7	12.2±3.3	11.8±3
L15	50	22.1	18.7±2.7	18.4±5.0	17.7±5
L16	60	30.4	31.4±7.0	30.1±8.4	28.7±7.6
L17	70	41.2	42.9±8.4	41.8±11.8	40.2±10.7
L18	80	63.0	63.8±12.5	59.1±11.8	54.5±10.9
L19	90	73.6	75.2±18.0	66.4±17.0	64.0±15.0
L20	100	74.0	78.9±5.3	78.6±6.8	78.2±6.7

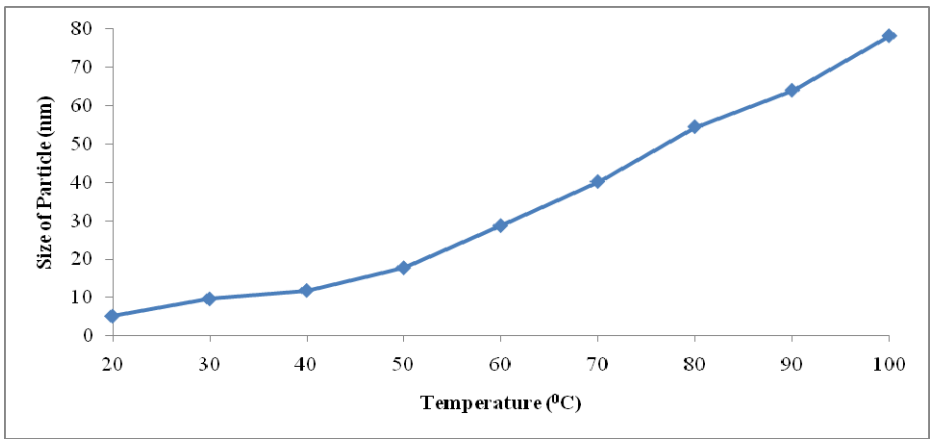

Figure 5.27. The Effect of Temperature on Particle Size.

5.1.2.5. Dye-doped Silica Nanoparticles

Finally, we synthesized dye-doped silica nanoparticles assisted by L-Lysine and investigated the effect of amount of dye on particle size. Firstly, the particle with use of 1 mL (0.1 g RBITC in 0.22 mL APTES) of APTES-RBITC conjugate dye was synthesized (**L21**). The size of synthesized particle was measured by DLS. When we compared the DLS results between **L1** and **L21,** it was observed that there was a significant difference between the particle sizes. Then, the silica particle with use of 100 µL of (0.1 g RBITC in 0.22 mL APTES) APTES-RBITC conjugates dye was synthesized (**L22**). However, the size distributions results of **L21** and **L22** are similar to each other. We synthesized the silica nanoparticles without dye in the presence of

APTES (**L23**) and without APTES in the presence of dye (**L24**) to determine which parameters affect the particle size more. According to DLS results that can be seen in Figure 5.28-5.29, it is verified that the formation of larger particles is led by mainly APTES and in minor by the presence of dye. The size distributions results of **L21**, **L22**, **L23** and **L24** are tabulated in Table 5.6.

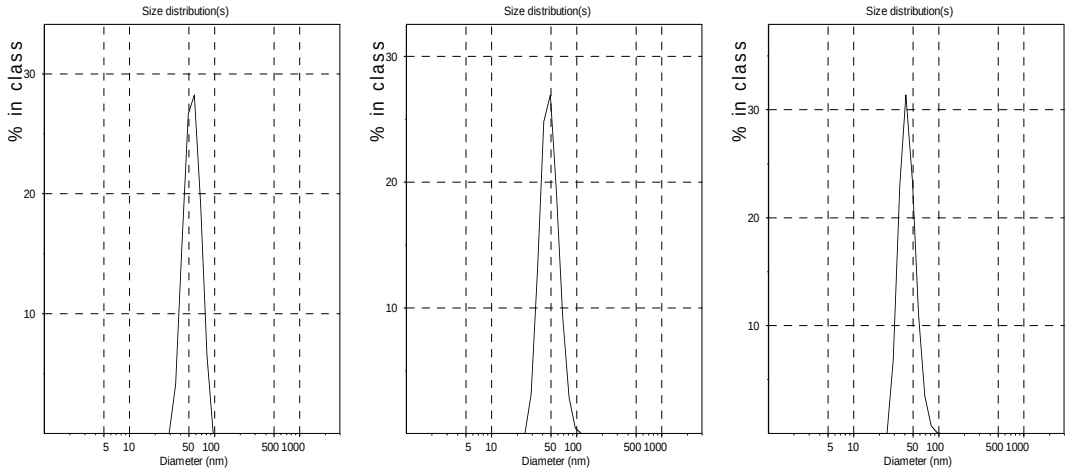

Figure 5.28. Size distributions of (**L21)** based on intensity, volume and number.

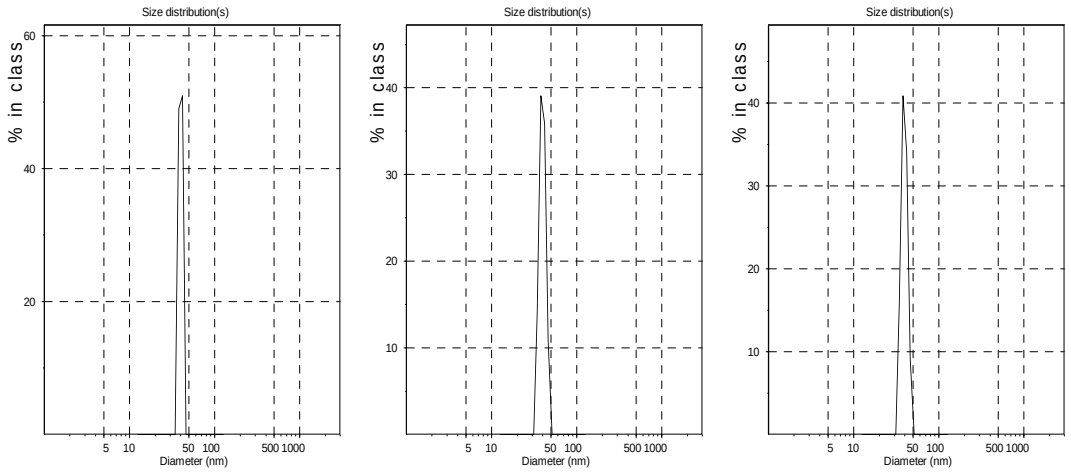

Figure 5.29. Size distributions of (**L22)** based on intensity, volume and number.

Table 5.6. Size distribution values of dye-doped silica nanoparticles.

Sample	Amount of Dye (1.0 mM) in APTES	Hydrodynamic Diameter (nm)	Intensity Distribution Peak Means (nm)	Volume Distribution Peak Means (nm)	Number Distribution Peak Means (nm)
L21	1000 µL	53.8	55.5±18.0	49.1±15	43.8±11.1
L22	100 µL	39.9	40.0±4.0	39.8±4.8	39.5±4.7
L23*	12 µL	93.8	108.9±24	109.8±20.6	77.3±12.5
L24**	0.2 mg	29.5	30.6±7.8	28.2±8.6	25.8±7.6

*** L23** was synthesized by addition of APTES (12 µL).
**** L24** was synthesized by addition of RBITC (0.2 mg in 1mL ethanol).

5.2. XRD Characterization of Silica Particles

The XRD pattern of synthesized silica particles (**S1**) using the general Stöber method revealed the diffraction at 23^0C indicating that the formation of amorph structure of silica as can be shown in Figure 5.30.

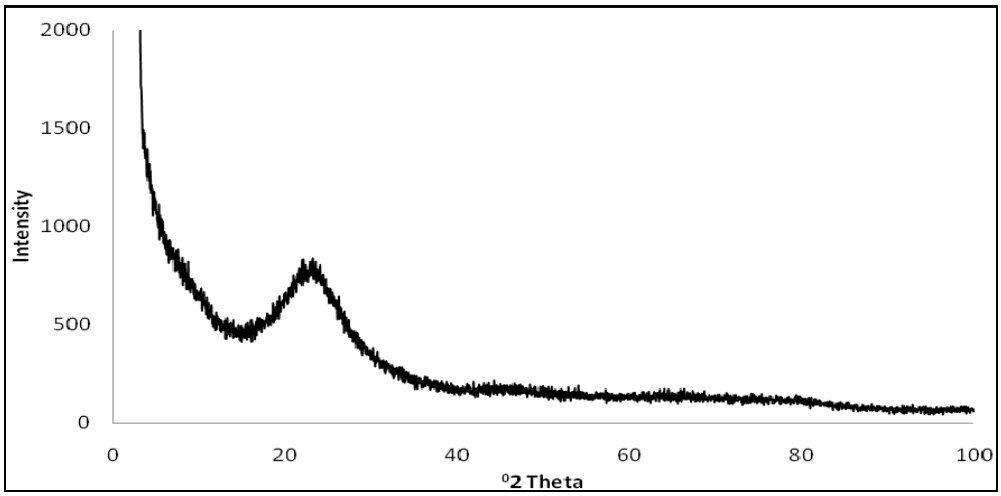

Figure 5.30. XRD Pattern of **S1**.

Figure 5.31 shows the XRD pattern of synthesized silica nanoparticles assisted by L-lysine (**L1**). According to this XRD pattern, the diffraction peaks of the sample are very broad. Because of these broad reflections (220) and (331) at 1.24^0 and 1.44^0 there is a long-range periodicity existing in powder form of silica nanoparticles. The full width at half maximum (FWHM) can be used to determine the crystallite size by using Debye-Scherer equation (Eqn.5-.1);

$$d = K*\lambda / \beta*\cos(\Theta) \quad (5.1)$$

where K is the shape factor, λ is the x-ray wavelength, typically 1.54 Å, β is the line broadening at half maximum intensity (FWHM) and Θ is the Bragg angle. The dimensionless shape factor has a typical value of about 0.9, but varies with the actual shape of the crystallite.

The orientation of a surface or a crystal plane may be defined by considering how the plane (or indeed any parallel plane) intersects the main crystallographic axes of the solid. The application of a set of rules leads to the assignment of the Miller Indices , (*hkl*) ; a set of numbers which quantify the intercepts and thus may be used to uniquely identify the plane or surface.

Table 5.7. Crystal Size of silica particles assisted by L-Lysine (**L1**)

^{0}2 Theta	**d/ nm**	**hkl**
1.24	11	220
1.44	9.6	331

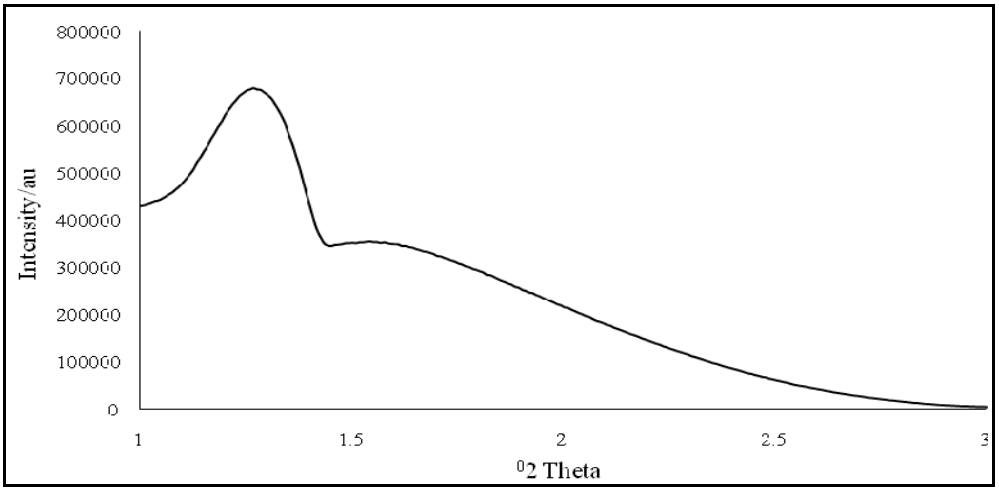

Figure 5.31. XRD Pattern of **L1**

5.3. Scanning Electron Microscopy (SEM) of Silica Particles

5.3.1. Silica Particles Synthesized by Stöber Method

SEM was conducted to observe the effect of ammonia, TEOS and water on the morphology and structure of the synthesized silica nanoparticles. Size of silica nanoparticles were evaluated as well.

5.3.1.1. Effect of Amount of Ammonia

The SEM images of silica nanoparticles prepared at different amount of ammonia are shown in Figure 5.32. It is observed that the maximum particle size obtained depended strongly on the ammonia concentration and we are able to obtain silica nanoparticles of 30nm-250nm in diameter, by controlling the amount of ammonia. These particles were monodisperse. These images represent the **S1**, **S2** and **S3** samples.

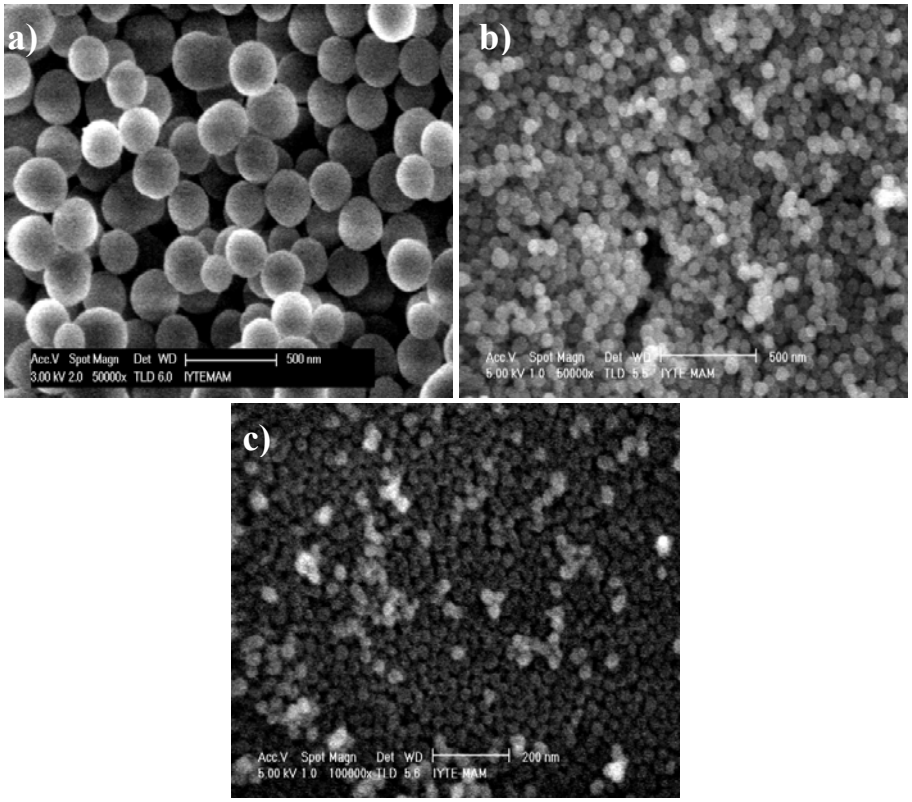

Figure 5.32. SEM images of a) **S1**, b) **S2**, and c) **S3**.

5.3.1.2. Effect of Amount of TEOS

As the amount of TEOS is increased, the silica nanoparticles ranging from 18nm to 150nm in diameter are formed that can be seen in Figure 5.33. It is observed that amount of TEOS is also important to control the size of the silica nanoparticles. These images represent the **S9**, **S10**, **S1**1and **S12** samples.

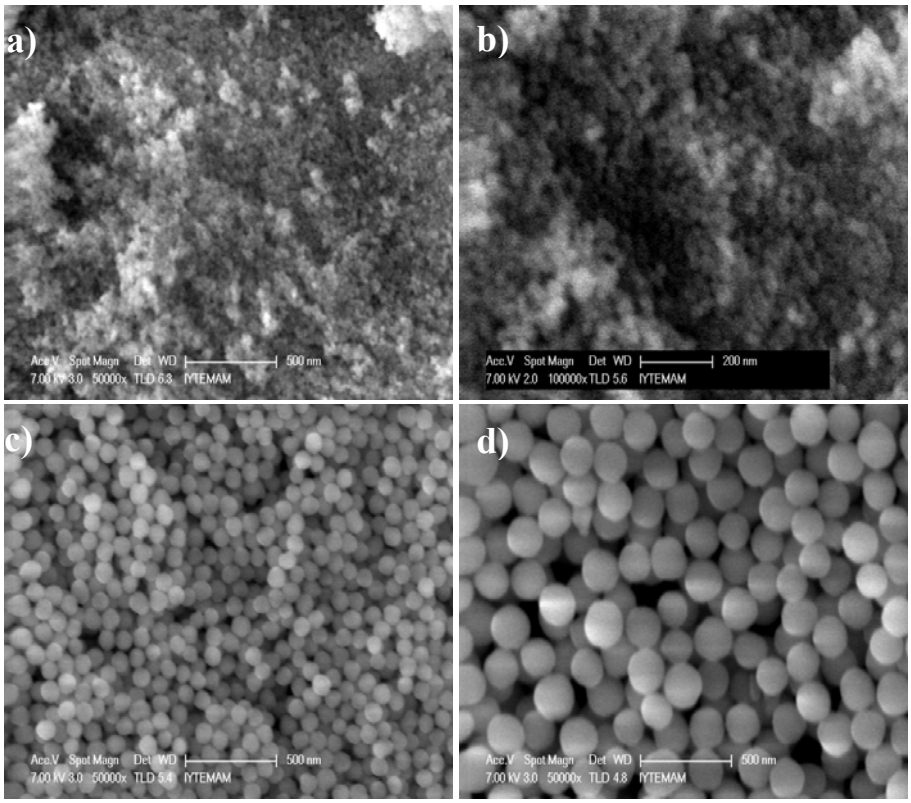

Figure 5.33. SEM images of a) **S9**, b) **S10**, c) **S11** and d) **S12**.

We also applied some purification process on particle size. The silica particles (**S13**) with a size around 500 nm was synthesized and then washed with water-ethanol mixture and centrifuged. This step repeated 2 times. According to SEM images, we observed that the particles are not washed showing a well-ordered array, while the particles are washed showing a disordered arrangement with the same size of the other particles that are washed. Because washing with water-ethanol mixture decreases the pH of the medium, this cause the weaker H-bonding and it is resulted of this disordered arrangement occurs.

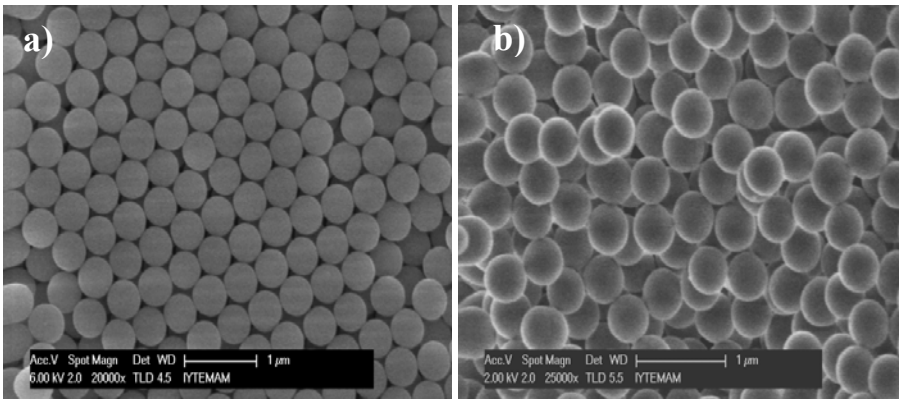

Figure 5.34. SEM images of **S13** that a) were not washed, b) were washed.

5.3.2. Synthesis of Silica Nanoparticles Assisted by Amino Acids

SEM was used to observe the effect of amino acids, amount of L-lysine and temperature on the morphology and structure of the synthesized silica nanoparticles. Size of silica nanoparticles were evaluated as well.

5.3.2.1. Effect of Type of Amino Acids

The SEM images of silica nanoparticles assisted with L-lysine, L-arginine and ammonia were taken. According to these images that can be shown in Figure 5.35, we observe the size differences between these synthesized silica nanoparticles. The differences between L1, A1 and N1 are caused by the basicity that higher basicity results the well-ordered arrangement silica nanoparticles. These images represent the **L1**, **A1** and **N1** samples.

5.3.2.2. Effect of Amount of L-Lysine

As we investigated the effect of amount of L-lysine on the morphology and structure of silica nanoparticles, SEM images were taken that can be seen in Figure 5.36. According to these images, it is observed that the particle size increases with the increasing amount of L-lysine in the range of 0.1 mmol- 4.0 mmol. Also we realized that the increase in the amount of L-lysine results the highly covered silica nanoparticles

with Lysine molecules, as can be seen in SEM images. These images represent L2, L3, L4, L5 and L6 samples.

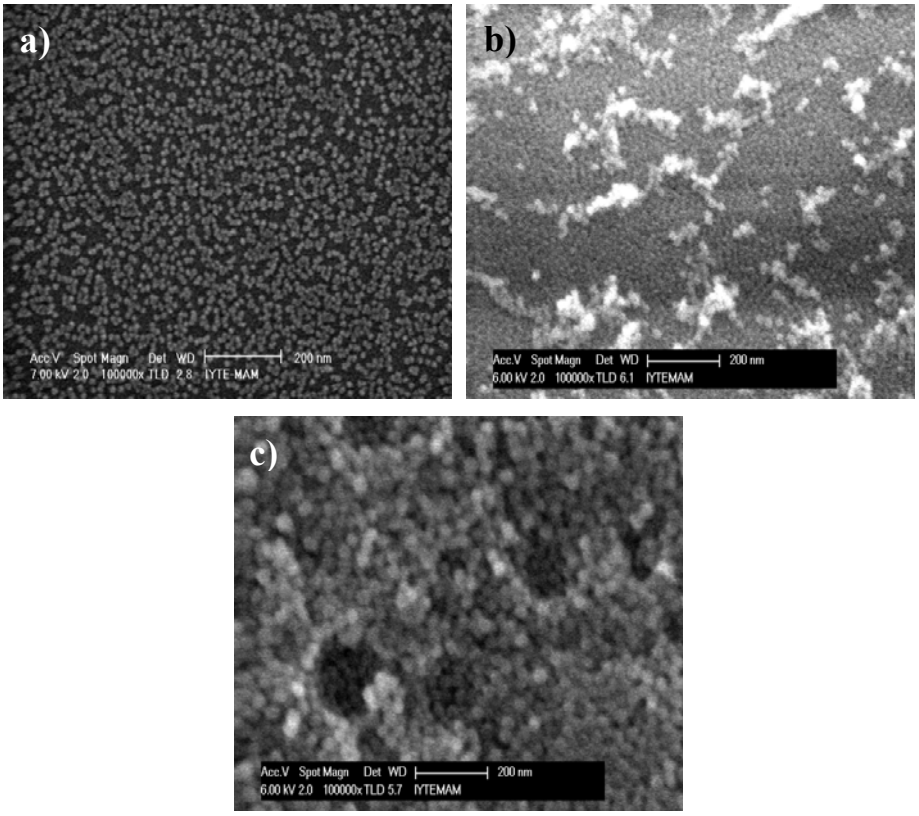

Figure 5.35. SEM images of a) **L1**, b) **A1** and c) **N1**.

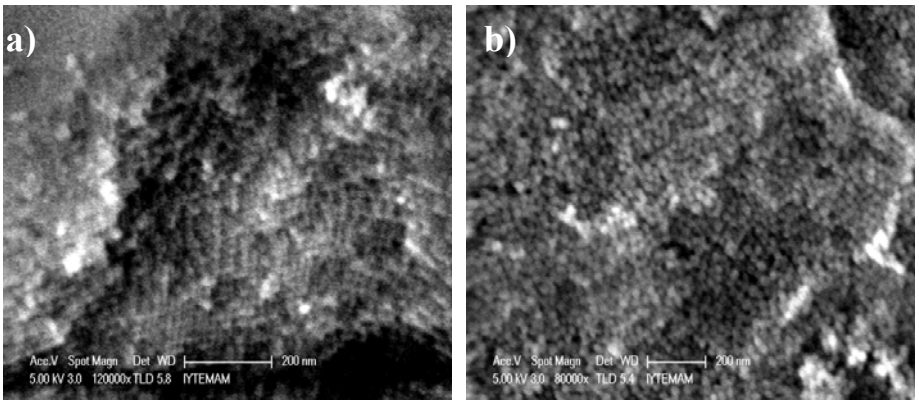

Figure 5.36. SEM images of a) **L2**, b) **L3**, c) **L4**, d) **L5** and e) **L6**

(**cont. on next page**)

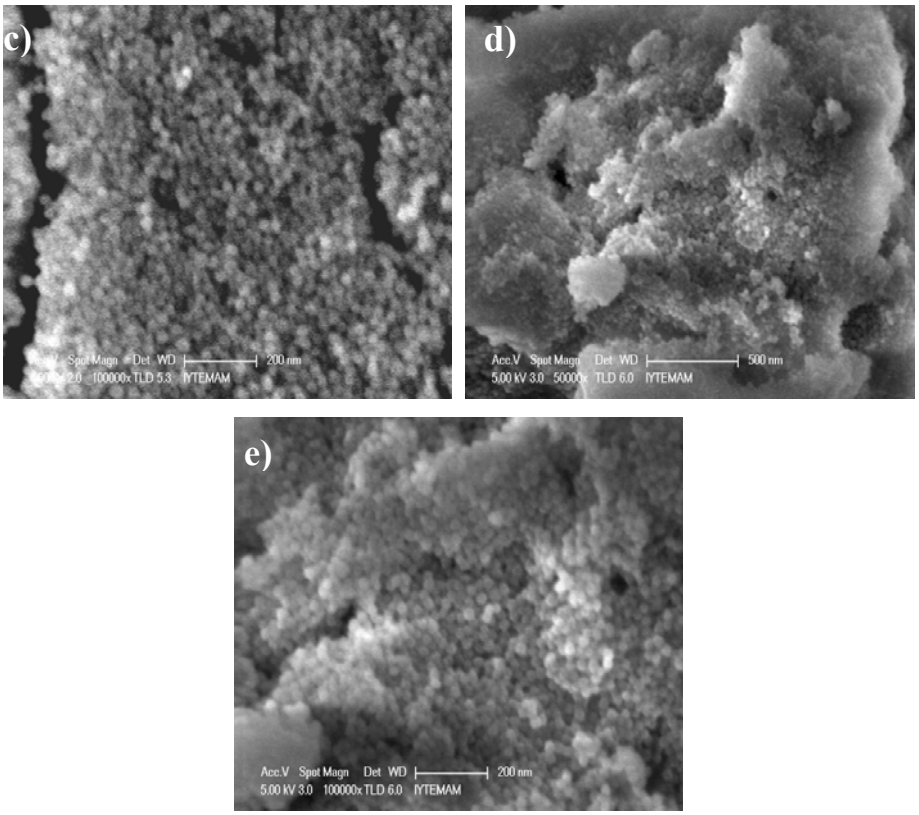

Figure 5.36. (**cont.**) SEM images of a) **L2**, b) **L3**, c) **L4**, d) **L5**, and e) **L6**

5.3.2.3. The effect of Amount of Dye

We also investigated the effect of dye on particle size and structure. The SEM images of dye-doped silica nanoparticles assisted by L-lysine were taken that can be seen in Figure 5.37. According to SEM images, there is no a significant differences between **L21** (1 mL dye was used) and **L22** (100 µL dye was used). However, there is a main difference of particle size between **L1** and **L21** (dye-doped particles) that is about 30nm. However, it is observed that the difference of particle size is resulted by the presence of APTES (major) and dye (minor) as mentioned in the measurement of particle size part.

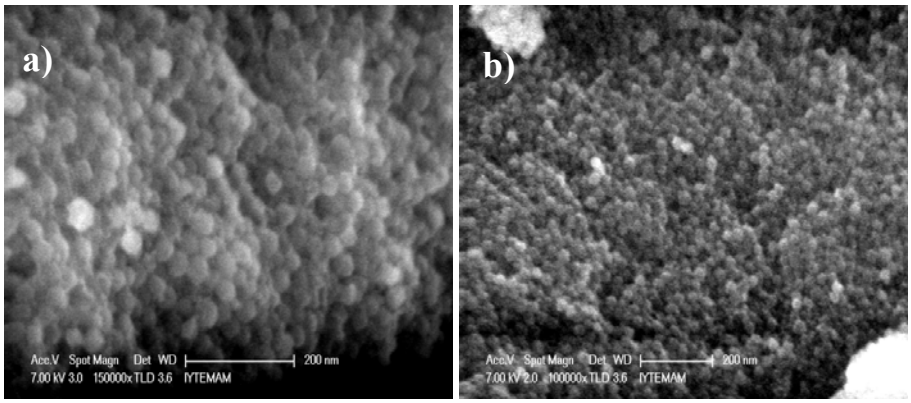

Figure 5.37. SEM images a) **L21** and b) **L22**.

5.4. Transmission Electron Microscopy (TEM) of Silica Particles

Size and morphology of silica nanoparticles can be determined easily by using transmission electron microscopy (TEM). This technique provideS information about the structural characteristics of silica nanoparticles. However, TEM gives information only about a small part of substance.

TEM grids were prepared by dropping diluted dispersions of L12 to observe size and structures of the nanoparticles. The particle size for L12 is determined to be 5.0 nm. The particles indicate almost same monodispersity (Figure 5.38).

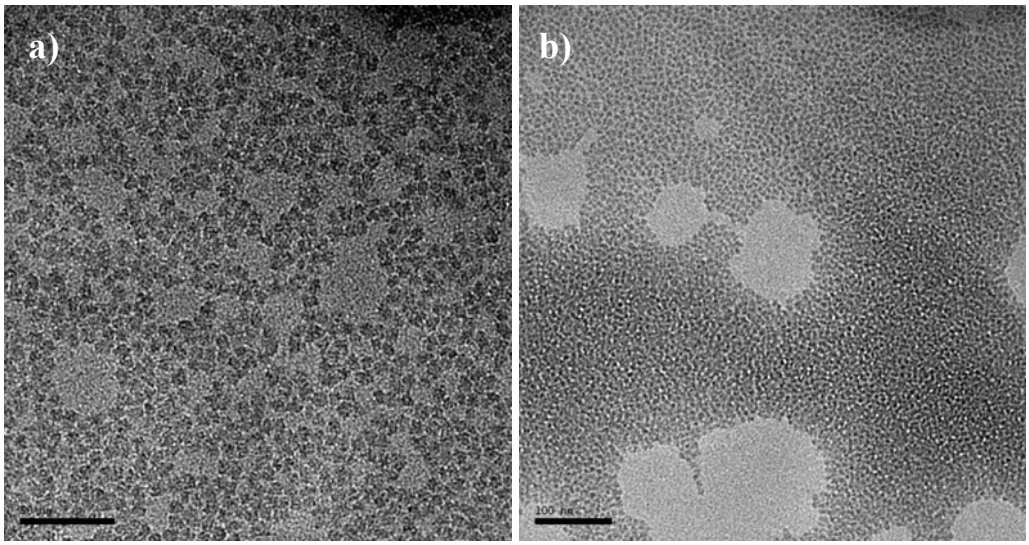

Figure 5.38. TEM images of **L12** (Scales are a)50nm and b)100nm)

5.5. Thermal Gravimetric Analysis (TGA) Characterization

The result of the thermal analysis of silica nanoparticles assisted by L-lysine is given in Figure 5.39 that shows the percent weight loss of silica particles with increase in temperature.

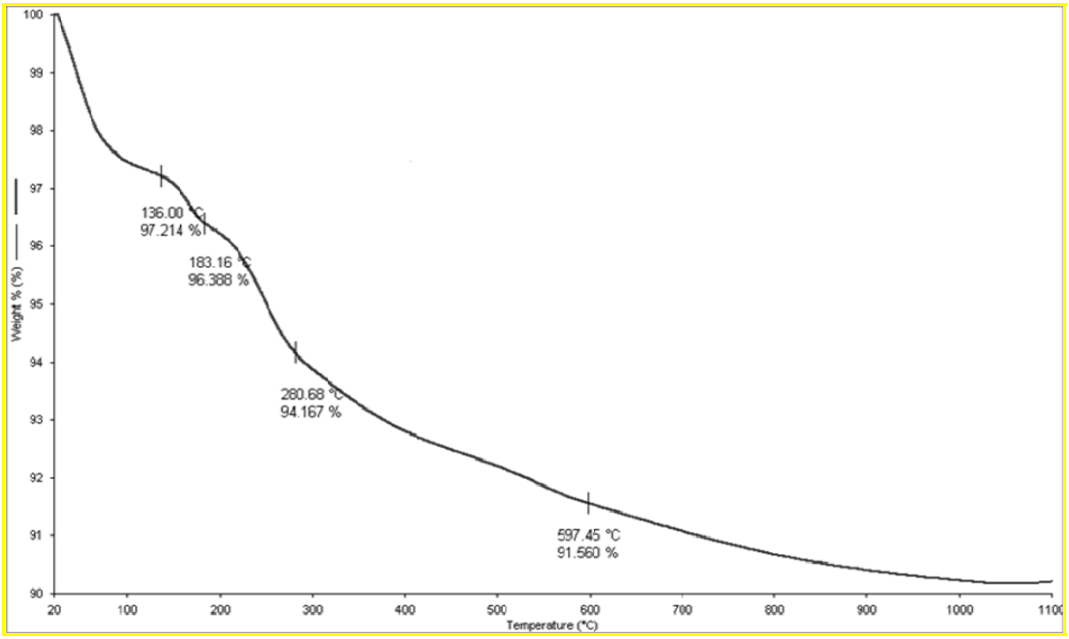

Figure 5.39. TGA curve of **L1**

According the TGA curves of L1, from the room temperature to 120^0C, the most of the weight losses were observed from the physical water removal. Actually the weight loss from the room temperature to 270^0C may be due to the removal of chemically bond water. The weight loss which occurs at about 135^0C was observed due to the octane removal. Also at about 180^0C, the removal of TEOS was observed and around 250^0C, the L-lysine was removed. In addition, we observed a gradual weight loss up to 1000^0C

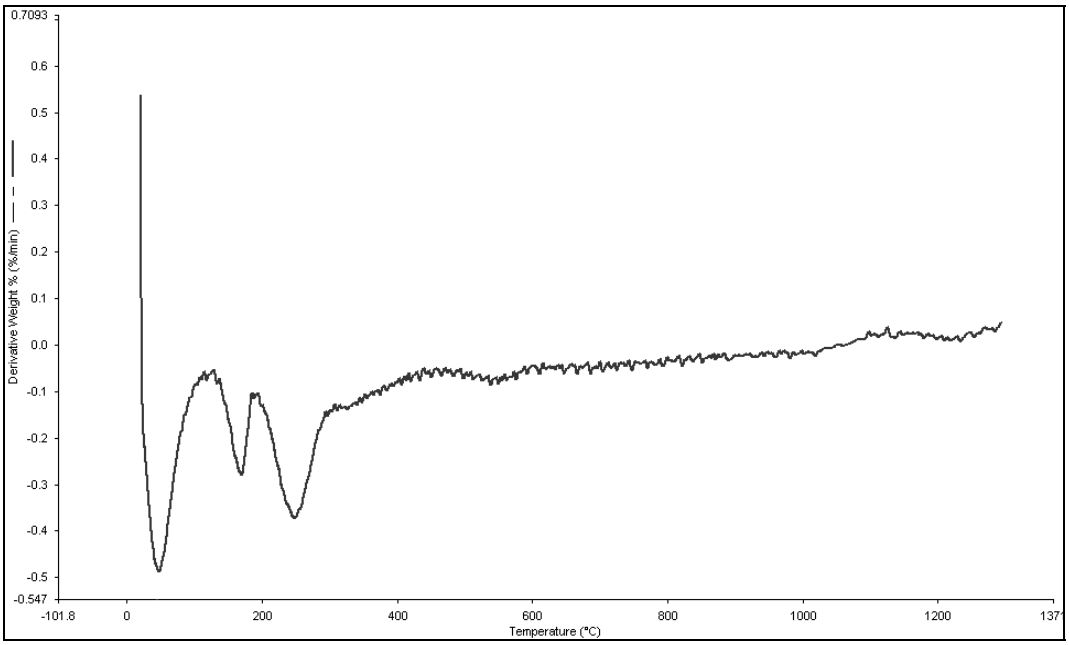

Figure 5.40. Derivative of TGA curve of **L1**

We also observed the weight loss from the derivative thermogravimetry (Derivative of TGA) curve as can be seen in Figure 5.40. This curve shows three separate steps occur in the range of 50^0C- 250^0C all probably due to the removal of water, octane and TEOS in different ways, respectively.

5.6. FTIR Analysis

The FTIR spectra of synthesized silica particles assisted by L-lysine, L-arginine and in the presence of ammonia are given in Figure 5.41.

Generally, silanol and silicon alkoxides groups appear in the range from 1400cm^{-1} to 400cm^{-1}. According to spectra, we observed the band at 800cm^{-1} which is attributed to silicon alkoxides (Si-O-Si stretching) and the band at 940cm^{-1} which is attributed to the bending modes of Si-O-H and Si-O. Moreover, the peak is observed at 1050cm^{-1} that may represents both the C-O/C-N and Si-O-Si bonding. We also observed the other important infrared vibrations of silica that are the band at: 1250-1020cm^{-1} which is attributed to asymmetric stretching of Si-O-Si and at 3400-3500 cm^{-1} which is belongs to stretching of Si-OH.

In the FTIR spectrum of silica nanoparticles assisted by L-Lysine, a double peak is observed in the range of 2800-3200 cm^{-1} which is attributed to stretching mode of NH

bonding that belongs to Lysine. Due to the broad band in the range 2800-3600cm^{-1} is attributed to the stretching modes of hydroxyl groups and molecular water; we are not able to observe the NH band clearly in the range of for the silica nanoparticles assisted by L-Arginine. Also the band with lower intensity in the range 1600-1700 cm^{-1} is attributed NH band (bending) at 1650- 1700 cm^{-1} which is hard to identify because it is too close C=O band at 1550-1700 cm^{-1}.

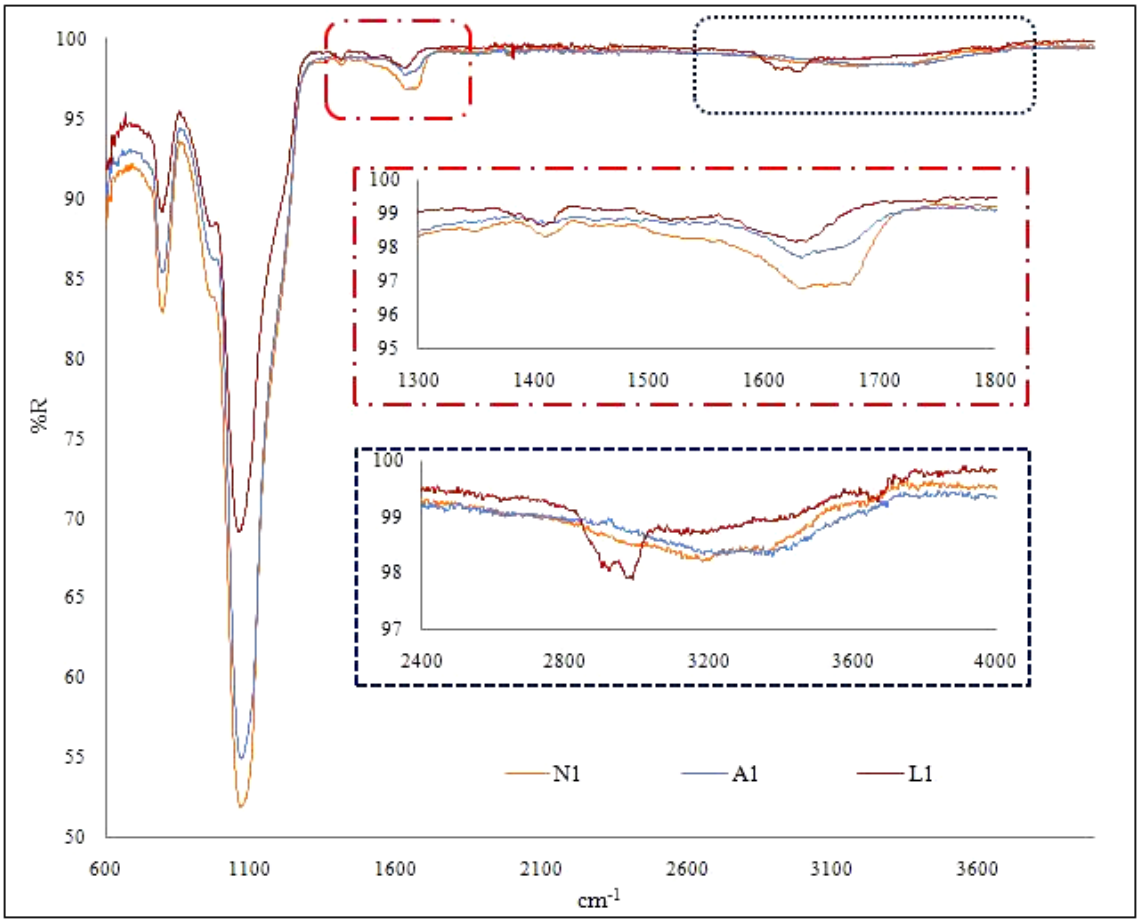

Figure 5.41. FTIR Spectra of **N1**, **A1** and **L1**

5.7. Spectroscopic Methods

The fluorescence and absorption spectra of the dye-doped silica nanoparticles were recorded by UV-visible and fluorescence spectrophotometer, respectively. The fluorescent dye-doped silica nanoparticles are characterized with respect to amount of dye, dialysis and centrifuge processes. Figures 5.42-43 shows the representative

absorption spectra of dye (RBITC-APTES) with 100(0.01mM) and 1000(0.001mM) times of diluted from the stock solution, respectively. The absorption maximum is found to be at 541 nm. The emission maximum is found to be at 568nm (excitation wavelength = 530nm).

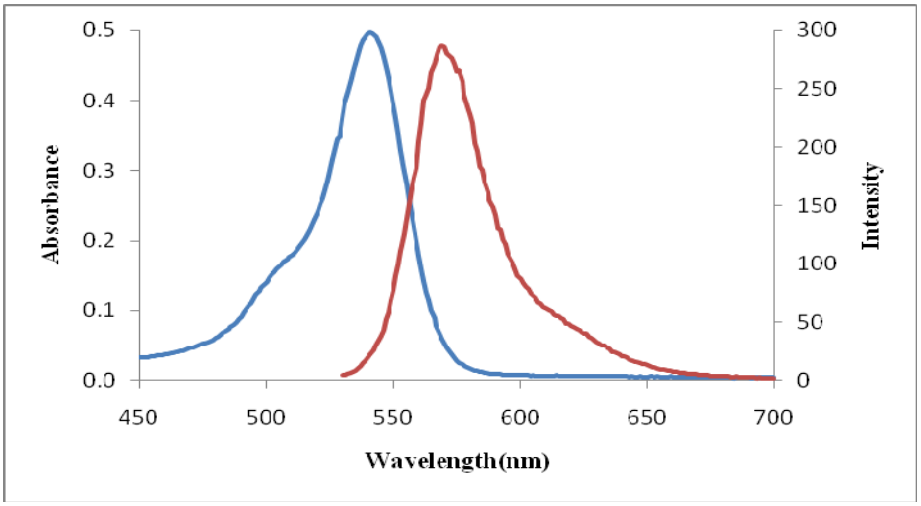

Figure 5.42. Absorption and fluorescence spectra of 10.0 µM RBITC-APTES.

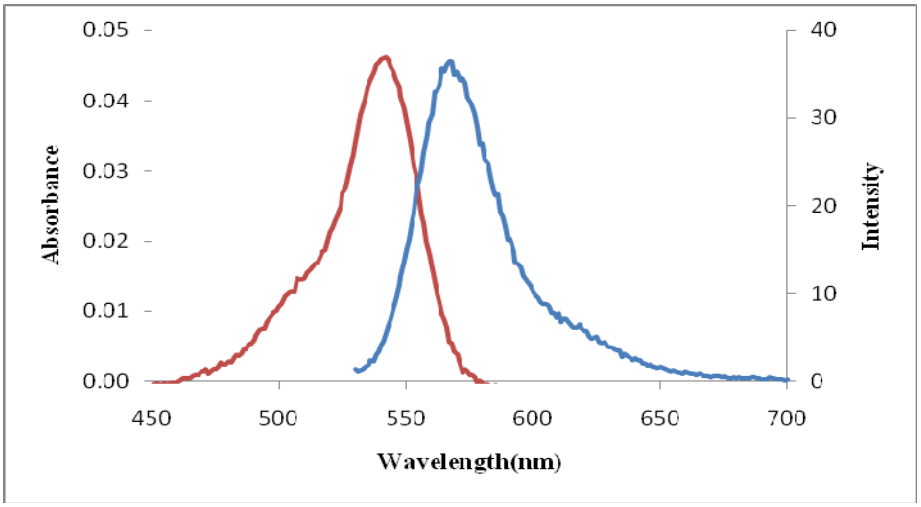

Figure 5.43. Absorption and fluorescence spectra of 1.0 µM RBITC-APTES.

As can be shown in Figures 5.44-47, the absorption and fluorescence spectra of dye-doped silica nanoparticles assisted by L-lysine (**L21-L22**) are taken. The medium of silica nanoparticles is water; however the medium of dye is ethanol. According to

both spectra, we observed strong peaks around 540nm and 570nm. However, the solvent effects, shift of absorbance and emission maxima are observed.

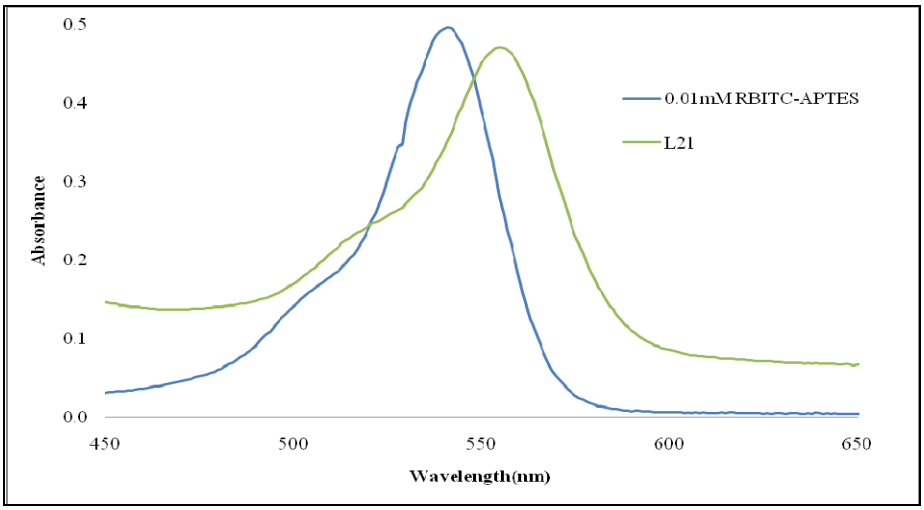

Figure 5.44. Absorption spectra of **10.0 µM RBITC-APTES** and **L21**.

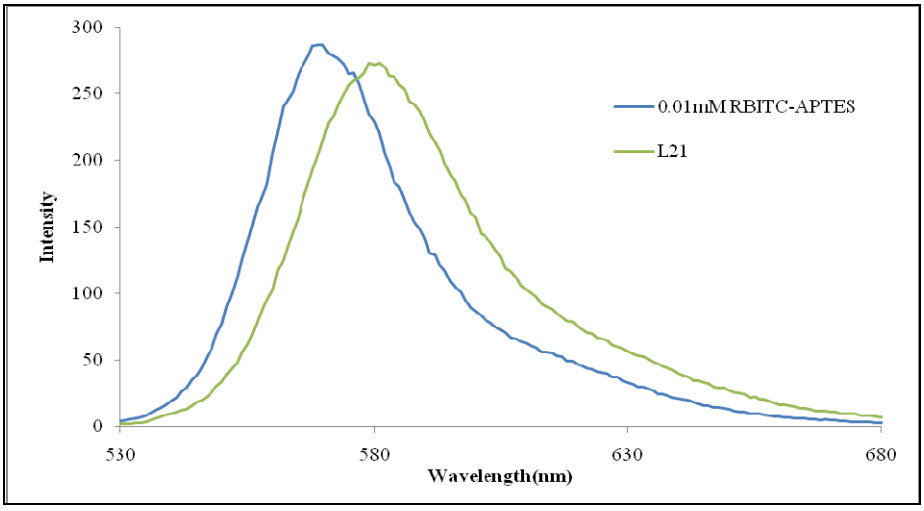

Figure 5.45. Fluorescence spectra of **10.0 µM RBITC-APTES** and **L21**.

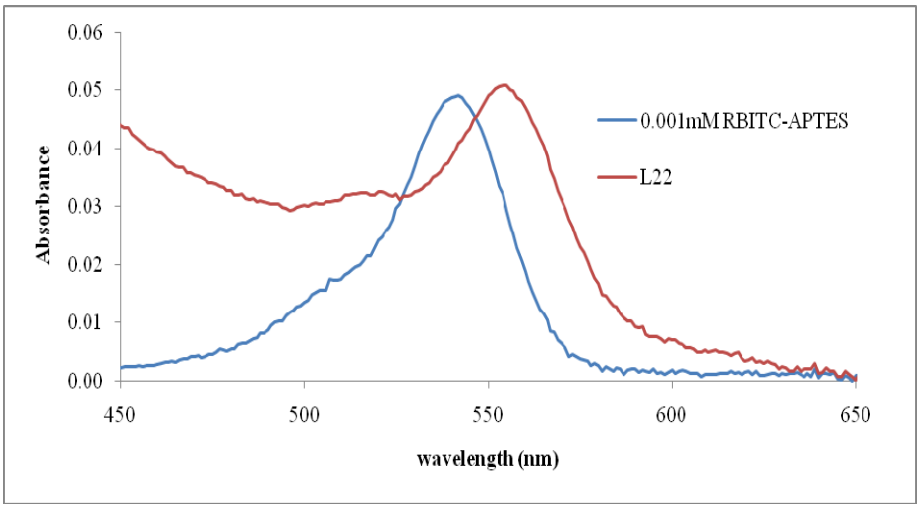

Figure 5.46. Absorption spectra of **1.0 µM RBITC-APTES** and **L22**.

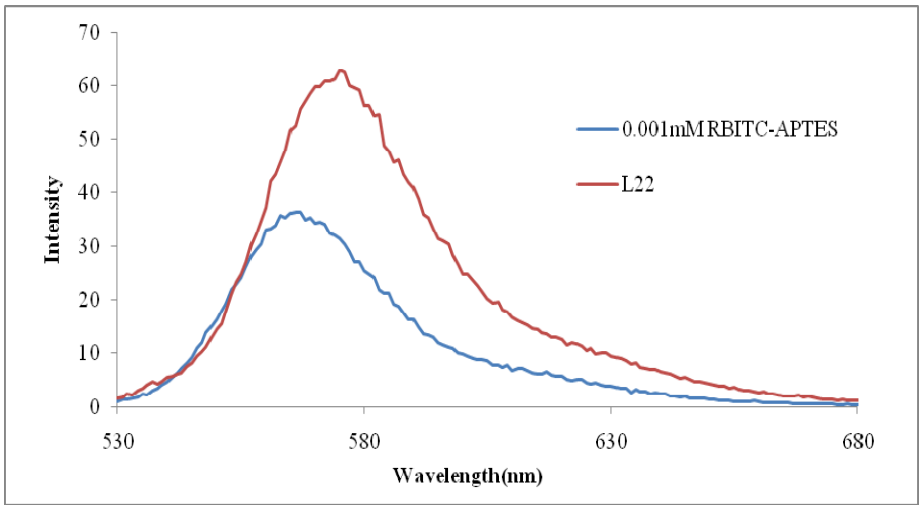

Figure 5.47. Fluorescence spectra of **1.0 µM RBITC-APTES** and **L22**.

After the synthesis of dye-doped silica nanoparticles assisted by L-lysine, we obtained silica powders applying the evaporation process. Although RBITC is covalently attached to APTES silane compound to dope into silica particles by a stable thiourea linkage, dye may be localized on the particle surface. Therefore, we used two purification methods to remove the unreacted RBITC from the particles. In first process, obtained silica powders were dispersed into ethanol water mixture to remove the unreacted RBITC. This process was repeated 5 times.

The absorption and fluorescence spectra were taken from supernatant of each these centrifugation steps. After the first centrifugation of **L21** sample, the supernatant

had a strong purple color, indicating that a significant fraction of the RBITC had not been incorporated into the silica particles. Also it is caused by using higher amount of RBITC-APTES **(1mL)** during the synthesis. After the fifth centrifugation, no color change is observed. On the other hand, the centrifugation of **L22** sample, there is no any significant color change observed between the centrifugation steps. It may be caused by using lower amount of RBITC-APTES **(100µL)** in the synthesis of the silica particles. These results can be seen in Figures 5.48-51 in both absorption and fluorescence spectra of dye-doped silica nanoparticles.

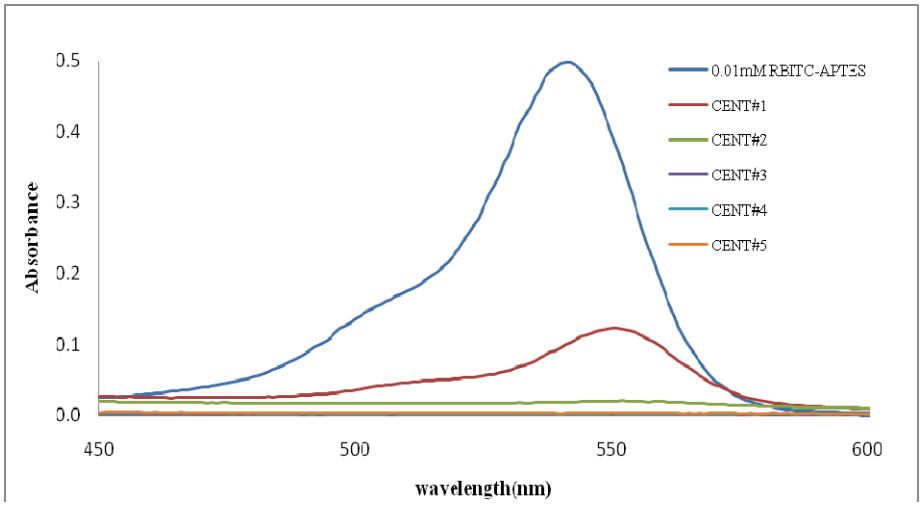

Figure 5.48. Absorption spectra of (**L21**) during the centrifuge process.

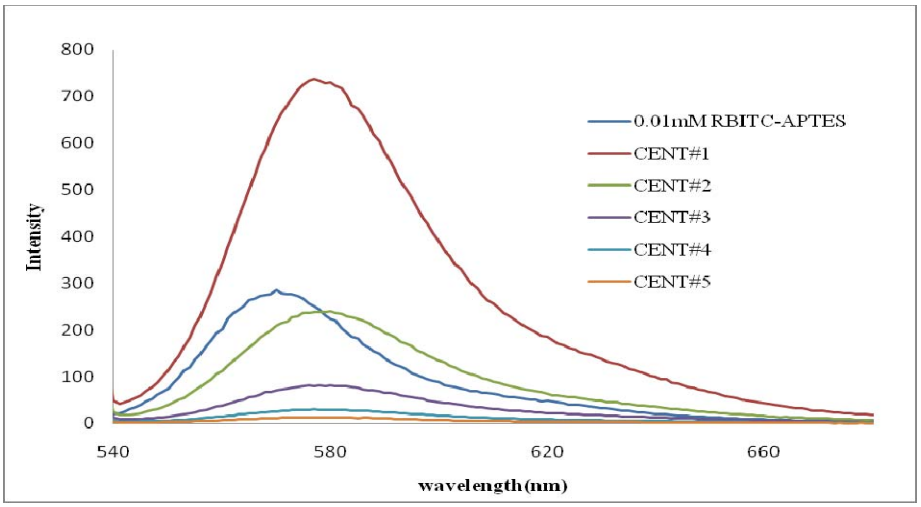

Figure 5.49. Fluorescence spectra of (**L21**) during the centrifuge process.

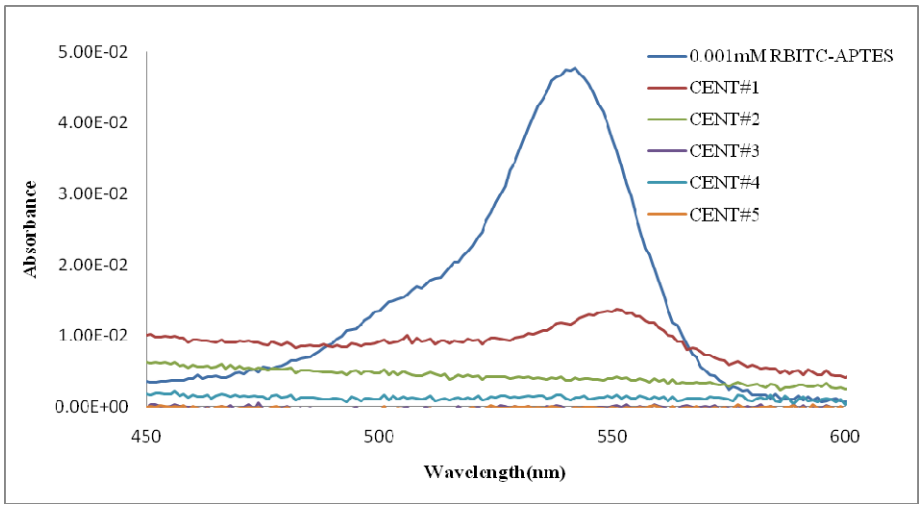

Figure 5.50. Absorption spectra of (**L22**) during the centrifuge process.

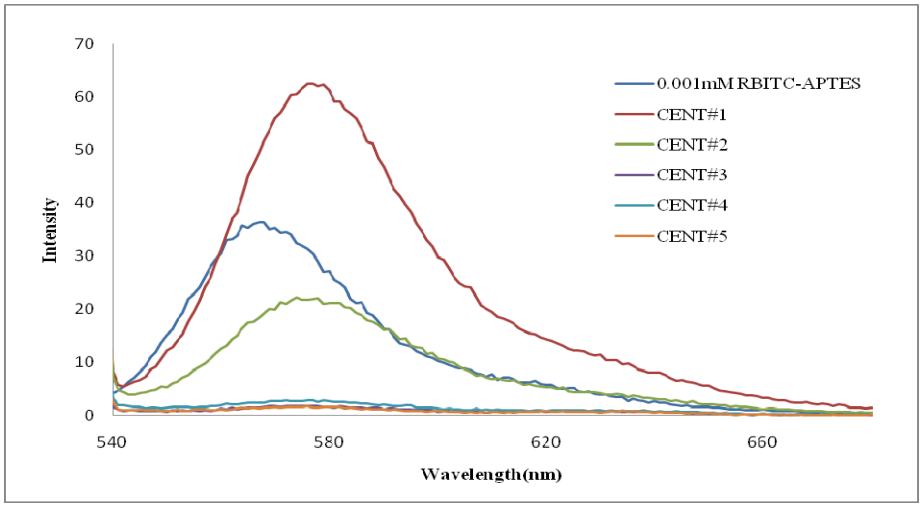

Figure 5.51. Fluorescence spectra of (**L22**) during the centrifuge.

We also used the second method to be sure the removal of unreacted RBITC from the particles. In this process, dialysis membrane was used to separate and remove the unreacted dye molecules from the silica particles. Thus, it is available in a range of molecular weight cut offs 500 Daltons from the particles. This dialysis process took 24 hours for each **L21** and **L22** samples. Every two hours, fluorescence spectrum of medium was taken to control the release of the RBITC-APTES from the sample in the dialysis tube.

As can be seen in Figures 5.52-53, we observed that after the dialysis, the significant amount of dye was removed from the **L21** sample. This may be due to using

higher amount of dye, thus there are lots of non-binding dye molecules in sample and during the dialysis, these unreacted dye molecules were removed easily from the sample. On the other hand, the release of dye molecules from the **L22** sample is much lower than the **L21** due to the use of lower amount of dye.

According to these purification process, we observed that using lower amount of dye is better than the higher amount of dye.

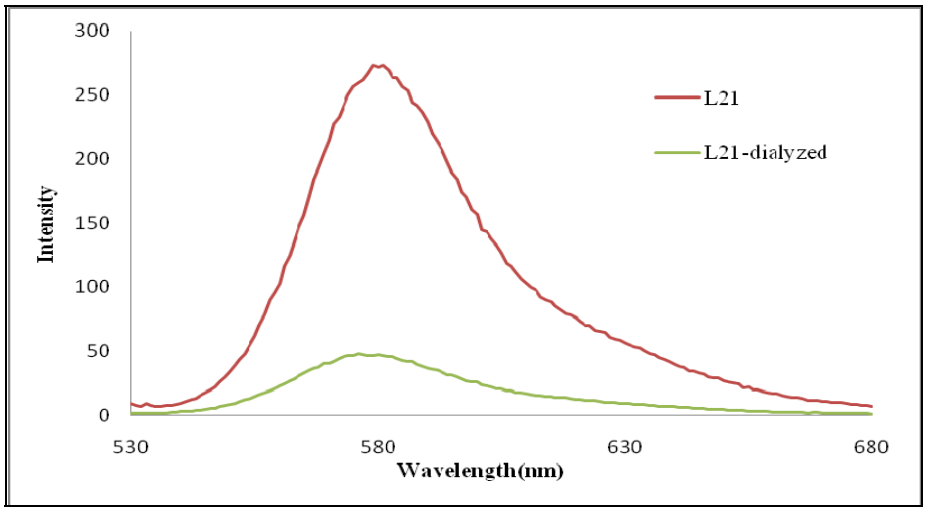

Figure 5.52. Fluorescence spectra of dye-doped and dialyzed (**L21**) sample.

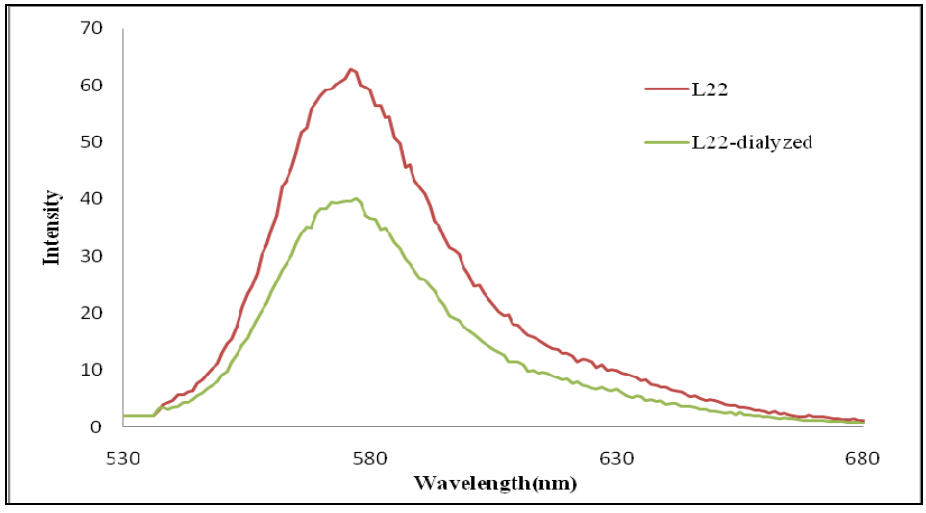

Figure 5.53. Fluorescence spectra of dye-doped and dialyzed (**L22**) sample.

5.8. Cytotoxic Evaluating

Cytotoxicity was evaluated by determining cell viability using MTT assay on MCF-7(human breast cancer cell lines) and PC-3(human prostate cancer cell lines) cell lines. By applying the MTT test, we examined the effect of size of silica nanoparticles which were synthesized in the presence of ammonia, amino acids and RBITC-APTES conjugate.

Firstly, we examined the effect of size of synthesized silica nanoparticles (in the presence of ammonia) on MCF-7 and PC-3 cells viability. Silica particles with a size of 10nm, 50nm and 500nm were dispersed in PBS at 5000µg/mL, 1000 µg/mL, 500 µg/mL, 100 µg/mL, 10 µg/mL, 1.0 µg/mL, and 0.1µg/mL and then exposed to cells. Cells were exposed 72 hours to silica nanoparticles. Each 24 hours, absorbance was measured at 540nm/570nm. Each measurement was repeated 3 times (triplicate).

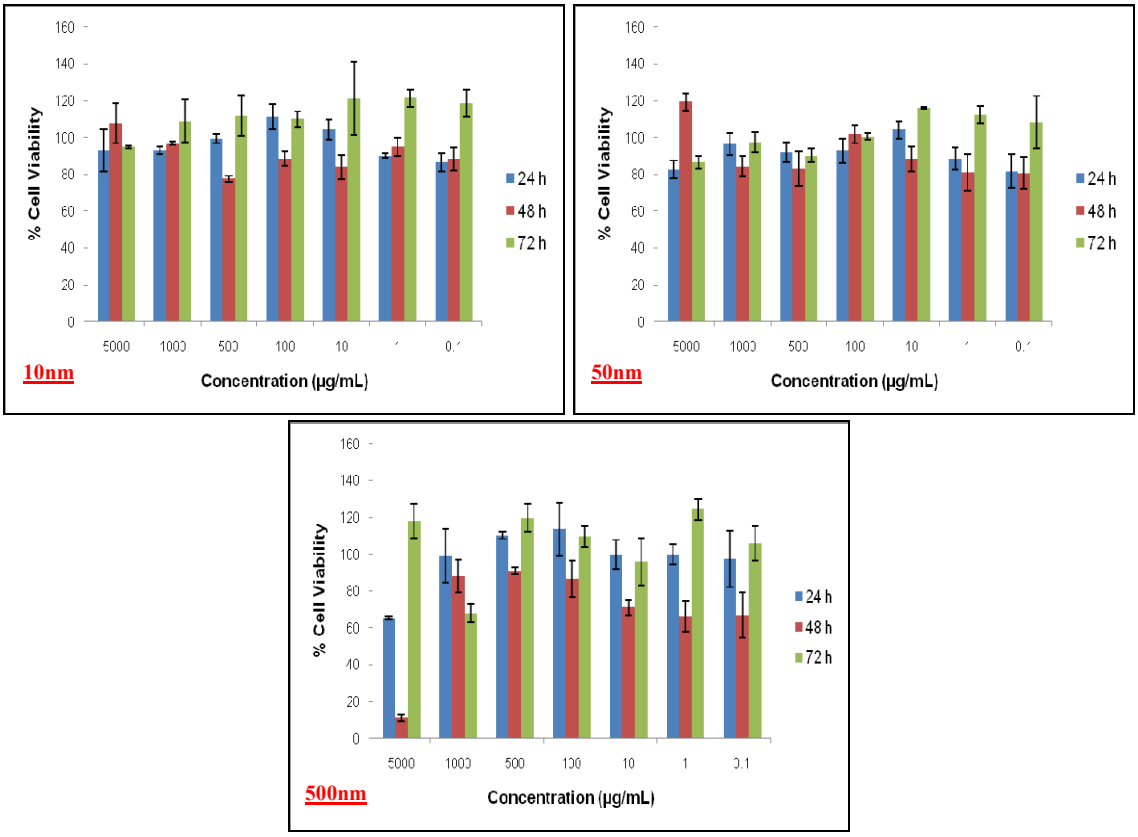

Figure 5.54. Viability of MCF-7 cells after 72-h exposure to silica nanoparticles with a size of **10nm**, **50nm** and **500nm**.

Figure 5.54-55 represent the MTT results of synthesized silica nanoparticles. According to these results, we observed that silica nanoparticles with a size of 10nm and 50nm do not show any significant toxic effect on both MCF-7 and PC-3 cells in the concentration range of 5000µg/mL to 0.1µg/mL.

On the other hand, silica nanoparticles with a size of 500nm shows toxic effect on MCF-7 cells above the concentration of 1000µg/mL and also have toxic effect on PC-3 cells above the concentration of 100µg/mL.

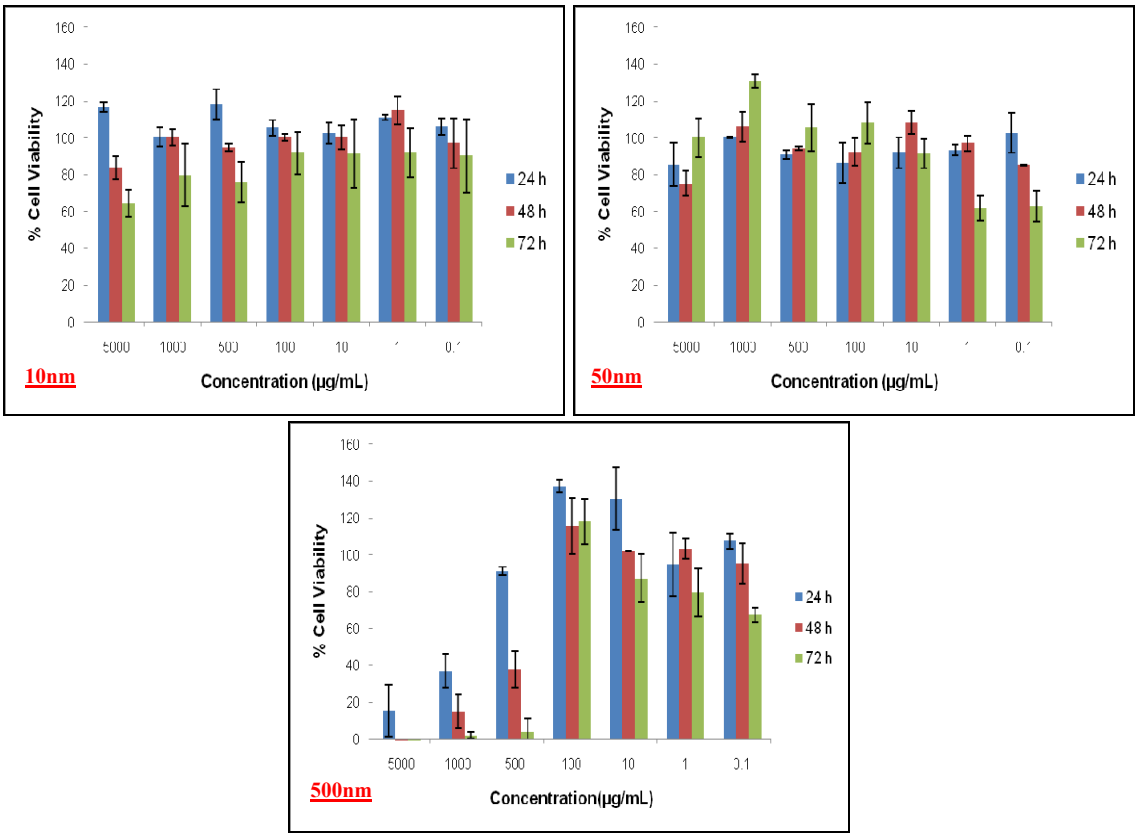

Figure 5.55. Viability of PC-3 cells after 72-h exposure to silica nanoparticles with a size of **10nm**, **50nm** and **500nm**.

We also applied MTT test on silica nanoparticles assisted by L-lysine to evaluate cytotoxicity in MCF-7 and PC-3 cells. First, silica particles with a size of 10nm, 40nm and 80nm were dispersed in PBS at 5000µg/mL, 1000 µg/mL, 500 µg/mL, 100 µg/mL, 10 µg/mL, 1.0 µg/mL, and 0.1µg/mL and then exposed to cells. Cells were exposed 72 hours to silica nanoparticles. Each 24 hours, absorbance was measured at 540nm/570nm. Each measurement was repeated 3 times (triplicate).

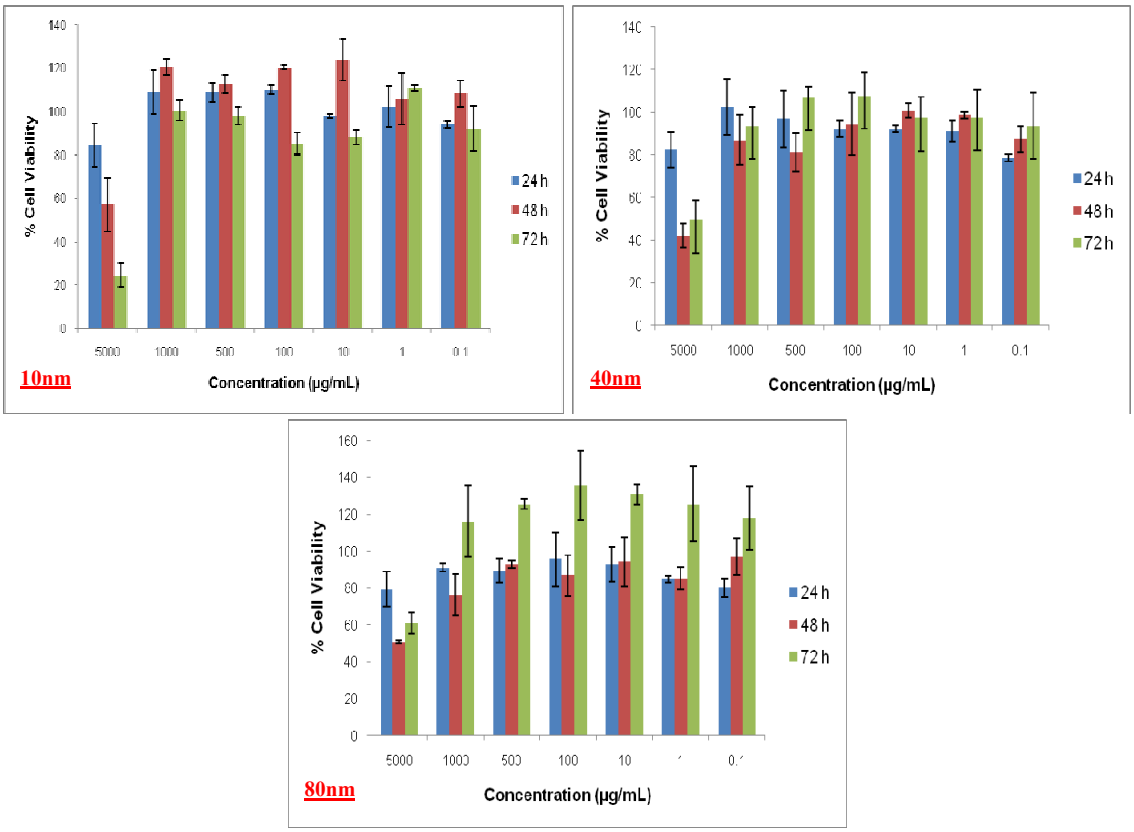

Figure 5.56. Viability of MCF-7 cells after 72-h exposure to silica nanoparticles with a size of **10nm**, **40nm** and **80nm**.

As can be seen in Figure 5.56, we observed that synthesized silica nanoparticles with a size of 10nm, 40nm and 80nm have no any significant toxic effect on MCF-7 cells below the concentration range of 1000µg/mL. Besides, these particles (10nm, 40nm and 80nm) show the toxic effect in the concentration of 5000µg/mL.

On the other hand, when these synthesized silica nanoparticles assisted by L-lysine were exposed to PC-3 cells, there was no any significant toxic effect observed in the both size of 10nm, 40nm and 80nm of particles on PC-3 cells in the range of 1000µg/mL to 0.1µg/mL that can be seen in Figure 5.57.

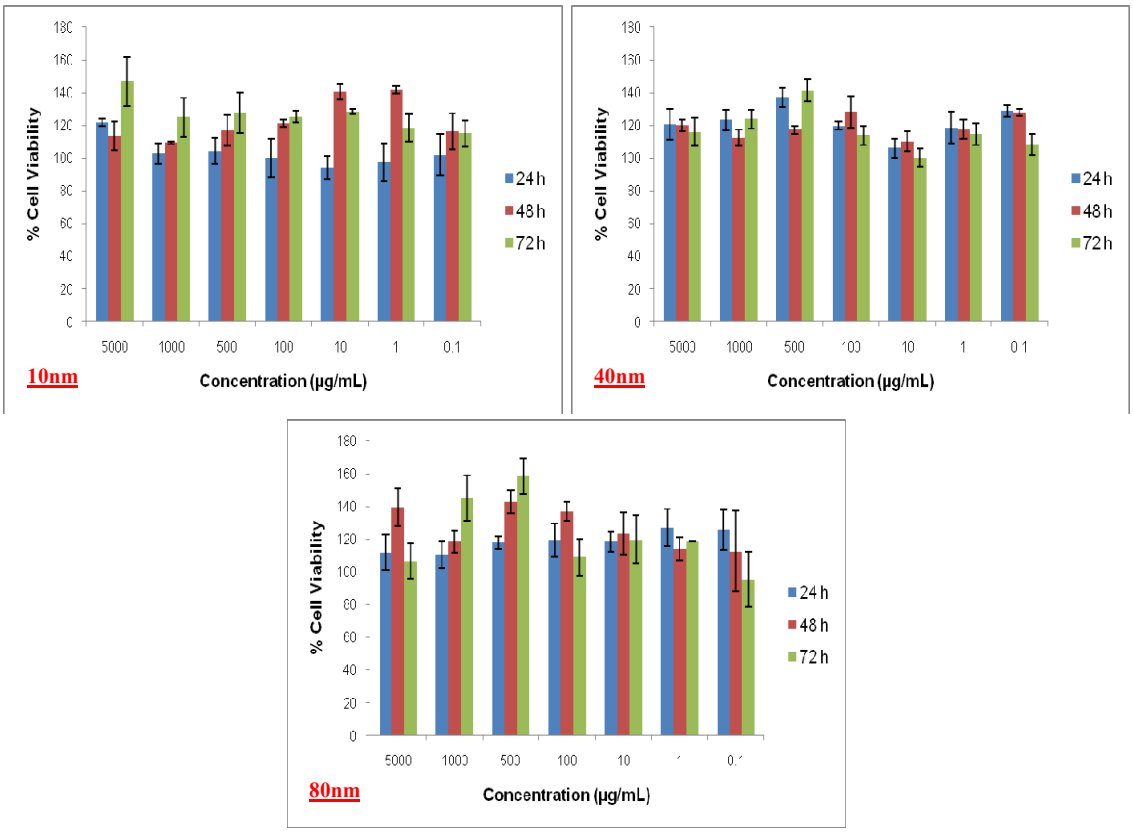

Figure 5.57. Viability of PC-3 cells after 72-h exposure to silica nanoparticles with a size of **10nm**, **40nm** and **80nm**.

To determine the cytotoxic effect of silica nanoparticles assisted by L-lysine (with a size of 14nm) and L-arginine (with a size of 23nm) on MCF-7 cells, MTT test was applied. Silica nanoparticles were dispersed in PBS at 500µg/mL, 400µg/mL, 300µg/mL, 200µg/mL, 100µg/mL, 50µg/mL, 1.0µg/mL, 0.1 µg/mL and 0.01µg/mL and then dosed to cells. Cells exposed 72 hours to silica nanoparticles. Each 24 hours, absorbance was measured at 540nm. Each measurement was repeated 3 times (triplicate).

As can be seen in Figure 5.58-59, we observed that silica nanoparticles assisted by L-lysine and L-arginine have no significant toxic effect on MCF-7 cells in the concentration range of 500µg/mL to 0.01µg/mL.

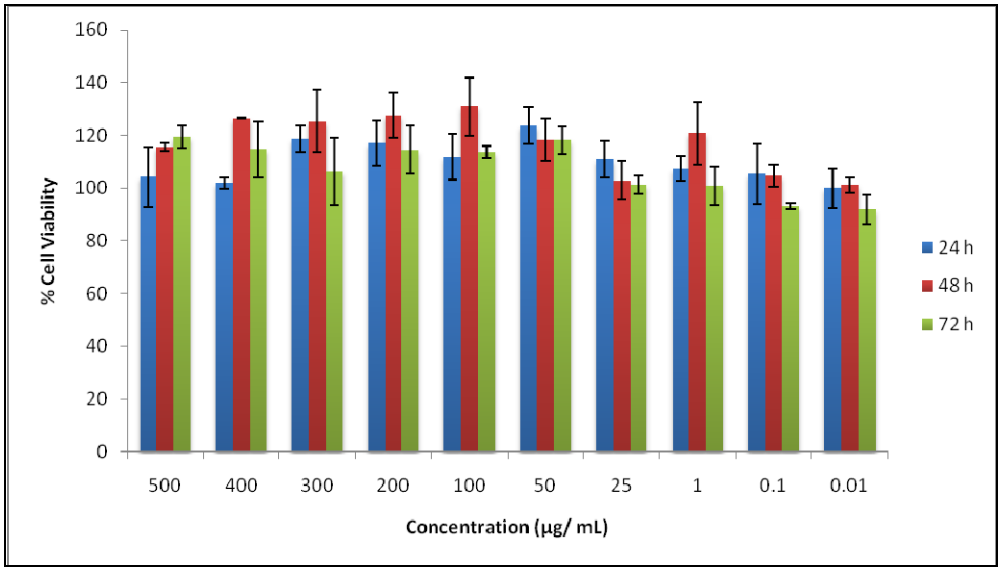

Figure 5.58. Viability of MCF-7 cells after 72-h exposure to **L1**.

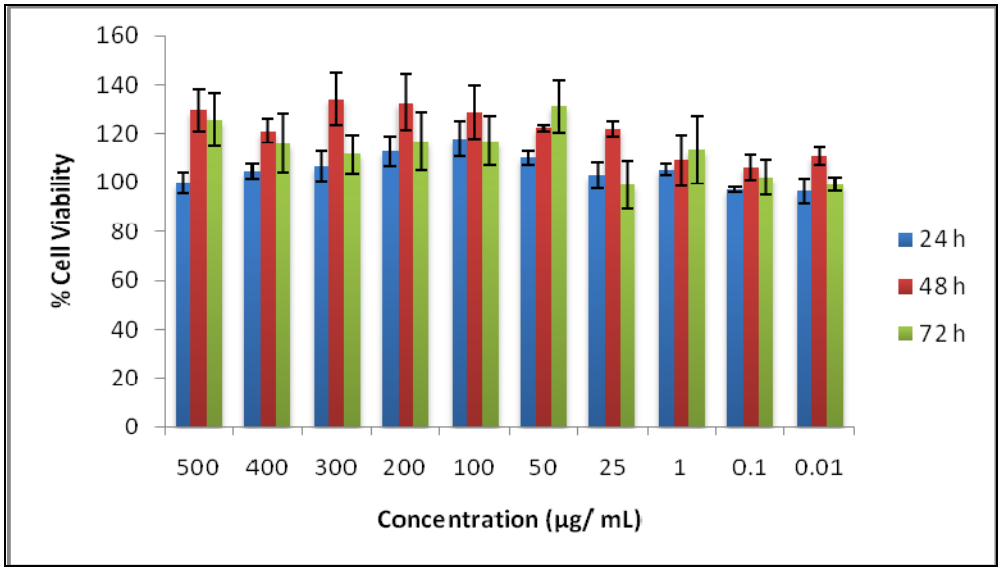

Figure 5.59. Viability of MCF-7 cells after 72-h exposure to **A1**.

Lastly, we examined the toxic effect of dye-doped silica nanoparticles assisted by L-lysine on MCF-7 and PC-3 cells. Dye-doped silica nanoparticles (**L21** and **L22**) were dispersed in PBS at 1000µg/mL, 500 µg/mL, 100µg/mL, 10 µg/mL, 1.0 µg/mL, and 0.1µg/mL and then dosed to cells. Cells were exposed 48 hours to silica nanoparticles. Each 24 hours, absorbance was measured at 540nm/570nm. Each measurement was repeated 3 times (triplicate).

According to MTT results (Figure 5.60-61), we observed that dye-doped silica nanoparticles assisted by L-lysine (both **L22** and **L23**) have no toxic effect on MCF-7 cells in the concentration of 1000µg/mL to 0.1µg/mL. However, these particles (**L22-L23**) have slightly toxic effect on PC-3 cells.

Also it is observed that the different amount of dye (**L22**-*1mL* and **L23**-*100µL*) have also no toxic effect on MCF-7 cells.

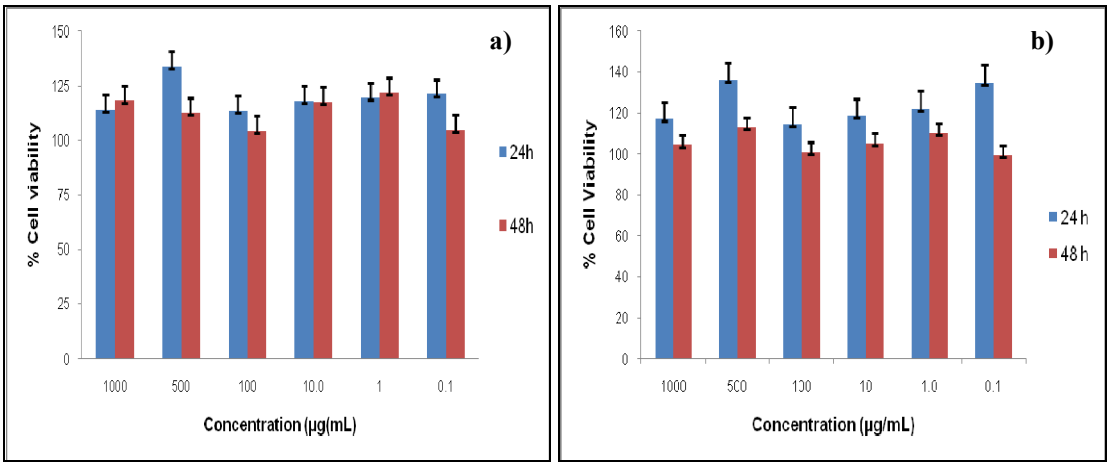

Figure 5.60. Viability of a) MCF-7 and b) PC-3 cells after 48-h exposure to **L22**.

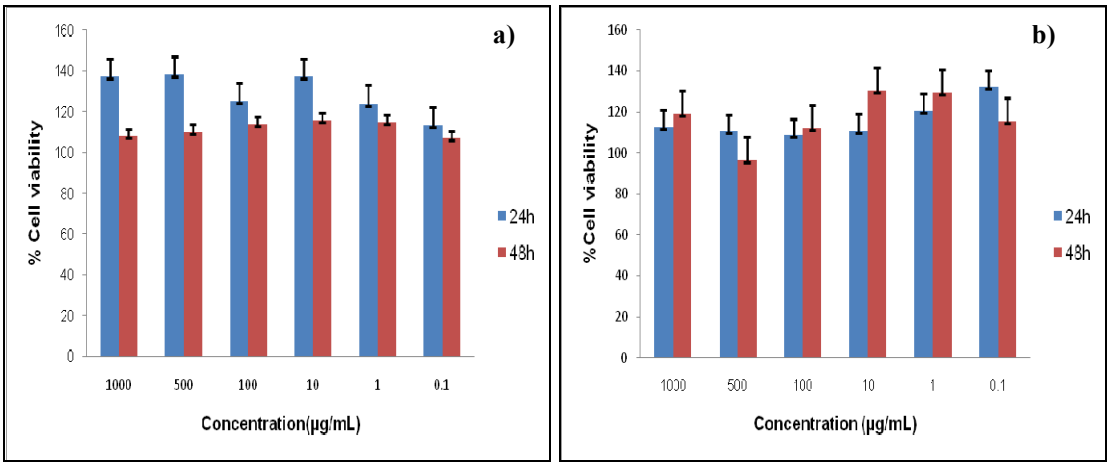

Figure 5.61. Viability of a) MCF-7 and b) PC-3 cells after 48-h exposure to **L23**.

5.9. Confocal Imaging

Confocal Microscopy was used to verify the location of the dye-doped silica nanoparticles (**L22**) synthesized by L-lysine relative to the cells. First, we investigated the effect of incubation period on cells exposed to silica particles. We took the images of MCF-7 cells in bright field mode from the confocal microscopy to observe the location of the dye-doped silica nanoparticles (Figure 5.62).

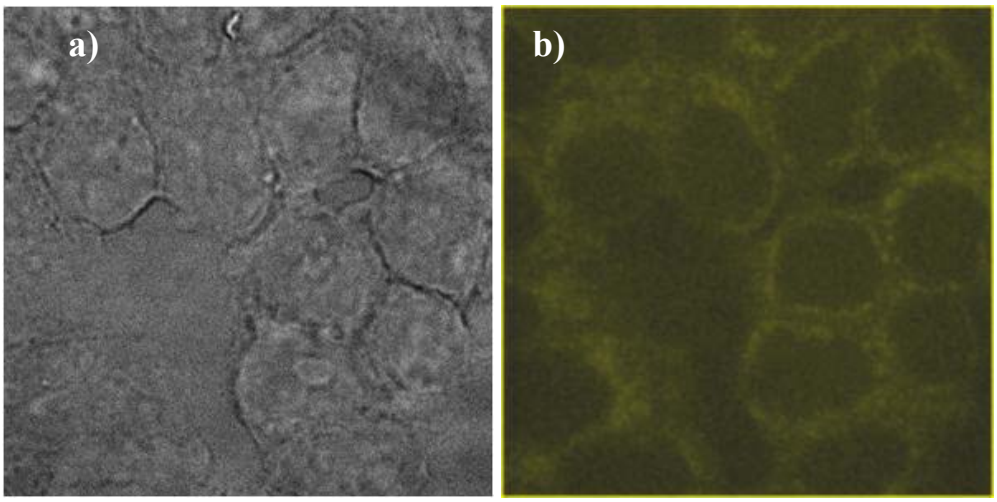

Figure 5.62. Confocal images of MCF-7 cells in bright field mode.

Dye-doped silica particles were incubated with MCF-7 cells for 5min, 10min, 15min, 20min and 60min and at a concentration of 1 µg/ mL. According to confocal images that can be seen in Figure 5.63, yellow points and regions represent dye-doped silica nanoparticles. A weak autofluorescence of cells was also observed.

When we compared the confocal images, there is no significant difference observed with varied incubation periods. After the 5min incubation period, silica particles show smaller amount of accumulation and were distributed throughout the cells. In contrast, after the 60min incubation period, the particles are well distributed throughout the cell.

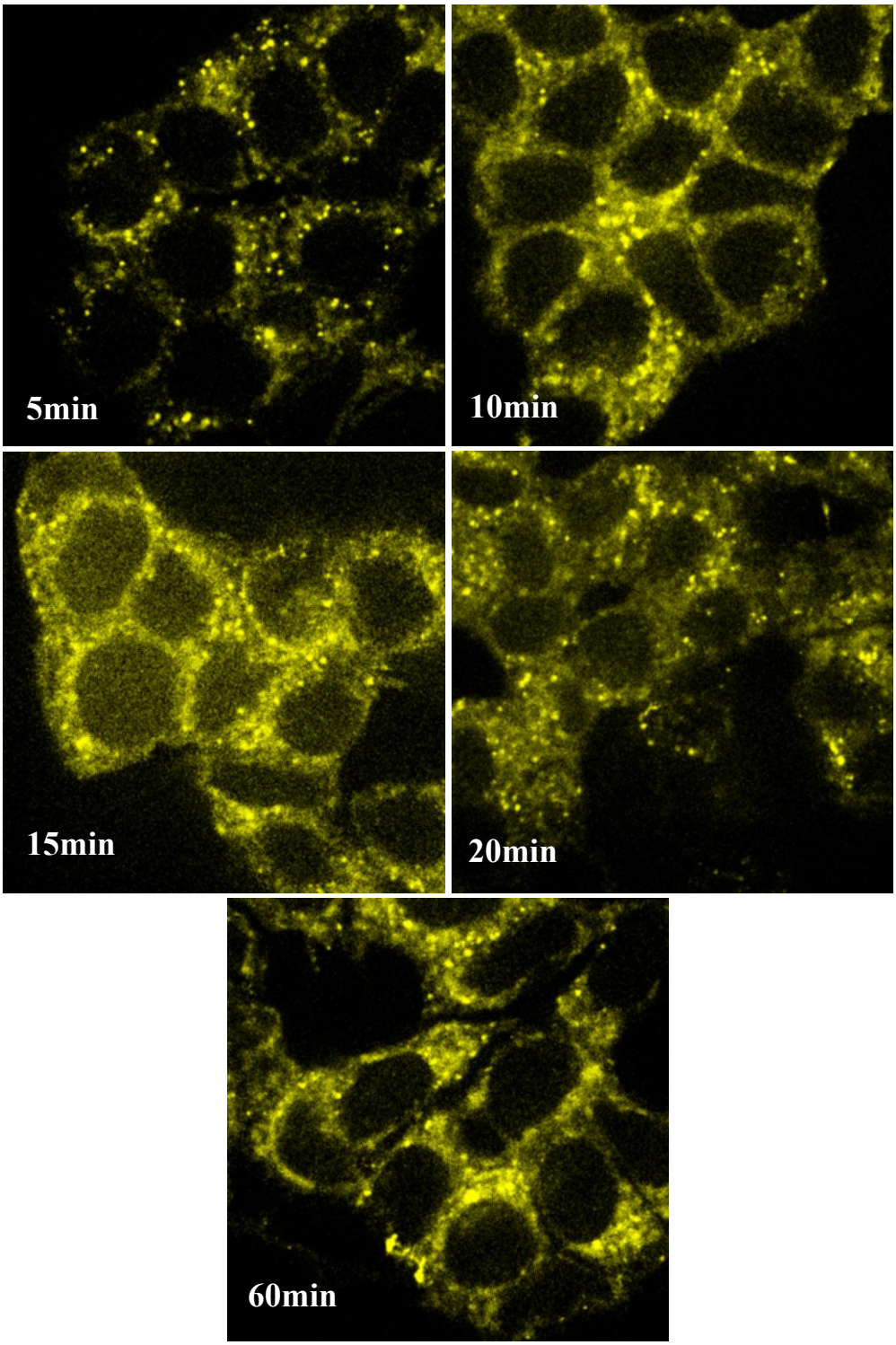

Figure 5.63. Confocal images of (**L17**) in MCF-7 cells in different incubation period.

We also investigated the effect of amount of particles on cells. Dye-doped silica nanoparticles (**L22**) were added 0.1µg/mL, 0.5µg/mL and 1.0µg/mL to cells at 60min incubation period. According to confocal images that can be seen in Figure 5.64, we

observed that increasing amount of particles incubated with cells results better spread of nanoparticles throughout the cells.

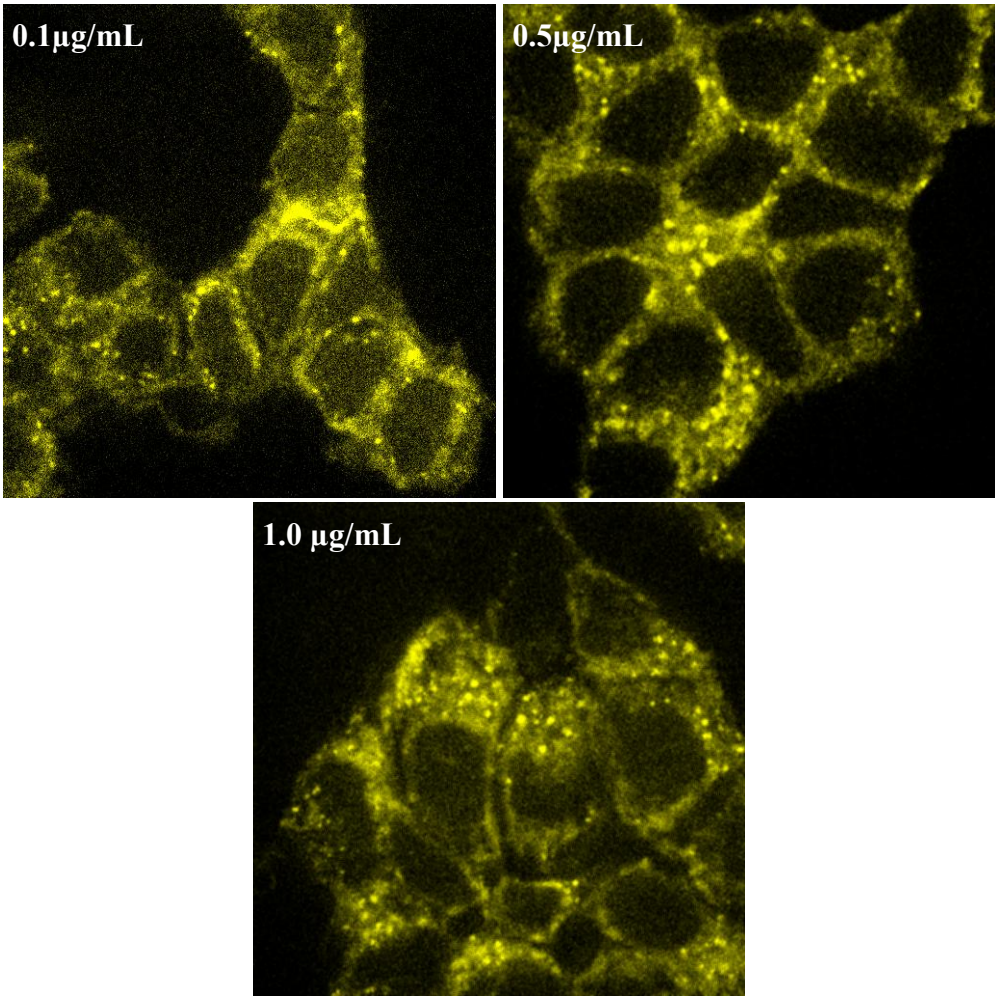

Figure 5.64. Confocal images of different amount of (**L22**) in MCF-7 cells .

CHAPTER 6

CONCLUSION

In this study, we synthesized monodisperse silica nanoparticles with a range of 100- 500nm by using Stöber method (Stöber 1979). Mainly three parameters play an important role in the size and the size distribution of particles; (i) amount of ammonia, (ii) amount of TEOS and (iii) amount of water (Bogush and Zukoski 1991). We optimized the effect of amount of ammonia, TEOS and water on particle size and the size distribution in our study. As a result of, we observed that increasing the amount of ammonia, TEOS and water is resulted in formation of larger particles that can be clearly seen in DLS results. Also, we realized that acidity or basicity of medium of the silica particles mainly alters the order of the particles arrangement. According to SEM images, we concluded that the order of the particles became disordered in the presence of weaker basic medium.

We also synthesized silica nanoparticles assisted by amino acids (Yokoi 2006). We investigated the effects of parameters on the particle size and the size distribution; especially (i) type of amino acids, (ii) temperature, (iii) amount of L-lysine, (iv) amount of TEOS and (v) amount of dye. First, we synthesized silica nanoparticles in the presence of basic amino acids, L-Lysine and L-Arginine. In literature, Histidine was also used however the use of histidine was unsuccessful due to the low basicity (Yokoi 2006). In addition, the use of L-lysine is resulted the formation of smaller particles (~10nm), on the other hand, the use of L-arginine is yielded larger particles (~27nm). XRD pattern shows the broadening peak that is caused by decreasing the particle size. Therefore, we decided to use of L-lysine during this study.

Moreover, the effect of the temperature of the reaction medium was examined. The silica nanoparticles were synthesized at 20^0C- 100^0C. The size of the particle at 20^0C is found to be 5nm, while the size of the particle at 100^0C is found to be 78nm.

According to DLS results we observed that as the temperature rises leads it to formation of the larger particles.

Furthermore, we investigated the effect of amount of L-lysine on particle size. Particles were synthesized in the presence of 0.1mmol, 0.5mmol, 1.0mmol, 2.0mmol and 4.0mmol of L-lysine. According to DLS results, we observed that increasing the amount of L-lysine favors the formation of larger particles. Also we examined the effect of amount of TEOS on particle size. Silica nanoparticles were synthesized in the presence of 5.0 mmol, 25.0 mmol, 50.0 mmol, 75.0 mmol and 100.0 mmol of TEOS. According to DLS results, the optimum, resulting the smallest size, amount of TEOS was determined to be 50.0 mmol. It was showed that controlling the amount of reactants and temperature, we prepared highly monodisperse silica nanoparticles with sizes tuned precisely.

For cellular applications and other immunoassays, it is best to have stable fluorescent probes. Therefore, dye molecules (RBITC-APTES) were randomly doped into the silica nanoparticles by using Stöber sol-gel synthesis. For cell labeling applications, positively charged free RBITC dye molecules could bind to the negatively charged phospholipids cellular membrane. This non-specific binding could contribute to false signals. To prevent dye leakage, we attached RBITC molecules covalently to the silica nanoparticles via a stable thiourea linkage. We synthesized dye-doped silica nanoparticles in the presence of 1ml and 100µl of RBITC-APTES conjugate. According to purification processes, the use of lower amount of dye is better than the use of higher amount of dye as can be shown in absorption and emission spectra.

Additionally, it is possible that most of the dye molecules would be localized on the nanoparticles surface due to small particle size. Actually, we should add an additional silica layer (post coating) to protect surface bound dyes from photobleaching (Santra et.al. 2006). Absorption and emission spectra of RBITC-APTES conjugate and dye-doped silica nanoparticles showed the presence of strong peaks around 540 and 570nm, respectively. These absorption and emission peaks are typical for RBITC molecules. In addition, these absorption and emission spectra of L21 and L22 matched well with corresponding spectra of RBITC. Both absorption and emission spectra of dye-doped silica nanoparticles were clearly confirmed successful doping of RBITC molecules in the silica nanoparticles.

Toxicity is a common characteristic of materials typically used for intracellular delivery because of their ability to alter cell membrane. Therefore, we evaluated the

effects of silica nanoparticles in the presence of ammonia and L-lysine(/L-arginine) both empty and dye-doped and the size of these particles on the viability of MCF-7 and PC-3 cancer cell lines. We incubated the silica nanoparticles in the range of 5000 mg/μL to 0.1 mg/μL into the cells. After the 24h, 48h and 72h, the absorbance of the cells exposed to silica particles was read. According to these absorbance values, we determined the cell viability of the cells. According to MTT results, silica nanoparticles assisted by L-lysine both empty and dye-doped has no significant toxic effect on MCF-7 and PC-3 cells based on the particle size.

Confocal microscopy was used to verify the location of the dye-doped silica nanoparticles assisted by L-lysine. We investigated the effects of amounts of particles exposed to cells and incubation time. First, cells were exposed to the dye-doped silica nanoparticles with a amount of 0.1 μg/ml, 0.5 μg/ml and 1.0 μg/ml for 60 min incubation time. We varied the incubation time (5min, 10min, 15min, 20min, 60min) of dye-doped silica nanoparticles at an amount of 1.0 μg/ml. We observed that dye-doped silica nanoparticles are well distributed throughout the cell with an increasing amount of particles. There are no important changes between the confocal images of silica nanoparticles with a concentration of 0.1 μg/ml, 0.5 μg/ml and 1.0 μg/ml

Due to their biocompatible properties, these dye-doped silica nanoparticles can be used for bioimaging and drug delivery applications.

REFERENCES

A Imhof, M. Mergens, J. J. Engelberts, D.T.N. de Lang, R. Sprik, and W. L. Vos. 1999. Spectroscopy of Fluorescein (FTIC) Dyed colloidal silica spheres. *Journal Physial Chemistry B* 103: 1408- 1415

A. van Blaaderen, and A. Vrij. 1992. Synthesis and characterization of colloidal dispersions of fluorescent, monodisperse silica spheres. *Langmuir* 8: 2921- 2931

Andre Nel, Tian Xia, Lutz Madler, and Ning Li. 2006. Toxic potential of materials at the nanolevel. *Science* 311: 622- 627

Anna M. Lipski, Christopher J. Pino, Frederick R. Haselton, I. Wei Chen, and V. Prasad Shastri. 2008. The Effect of silica nanoparticles-modified surfaces on cell morphology, cytoskeletal organization and function. *Biomaterials* 29: 3836- 3846

B. Viwanathanrinker, C. J., and Scherer G.W. 1990. Sol-gel science: The Physics and Chemistry of Sol-gel Processing. *Acedemic Press*

Brian Matsumoto. 2002. *Cell biological applications of confocal microscopy.* Academic Press

Brinker, C. J., and Scherer G.W. 1990. Sol-gel science: The Physics and Chemistry of Sol-gel Processing. *Acedemic Press*

C. A. R. Costa, L.F.Valadares, F.Galembeck. 2007. Stöber silica particle size effect on the hardness and brittleness of silica monoliths. *Colloids and Surfaces A: Physicochem. Eng.* Aspects 302: 371- 376

Chemical Materials. http://www.chemat.com. (accessed may 5, 2009)

C. N. R. Rao, A. Müller, A. K. Cheetham, eds. 2004. *The Chemistry of nanomaterials*. John Wiley & Sons

Cornell Nanobiotechnology Center. http://www.. N. R. Rao, A. Müller, A. K. Cheetham, eds. 2004. *The Chemistry of nanomaterials*. John Wiley & Sons

David B. Mitzi. 2009. *Solution processing of inorganic materials*. John Wiley & Sons

D. L. Green, J. S. Lin, Yui- Fai Lam, M. Z. C. Hu, Dale W. Schaefer, and M. T. Harris. 2003. Size, volume fraction and nucleation of stöber silica nanoparticles. *Journal of Colloid and Interface Science* 266: 346- 358

Dong- Wook Lee, Son- Ki Ihm, and Kew- Ho Lee. 2005. Mesoporous silica framed by sphere-shaped silica nanoparticles. *Microporous and Mesoporous Material* 83: 262- 268

Elisabeth S. Papazogluo, Aravind P, eds. 2007. *Bionanotechnology*. Morgan and Claypool Publishers

Eugenii Katz, and Itamar Willner. 2004. Integrated nanoparticles-biomolecule hybrid systems: synthesis, properties and applications. *Angew. Chem. Int. Ed.* 43: 6042-6108.

Fang Wang, J. Liu, Zhongkuan Luo, Qianling Zhang, Peixin Wang, Xun Liang, C.Li, J.Chen. 2007. Effects of dimethyldiethoxysilane addition on the sol-gel process of tetraethylorthosilicate. *Journal of Non-Crystalline* 353: 321-326

G.H. Bogush, and C. F. Zukoski. 1991. Uniform silica particles precipitation: An aggregative growth model. *Journal of Colloid and Interface Science* 142: 1- 18

Hiroshi Nakamura, Masahiko Ishii, Azusa Tsukigase, Msashi Harada, and Hideyuki Nakano. 2006. Close-packed colloidal crystalline arrays composed of silica spheres coated with titania. *Langmuir* 22: 1268- 1272

Hooisweng Ow, Daniel R. Larson, Mamta Srivastava, Barbara A. Baird, Watt W. Webb, and Ulrich Weisner. 2005. Bright and stable core-shell fluorescent silica nanoparticles. *Nano Letters* 5: 113- 117

I. A. Rahman, P. Vejayakumaran, C. S. Sipaut, J. Ismail, M. Abu Bakar, R. Adnan, and C. K. Chee. 2007. An optimized sol-gel synthesis of stable primary equilavent silica particles. *Colloids and Surfaces A: Physicochem. Eng. Aspects* 294: 102- 110

I. A. Rahman, P. Vejayakumaran, C. S. Sipaut, J. Ismail, and C. K. Chee. 2008. Effect of the drying techniques on the morphology of silica nanoparticles synthesized via sol-gel process. *Ceramics International* 34: 2059- 2066

Iler, R. K. 1979. *The Chemistry of Silica*. JohnWiley & Sons

Jason E. Fuller, Gregory T. Zugates, Lino S. Ferreira, Hooisweng S. Ow, Nicholas N. Nguyen, Ulrich B. Weisner, Robert S. Langer. 2007 Intracellular delivery of core-shell fluorescent silica nanoparticles. *Biomaterials* 1-7

K. Nozawa, H. Gailhanou, L. Raison, P. Panizza, H. Ushiki, E. Sellier, J. P. Delville, and M. H. Delville. 2005. Smart control of monodisperse stöber silica particles: effect of reactant addition rate on growth process. *Langmuir* 21: 1516- 1528

Kewal K. Jain. 2005. Nanotechnology in clinical laboratory diagnostics. *Clinica Chimica Acta* 258: 37- 54

Kota Sreenivasa Rao, Khalil El- Hami, Tsatomu Kodaki, Kazumi Matsushige, and Keisuke Makino. 2005. A novel method for synthesis of silica nanoparticles. *Journal of Colloid and Interface Science* 289: 125- 131

Lide Zhang, X. Fang, Changhui Ye, eds. 2007. *Controlled growth of nanomaterials*. World Scientific Publishing.

Lingzhi Wang, Juying Lei, and Jinlong Zhang. 2009. Building of multifluorescent mesoporous silica nanoparticles. Chem. Commun. 2195-2197

Michele Marini, Behzad Pourabbas, Francesco Pilati, and Paola Fabbari. 2008. Functionally modified core-shell silica nanoparticles by one-pot synthesis. *Colloids and Surfaces A: Physicochem. Eng. Aspects 317: 473- 481*

N. Venkatathri. 2007. Synthesis of silica nanospheres from homogeneous and heterogeneous systems. *Bull. Mater. Sci.* 30: 615- 617.

Neelam Azad, and Yon Rojanasakul. 2006. Nanobiotechnology in drug delivery. *J. Am. Drug Delivery* 4: 79- 88

Ntsc. http://www.ntsc.in (accessed June 5, 2009)

Patrick M. Johnson, Carlos M. van Kats, and Alfons van Blaaderen. 2005. Synthesis of colloidal silica dumbels. *Langmuir* 21: 11510- 11517

Rahul P. Bagwe, Lisa R. Hilliard, and Weihong Tan. 2006. Surface modification of silica nanoparticles to reduce aggregation and nonspecific binding. *Langmuir* 22: 4357- 4362.

Rahul P. Bagwe, Chaoyong Yang, Lisa R. Hillard, and Weihong Tan. 2004. Optimization of dye-doped silica nanoparticles prepared using a reverse microemulsion method. *Langmuir* 20: 8336- 8342

S. Tabatabaei, A. Shukohfar, R. Aghababazadeh, A. Mirhabibi. 2006. Experimental Study of the synthesis and characterization of silica nanoparticles via the sol-gel method. *Journal of Physics: Conference Series* 26: 371- 374

Sumio Sakka. 2007. *Sol-gel Science and Technology: Processing Characterization and Applications.* Kluwer Academic Publishers

Stöber, W., Fink, A., and Bohn, E. 1968. Controlled growth of monodisperse silica nanospheres in the micron size range. *Journal of Colloid Interface Science* 26: 62-69

Swadeshmukul Santra, Bernd Liesenfeld, Chiara Bertolino, Debemitra Dutta, Zehui Cao, Weihong Tan, Brij M. Moudgil, and Robert A. Mericle. 2006. Fluorescence lifetime measurements to determine the core-shell nanostructure of FTIC-doped silica nanoparticles: An optical approach to evaluate nanoparticles photostability. *Journal of Luminescence* 117: 75- 82

Tracy M. Davis, Mark A. Snyder, John E. Krohn, and Micheal Tsapatsis. 2006. Nanoparticles in lysine-silica sols. *Chem. Mater.* 18: 5814-5816

Toshiyuki Yokoi, Yasuhiro Sakamoto, Osamu Terasaki, Yoshihiro Kubota, Tatsuya Okubo, and Takashi Tatsumi. 2006. Periodic arrangement of silica nanospheres assisted by amino acids. *Journal American Chemical Society* 128: 13664- 13665

V.Renugopalakrishnan, Randolph V.Lewis, eds. 2006. *Bionanotechnology: Proteins to nanodevices*. Springer.

Valter Reedo. 2008. Elaboration of IVB group metal oxide structures and their possible applications. *Phys. Status Solidi A.* 205: 1511- 1514.

Weihong Tan, Kemin Wang, Xiaoxiao He, Xiaojun Julia Zhao, Timothy Drake, Lin Wang, and Rahul P. Bagwe. 2003. Biotechnology based on silica nanoparticles. *Medicinal Research Reviews* 24: 621- 638

Weisheng Lin, Yue-wern Huang, Xiao- Dong Zhou, and Yinfa Ma. 2006. In vitro toxicity of silica nanoparticles in human lung cancer cells. *Toxicology and Applied Pharmacology* 217: 252-259

Yale Strausser. 1993. *Characterization in silicon processing*. Butterworth Heinemann.

Yu-Shen Lin, Chih-Pin Tsai, Hsing-Yi Huang, Chieh-Ti Kuo, Yann Hung, Dong-Ming Huang, Yao-Chang Chen, and Chung-Yuan Mou. 2005. Well-ordered mesoporous silica nanoparticles as cell markers. *Chem. Mater.* 17: 4570-4573